**The Thesis Committee for Robert Anthony Schomp**

**Certifies that this is the approved version of the following thesis:**

# Estimating Inundation Extent and Depth from National Water Model Outputs and High Resolution Topographic Data

**APPROVED BY**

**SUPERVISING COMMITTEE:**

Paola Passalacqua, Supervisor

David R. Maidment

# Estimating Inundation Extent and Depth from National Water Model Outputs and High Resolution Topographic Data

by

**Robert Anthony Schomp**

**Thesis**

Presented to the Faculty of the Graduate School of

The University of Texas at Austin

in Partial Fulfillment

of the Requirements

for the Degree of

**MASTER OF SCIENCE IN ENGINEERING**

**The University of Texas at Austin**

**May 2021**

**Dedication**

To my friends and family

**Acknowledgments**

First, I am grateful for Dr. Paola Passalacqua's guidance, support, and persistence. Her confidence in my ability to learn quickly encouraged me to flourish in my Master's program. Next, many thanks go to my CWE project collaborators including: Alec and Daniel for your patience in teaching me how computers work, Dr. Arctur, Harry, and Christine for your contributions and connections to the community, Andy for your post-graduation career advice, and Dr. Maidment for your limitless vision.

Special thanks go to Tom, Nicky, and Yacoub at AECOM for creating a previously nonexistent environmental intern position and offering three years of enjoyable experience. Thank you to my favorite Portland State University professors Dr. Khosravifar and Dr. Dietz. My nontraditional path through four colleges allowed me gain enriching experiences with professors Dr. Lee and Leif Eccles as well as lasting friendships with David and Chris. Additionally, I could not have kept my momentum without my UT EWRE friends Emma, Daniel, and Megan.

My deepest gratitude goes to Ana for your unwavering trust, reassurance, and optimism. As a first generation college student, a special thank you goes to my parents, Chris and Ken, and grandparents, Helen and Tony, for supporting my academic journey. This thesis is a direct result of my family's hard work and generational improvement. As my late grandpa Tony once said, "*Break your brain, not your back*".

Finally, I would like to thank Planet Texas 2050 and NOAA for funding this project. Specifically, the following thesis received financial support from the NOAA-JTTI Program, Grant No. NA19OAR4590229.

# Estimating Inundation Extent and Depth from National Water Model Outputs and High Resolution Topographic Data

Robert Anthony Schomp, M.S.E.

The University of Texas at Austin, 2021

Supervisor: Paola Passalacqua

Recent flood disasters, such as Hurricane Harvey in 2017, have emphasized the need for computationally quick simulations of flood inundation over large spatial scales. The purpose of this study is to address the National Oceanic and Atmospheric Administration's priority goal by enhancing inundation mapping with the GeoFlood workflow. The GeoFlood flood inundation mapping approach integrates the GeoNet and Height Above Nearest Drainage methods. GeoNet utilizes high-resolution topographic data and geodesic minimization principles to extract channel networks. Then, the Height Above Nearest Drainage method is used to determine synthetic rating curves and channel hydraulic properties. Finally, the National Water Model discharge forecasts are correlated with stage heights to produce real-time flood inundation extent and depth maps. For this study, GeoFlood's computational advantages were leveraged at the Texas Advanced Computing Center to produce Hurricane Harvey flood inundation maps across seven Texas counties on a Hydrologic Unit Code 12 watershed scale. Improvement was quantified by comparing a traditional medium-resolution Height Above Nearest Drainage approach versus the GeoFlood workflow. The most significant channel and terrain characteristics used to quantify improvements were topographic relief,

slope, and stream order. Performance was measured by comparing the 10-meter resolution Height Above Nearest Drainage and 1-meter resolution GeoFlood inundation maps versus the Federal Emergency Management Agency Hurricane Harvey flood depths grid and United States Geological Service Hurricane Harvey High Water Mark benchmarks. GeoFlood performance enhancements were greatest in low relief, low slope, and densely developed regions as well as across a majority of Strahler stream orders. GeoFlood increased inundation mapping performance in both extent and depth. Limitations of the approach included segment catchment filling as well as the lack of pluvial and coastal flood hazard components. Overall, this study supports the integration of high-resolution terrain data into flood inundation mapping via the GeoFlood workflow.

Keywords: Flood Inundation Mapping; GeoNet; GeoFlood; Height Above Nearest Drainage; High-Resolution Terrain Data; Raster Comparison

## Table of Contents

## List of Tables

## List of Figures

# Acronyms

**3DEP** 3D Elevation Program. 19, 27

**AMSL** Average Mean Sea Level. 18

**CONUS** Continental United States. 1

**DEM** Digital Elevation Model. xv, 2–4, 8, 19, 27–31, 34–36, 88, 92

**Dinf** D-infinity Flow Directions. 35

**ESRI** Environmental Systems Research Institute. 21

**FEMA** Federal Emergency Management Agency. xiii, xv, xix–xxii, 3, 4, 9, 21, 22, 55, 67–82, 89, 90, 92–94, 96

**HAND** Height Above Nearest Drainage. xi–xiii, xv–xxi, 2–5, 7, 8, 22, 24, 26, 33, 36, 41, 43–73, 75–78, 81, 83, 84, 87–97

**HEC-RAS** Hydrologic Engineering Center's River Analysis System. 6, 7

**HR** High Resolution. 20

**HRT** High Resolution Topography. xii, 2–5, 72, 93

**HUC** Hydrologic Unit Code. xiii, xv–xvii, xxii, 26–28, 34, 36, 39–43, 47, 83–86, 94

**HWM** High Water Marks. xiii, 3, 23, 25, 45, 75–77, 86, 87, 96

**IfSAR** Interferometric Synthetic Aperture Radar. 22

**IQR** Interquartile Range. xi–xiii, 13, 14, 18, 52, 55, 71, 72, 76

**JTTI** Joint Technology Transfer Initiative. 1, 2

**LiDAR** Light Detection and Ranging. 3, 8, 10, 19, 22, 27, 70, 90, 96

**MAE** Mean Average Error. xi–xiii, xx, xxi, 54, 55, 72–77, 88, 90, 93, 96

**ME** Mean Error. xi–xiii, xviii, xx, xxi, 53–55, 71–77, 88, 90, 93, 96

**MR** Medium Resolution. xiv, xv, xviii, xxi, xxii, 2, 3, 13, 17, 20, 21, 28, 33, 34, 56–58, 79, 82, 92, 93

**MRLC** Multi-Resolution Land Characteristics. 10

**NAD83** North American Datum of 1983. 23

**NAVD88** North American Vertical Datum of 1988. 23

**NED** National Elevation Dataset. 20

**NFIE** National Flood Interoperability Experiment. 2, 3, 20

**NHD** National Hydrography Dataset. xiv, xv, xvii–xxii, 2–4, 13, 14, 16–21, 26, 28, 33, 34, 48–50, 54–59, 62–66, 68, 71, 74, 78, 79, 81, 82, 84, 88–95

**NLCD** National Land Cover Database. 10–13

**NOAA** National Oceanic and Atmospheric Administration. 1, 2, 26

**NWM** National Water Model. 1–4, 8, 21, 39, 87, 94, 96, 97

**RMSE** Root Mean Squared Error. xi–xiii, xviii–xxi, 53, 55–57, 65, 71–77, 82, 88, 90–93, 96

**StratMap** Strategic Mapping Program. 19

**TACC** Texas Advanced Computing Center. 19

**TauDEM** Terrain Analysis Using Digital Elevation Models. 35

**TIN** Triangulated Irregular Network. 22

**TNM** The National Map. 19, 27

**TNRIS** Texas Natural Resources Information System. 19, 27

**TPP** Transportation Planning and Programming. 26

**TxDOT** Texas Department of Transportation. 26

**US** United States. 20, 94

**USACE** United States Army Corps of Engineers. 7

**USFIMR** United States Flood Inundation Mapping Repository. 95

**USGS** United States Geologic Survey. xiii, xv, xxi, xxii, 3, 4, 10, 19, 20, 22–25, 27, 45, 55, 75–77, 84, 86, 87, 96

**UTM** Universal Transverse Mercator. 10

**WBD** Watershed Boundary Dataset. 20

**WSE** Water Surface Elevation. 45, 46

# Chapter 1: Introduction

On August 25th, 2017, Hurricane Harvey made landfall near Rockport, Texas as a category 4 hurricane (National Oceanic and Atmospheric Administration, 2018a). Wind gusts exceeded 150 miles per hour (240 kilometers per hour) as tremendous amounts of rainfall poured over southeastern Texas and southwestern Louisiana (National Oceanic and Atmospheric Administration, 2018a). As Harvey stalled inland, up to 60 inches (1524 millimeters) of precipitation fell within an eight day period in some parts of Texas (Blake and Zelinski, 2018). Historic levels of flood inundation were observed as Harvey moved slowly until diminishing in strength on September 4th, 2017. Flooding impacted 500,000 vehicles and 300,000 structures causing nearly $125 billion in damage (National Oceanic and Atmospheric Administration, 2018b). Hurricane Harvey, the second costliest event behind Hurricane Katrina, was also responsible for 68 direct and 35 indirect fatalities (National Oceanic and Atmospheric Administration, 2018b).

The need for computationally quick predictions of flood inundation extent and depth over large regions has been emphasized by recent hurricane disasters. The National Oceanic and Atmospheric Administration's (NOAA) 2018 Joint Technology Transfer Initiative (JTTI) prioritizes the improvement of flood inundation mapping (National Oceanic and Atmospheric Administration, 2018c). A secondary goal of NOAA's JTTI includes enhancing hydrologic prediction. The National Water Model NWM simulates observed and forecasted channel discharges for all stream reaches in the entire continental United States (CONUS) on an hourly basis (Office of Water Prediction, 2020). The GeoFlood workflow addresses the

NOAA JTTI goals by utilizing NWM outputs and high-resolution terrain (HRT) to enhance flood inundation mapping performance.

Zheng et. al. (2018a) and Liu et. al. (2016) tested the Height Above Nearest Drainage method at the National Flood Interoperability Experiment (NFIE) with 10-meter resolution digital elevation models (DEMs) and the National Hydrography Dataset Plus medium-resolution (NHDPlus MR) flowlines. However, a lack of accuracy becomes apparent when comparing the NHDPlus MR flowlines to the high-resolution terrain. As noted by Johnson et. al. (2019), inaccuracies from the NHDPlus MR flowlines may perpetuate errors into the inundation extent and depth predictions. The goal of this study is to test the GeoFlood workflow across seven Texas counties to determine if and where high-resolution terrain enhances inundation mapping performance.

First, GeoFlood uses high-resolution topographic data and geodesic minimization principles to extract a channel network between NHDPlus MR nodes. Next, the Height Above Nearest Drainage HAND method is used to compute channel hydraulic properties and synthetic rating curves. Then, the NWM discharges are correlated with the synthetic rating curve to determine stage height. Pixels with values less than or equal to the stage height will become inundated. Finally, flood inundation extent and depth maps are produced. The GeoFlood workflow is computationally quick while also incorporating real-time streamflow data from the NWM.

While other studies have applied HAND based inundation mapping approaches to smaller regions, this study is focused on understanding inundation prediction improvements and performance across seven Texas counties covering a total of 31,938 square kilometers (Afshari et. al., 2018; Jafarzadegan and Mer-

wade, 2018; Zheng et. al., 2018a; Johnson et. al., 2019). The GeoFlood 1-meter inundation mapping workflow was compared to the Height Above Nearest Drainage (HAND) method at 10-meter resolution. The HAND at 10-meter inundation maps, often referred to as the medium-resolution (MR) simulation, were generated using 10-meter DEMs and the NHDPlus MR flowlines. HAND at 10-meter is the original HAND-NWM inundation mapping method tested at the NFIE. The 1-meter resolution inundation maps, frequently referred to as the GeoFlood 1-meter or high-resolution terrain (HRT) simulation, utilizes the most recent LiDAR flights and topographical data available as well as GeoNet extracted channel networks.

*Improvement* is defined as the beneficial differences from the GeoFlood 1-meter workflow versus the traditional HAND at 10-meter workflow. *Performance* is defined as the favorable enhancements provided by the HRT inclusion in the GeoFlood workflow as compared to reference datasets. Beneficial differences and favorable enhancements are quantified by statistical inundation extent and depth comparison metrics as well as geospatial observations. For example, inundation extent accuracy may be greater for the HRT GeoFlood model as compared to a reference because the difference between the enhanced GeoFlood 1-meter workflow and HAND at 10-meter simulation is significant. Two references were used for comparison; the Federal Emergency Management Agency (FEMA) 3-meter Harvey Flood Depths Grid and United States Geological Survey (USGS) Hurricane Harvey High Water Marks (HWMs) (Federal Emergency Management Administration, 2020a; Watson et. al., 2018). The FEMA reference was used to compare NHD catchment scale inundation extent and depth, while the USGS reference compared inundation depth at point locations.

This thesis is organized as follows: Four research questions are proposed,

then, a literature review and background for GeoNet and GeoFlood are presented in Chapter 2. Chapter 3 characterizes the terrain and channel characteristics of the seven Texas counties. Additionally, the input datasets including the DEMs, NHDPlus, and NWM forecasts are introduced. Descriptions of the reference FEMA and USGS datasets follow. Chapter 4 reviews the input data preparation, channel network extraction, channel hydraulic property, and inundation mapping methods of the GeoFlood workflow. Then, the inundation extent and depth statistical comparison metrics are presented. Results are presented in Chapter 5. *Improvement* is evaluated for inundation extent and depth for the GeoFlood model to HAND model comparison. *Performance* is assessed for inundation extent and depth for the GeoFlood models to FEMA and USGS references comparison. Correlations of terrain and channel characteristics to the statistical comparisons are examined in the proceeding sections. Finally, limitations in the GeoFlood workflow are introduced. Chapter 6 answers the four research questions by proposing new hypothesis as well as discussing the support of prior hypothesis in this study. Finally, chapter 7 summarizes the improvements and enhancements provided by HRT and offers opportunities for future work.

## 1.1 Research Questions

*Which terrain characteristics significantly impact GeoFlood's performance?*

*Which channel characteristics significantly impact GeoFlood's performance?*

*Where does high-resolution terrain improve inundation mapping performance using the GeoFlood workflow?*

We will test the hypothesis that performance enhancements brought by

HRT data in estimation accuracy are quantifiable in inundation depth and to a lesser degree in extent.

*Where is the HAND approach and related estimation of hydraulic geometry appropriate?*

We will test the hypothesis that the HAND approach and related estimation of hydraulic geometry is less appropriate in short and flat reaches as well as where backwater effects dominate behavior.

---

# Chapter 2: Literature Review and Background

## 2.1 Flood Inundation Models

Flood inundation modeling has permeated many aspects of water resources and environmental engineering. The models may be used in flood damage assessments (Watson et. al., 2018; Jamali et. al., 2018), real-time flood forecasting (Robson et. al., 2017), flood risk mapping (Federal Emergency Management Administration, 2020b), and contaminant transport (Sämann et. al., 2019). According to Teng et. al. (2017), flood inundation models can be classified into three categories: empirical methods, hydrodynamic models, and simplified conceptual models.

Empirical flood inundation models use historical data, such as rainfall, water levels, and stage height, as well as rating curves to forecast flood inundation (Chang et. al., 2016). Recent empirical flood inundation models have utilized remote sensing, social media information, and topographic data sources (Rosser et. al., 2017). The strengths of empirical flood inundation models are the rapid estimation of potential flood risk and post-event model calibration (Rosser et. al., 2017). The disadvantages of empirical flood inundation models are their susceptibility to inaccuracies due to environmental factors as well as their lack of ability to explain the underlying hydrodynamic processes.

Hydrodynamic models commonly solve one-dimensional Saint-Venant equations or two-dimensional shallow water equations. Modern high-resolution FEMA flood inundation maps are created with HEC-RAS hydrodynamic models (Brunner, 2020). HEC-RAS is developed by the Hydrologic Engineering Center of

the United States Army Corps of Engineers (USACE). HEC-RAS performs one-dimensional steady flow and two-dimensional unsteady flow calculations using high-resolution terrain inputs. HEC-RAS is used to simulate dam and levee failures in major drainage basins and can provide important insight in such applications. The strength of HEC-RAS is its widespread international adoption, accessibility, and accuracy. The computational power required by HEC-RAS to produce a flood inundation map can be on the order of weeks to months. The disadvantages of HEC-RAS are its substantial computational requirements. Thus, the computationally intensive HEC-RAS method is currently impractical to model real-time flood events over large regions.

Simplified conceptual models require less computational power than conventional hydrodynamic models (Teng et. al., 2017). Computational time savings mean that simplified conceptual models are well-suited for large-scale inundation mapping as well as probabilistic risk assessments that require a large number of simulations. The relevant simplified conceptual model for this study is the Height Above Nearest Drainage HAND method (Rodda, 2005; Rennó et. al., 2008; Nobre et. al., 2011; Tesfa et. al., 2011). The HAND method determines the vertical height difference between a pixel within a delineated drainage area and its nearest drainage path. Liu et. al., 2016 discussed the applicability of using the HAND raster and workflow to conduct large-scale inundation mapping research. The pre-processing of the input datasets (i.e. HAND) allows for the rapid conversion of real-time streamflow forecasts to flood inundation models.

## 2.2 GeoNet and GeoFlood

Automated channel extraction from LiDAR data has been developed using diverse approaches and methods (Johansen et.al., 2013; Orlandini et. al., 2011; Passalacqua et. al., 2010; Pelletier, 2013; Sangireddy et. al., 2016). Barták (2010) concluded that the availability of a suitable range of automated channel extraction methods is desirable because the optimal algorithms needed for study areas often differ substantially and the aim of the analysis depends on individual choice. GeoNet is a method for the extraction of channel networks from LiDAR-derived DEMs (Passalacqua et. al., 2010). The GeoNet approach combines nonlinear filtering and geodesic minimization principles to extract the channel network while overcoming high-resolution topography issues. GeoNet is a suitable method for this study because adjustable parameters can be optimized while retaining the general workflow; as explained in Section 4. Additionally, GeoNet has been integrated with HAND and NWM outputs to create the novel GeoFlood approach for high-resolution flood inundation mapping (Zheng et. al., 2018a).

GeoFlood, a simplified conceptual model, can produce flood inundation maps within minutes using real-time precipitation forecast data from the National Water Model (NWM). First, the HAND raster is used to derive the channel geometric properties of each stream segment (Zheng et. al., 2018b). Next, a synthetic rating curve is computed for each stream segment using the channel geometric properties. Then, a flow time series is converted into a stage height time series. Finally, a NWM discharge is correlated with a stage height and associated with the HAND raster to determine the inundation depth and extent within the stream segment catchment.

The GeoFlood workflow detailed in Zheng et. al., 2018a was applied to the Onion Creek watershed in Central Texas. The Zheng et. al., 2018a sensitivity analysis showed that the Manning's n roughness coefficient and correctness of channel delineation may significantly impact the accuracy of inundation depth and extent. GeoFlood inundation extent results were shown to overlap with 60% to 90% of the FEMA 100-year inundation maps derived from hydrodynamic inundation models (Zheng et. al., 2018a). Furthermore, Zheng et. al., 2018a recommended using GeoFlood as an approximate inundation mapping method for fluvial flooding in hilly areas over large scales.

---

# Chapter 3: Study Area and Data Sources

## 3.1 Study Area

The state of Texas encompasses a variety of topography ranging from flat bayous and man-made metropolises to hilly drainage basins and rural agricultural land. Of the 254 counties in Texas, the seven shown in Figure 3.1 were chosen for this study. Each county allowed for a unique assessment of GeoFlood performance across diverse terrain and channel characteristics. Qualities of the counties considered in the selection process included minimum and maximum elevations, USGS Multi-Resolution Land Characteristics (MRLC) National Land Cover Database (NLCD) land cover, number of active storm gauges, LiDAR coverage, population, Universal Transverse Mercator UTM zone, and historical flood events. Only counties with complete LiDAR coverage and are fully contained within a single UTM zone were considered for selection.

Jefferson county borders the Gulf of Mexico in southeast Texas. Jefferson is best characterized by flat drainhead complexes near the coast and low relief coastal plains. The county lies within the Coastal Praries physiographic region of Texas. The Neches River forms the northeast boundary, the Pine Island Bayou forms the northern boundary, and Sabine Lake forms the eastern boundary. Waterbodies cover 27.2% of the 4141 $km^2$ Jefferson study area. The population of Jefferson County was 252,273 according to the 2010 US Census (United States Census Bureau, 2020). Four deep-water ports at Beaumont, Port Arthur, Orange, and Sabine Pass serve robust petrochemical and manufacturing industries.

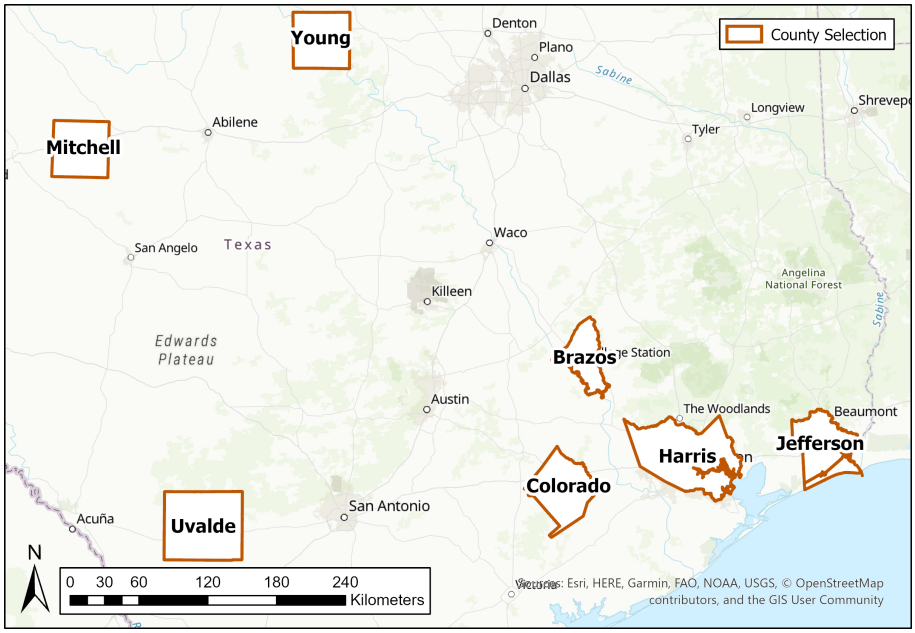


Figure 3.1: Brazos, Colorado, Harris, Jefferson, Mitchell, Uvalde, and Young counties were selected to represent the variety of terrain and channel characteristics in Texas.

Harris county is a densely populated southeast Texas county connected to the Gulf of Mexico via Galveston Bay. Similar to Jefferson county, Harris county is within the Coastal Praries physiographic region of Texas. Harris county is bordered by Spring Creek to the North, Cedar Bayou to the east, and partially by Clear Creek to the South. The Houston metropolitan area encompasses a majority of Harris county. In comparison to the other counties in this study, Harris County has the highest population of 4,092,459 according to the 2010 US Census (United States Census Bureau, 2020). The Harris study area covers 6898 $km^2$ including portions of Galveston Bay. The 2016 NLCD developed area land cover classification represents 15.0% of the Harris study area (Dewitz, 2019). The prominent Harris county features are man-made infrastructure including roadways, conveyance channels, and buildings.

Colorado is a rural county bisected by the Coastal Praries and Interior Coastal Plains physiographic provinces of Texas. Colorado county is bordered by the San Bernard River to the northeast. The Colorado study area covers 4074 $km^2$. Major industries include agriculture, petrochemical services, and gravel mining. Colorado's cropland is intersected by the major thruways of Interstate 10 and U.S Highway 90.

Brazos county is considered "The Heart of Aggieland". Similar to Colorado, Harris, and Jefferson counties, Brazos is within the Gulf Coastal Plains physiographic province of Texas. The Bryan and College Station metropolitan area hosts Texas A&M University. Brazos county is bordered by the Brazos River to the west and the Navasota River to the east. The Brazos study area covers 3020 $km^2$. A low relief area drains the southern end of the Brazos study area. The population of Brazos county was 194,851 according to the 2010 US Census (United States Census Bureau, 2020). The primary 2016 NLCD land cover classification is hay and pasture.

Uvalde county is bisected by the east-west running Balcones Escarpment. The northern Edwards Plateau is comprised of flat upper surfaces and steep-walled canyons. The southern plains are characterized by low, rolling terrain with ephemeral streams. There are distinct differences between the northern and southern terrain features of Uvalde county. The Frio, Nueces, and Sabinal Rivers emerge from the north and run south-southeast towards the Gulf of Mexico. The Uvalde study area covers 5983 $km^2$.

Mitchell county is located in the North Central Plains physiographic province of Texas. The main industries include agriculture, livestock, and oil production. Mitchell County is the least populated county in the study with a population of

9,403 according to the 2010 US Census (United States Census Bureau, 2020). The primary 2016 NLCD land cover classification is shrubland. The man-made reservoirs of Lake Colorado City and Champion Creek Reservoir cover 30 $km^2$ of the 3930 $km^2$ Mitchell study area.

Young county is located in the Grand Prarie physiographic province of Texas. Low relief Young county is best characterized by the 2016 NLCD land cover classification herbaceous. Main industries include oil production, agriculture, and hunting. The connected man-made reservoirs Lake Graham and Lake Eddleman, popular for recreation, cover a combined total of 9.90 $km^2$. The Young study area covers 3892 $km^2$. Young county is bisected by the northwest to southeast flowing Brazos River.

Study area terrain and channel characteristics are summarized in the following box plots to further exemplify the unique qualities of each selected county. Each county was selected to represent a diverse set of distinctive topographic features. Often channel and terrain characteristics are related due to macro-scale physiogeographic trends across the state of Texas.

Figure 3.2 shows the box plots for channel slopes within the selected Texas county study areas. The slope of 0.00001 is the minimum slope defined by the NHDPlus MR database. Figure 3.3 shows the percentage of channels in each county with slopes equal to the minimum 0.00001. Jefferson county has the lowest slope median at 0.00001 and lowest interquartile range (IQR) at 0.0002768. The low relief characteristics of Jefferson County are supported by the low slope median and IQR. Uvalde county has the highest slope median at 0.004893 and highest IQR at 0.007909. The high slope median and IQR in Uvalde county is due to the topographical transition from the flat upper surfaces to low rolling terrain through

the steep canyons of the Balcones Escarpment.

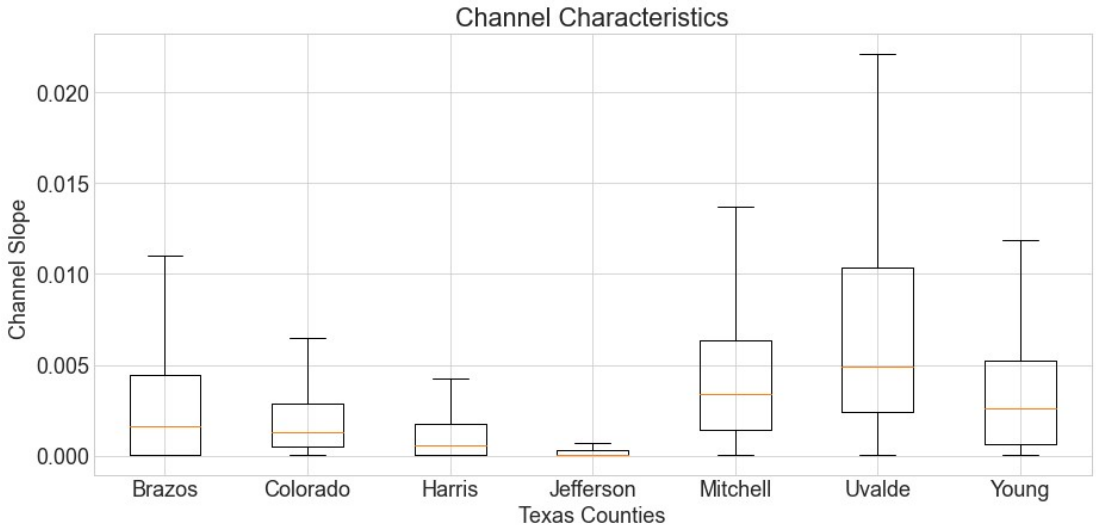


Figure 3.2: Channel slopes box plot for each selected Texas county. Reach slopes are defined by the Medium Resolution National Hydrography Datasets (Fagan, 2015a; Fagan, 2015b).

Figure 3.4 shows the box plots for Strahler stream order. Brazos, Harris, and Young county share a stream order median of one. Brazos, Harris, and Young county contain one or more major, sinuous rivers. Colorado county has an IQR spanning the entire stream order range. The high IQR indicates that Colorado county contains a wide distribution of channel characteristics including channels that originate within the county as well as major rivers that run through.

Figure 3.5 shows the box plots for the geodesic distances from the NHD catchment centroids to the Gulf of Mexico coastline to quantify the distance from each study area to the coast. Figure 3.6 shows that channel slope increases with increasing distance from the Gulf of Mexico, with the exception of Uvalde county due to its unique topography along the Balcones Escarpment.

The mean annual flow box plots for the selected Texas counties are shown in

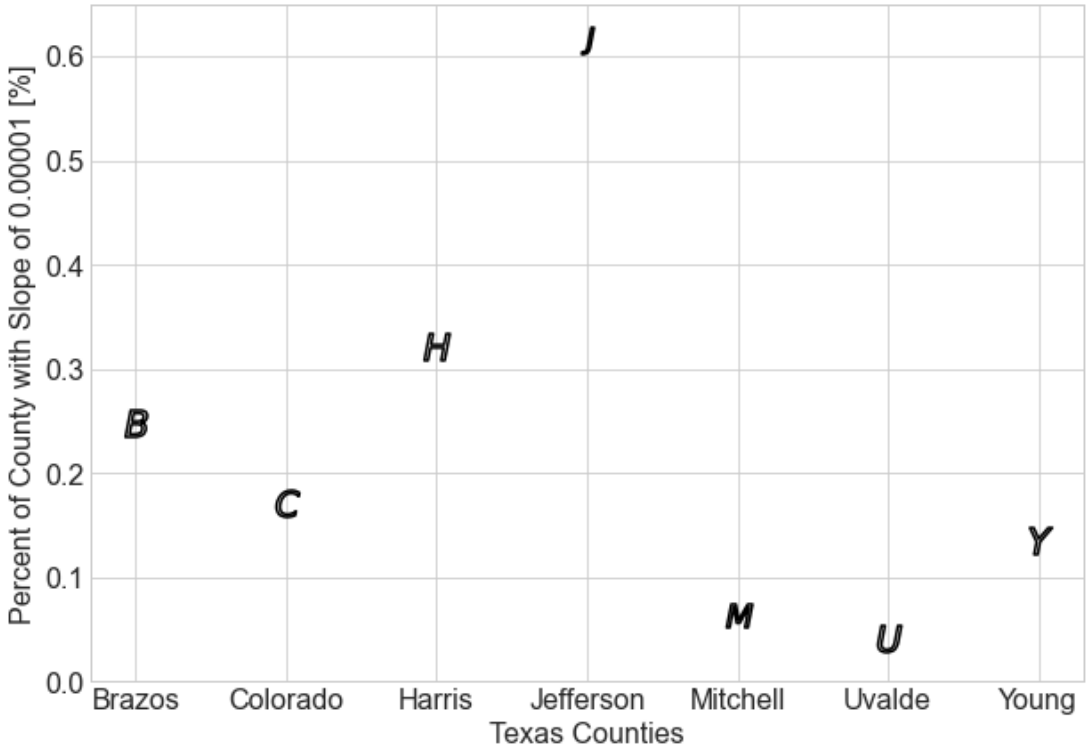


Figure 3.3: Percent of each county with a channel slope of 0.00001. Reach slopes are defined by the Medium Resolution National Hydrography Datasets (Fagan, 2015a; Fagan, 2015b).

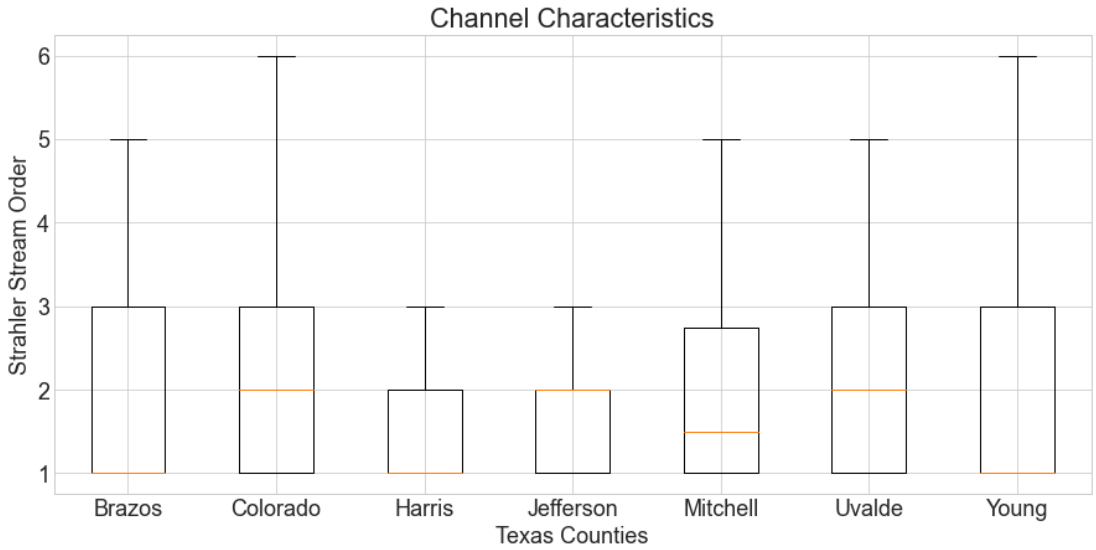


Figure 3.4: Strahler stream order box plot for each selected Texas county. Stream orders are defined by the Medium Resolution National Hydrography Datasets (Fagan, 2015a; Fagan, 2015b).

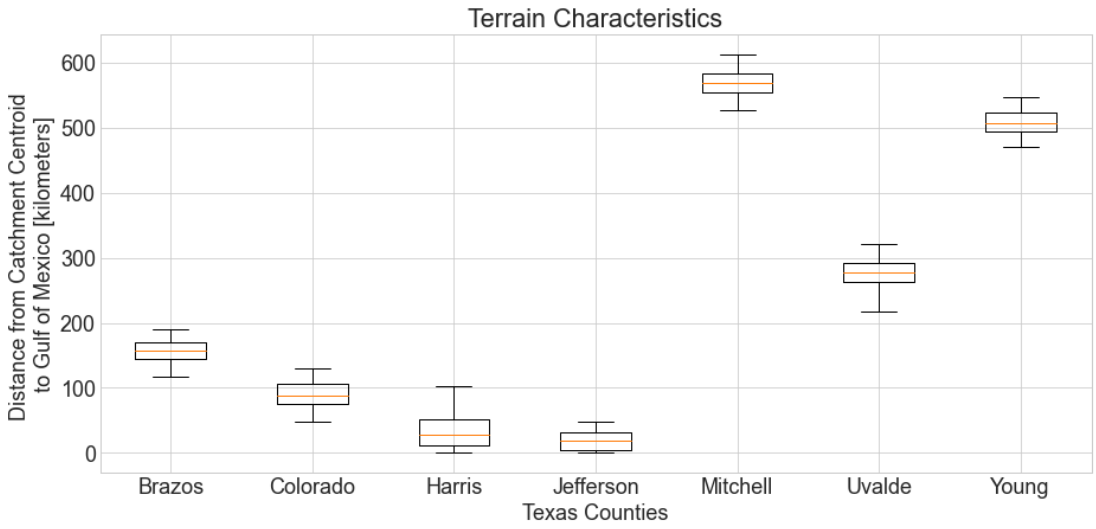


Figure 3.5: Distance from NHD catchment to the Gulf of Mexico box plot for each selected Texas county. Distances were computed using the ArcGIS Pro "Near" Spatial Analyst tool. The computation measures the geodesic distance between the centroid of a NHD catchment polygon to the nearest vertice of the Gulf of Mexico coastline polyline.

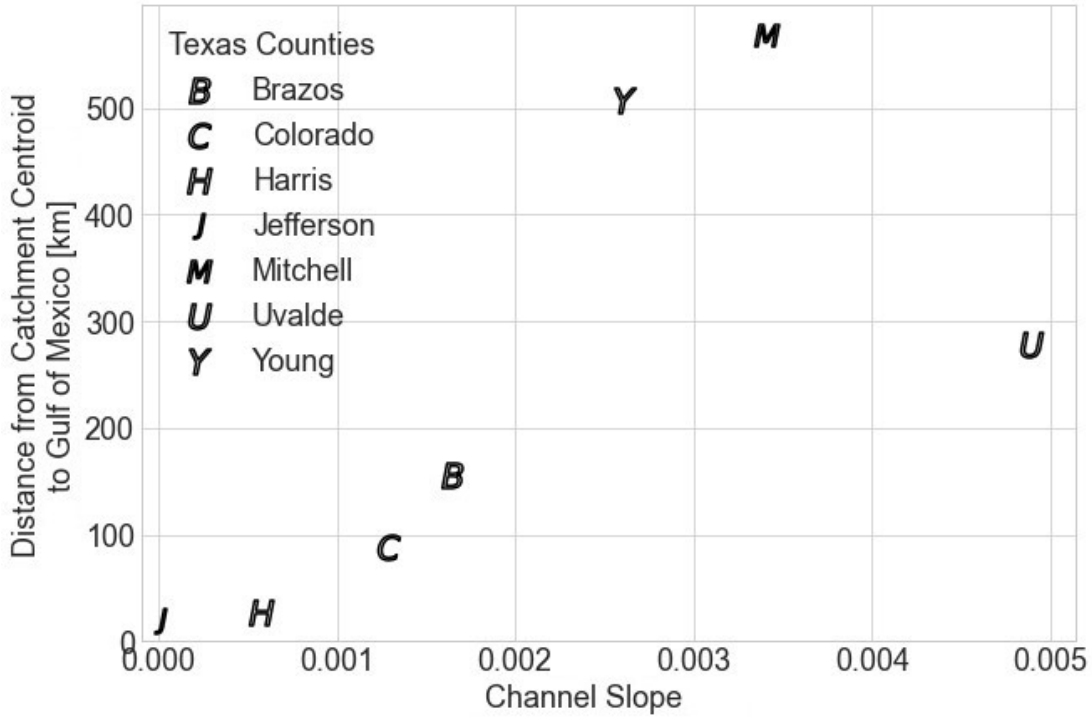


Figure 3.6: Median distance from NHD catchment centroid to the Gulf of Mexico versus median NHDPlus MR reach slope.

Figure 3.7. Jefferson county has the highest mean annual flow median at 17.5 $m^3/s$ as well as the highest IQR at 96.1 $m^3/s$. The mean and maximum of mean annual flows in the Jefferson county study area is 534 $m^3/s$ and 11,504 $m^3/s$, respectively.

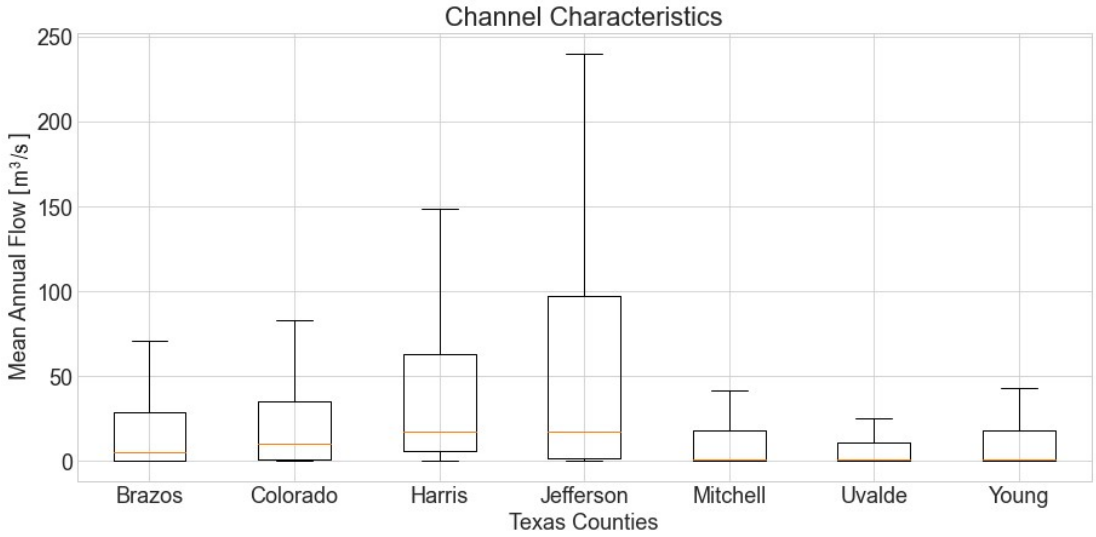


Figure 3.7: Mean annual flow in $m^3/s$ for each selected Texas county. Mean annual flows are defined by the National Hydrography Datasets Medium Resolution (Fagan, 2015a; Fagan, 2015b).

Catchment areas are the spatial scope for the computed statistics in this study. The NHD catchment area box plots for each selected Texas county are shown in Figure 3.8. The smallest median catchment area of 1.11 $km^2$ is attributed to Jefferson county. Jefferson county was expected to have smaller catchments areas because low relief regions tend to produce a dense, complex network of drainage basins especially where waterbodies and below average mean sea level (AMSL) elevations exist. Mitchell county has the largest median catchment area at 8.39 $km^2$ and largest IQR at 17.1 $km^2$. Mitchell county's catchment features are larger relative to the other counties due to its low population, lack of man-made features, and lesser stream network density. Artificial landscape features,

like roads and levees, tend to divide drainage areas into smaller regions. The size of the NHD catchment areas is inversely related to the stream network density.

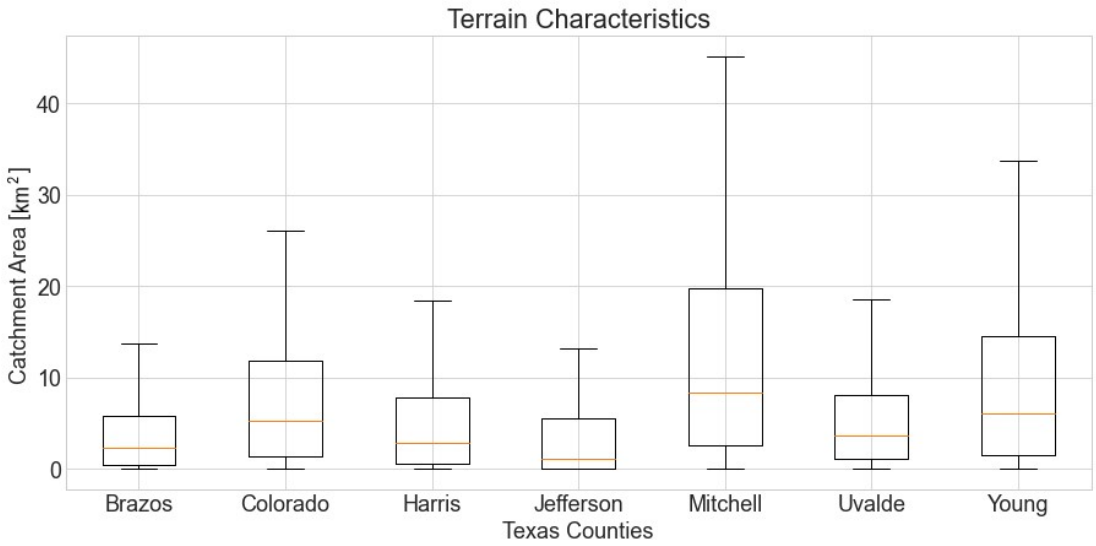


Figure 3.8: NHD catchment areas in km$^2$ for each selected Texas county. Catchment areas are defined by counting the number of 1-meter resolution pixels within the NHD catchment polygons.

### 3.2 Digital Elevation Model

The 1-meter and 10-meter Digital Elevation Models (DEM) were developed from USGS The National Map (TNM) and Texas Natural Resource Information System (TNRIS) resources. After specifying the boundary of analysis within the TNM interactive viewer, 1-meter and 10-meter resolution 3D Elevation Products (3DEP) were downloaded using TNM's Download Manager uGET. Additionally, TNRIS Strategic Mapping Program (StratMap) LiDAR datasets were downloaded from the Texas Advanced Computing Center (TACC). The TNRIS LiDAR Coverage Map was used to identify the required LiDAR tiles that fully cover each study area when combined.

### 3.3 National Hydrography Dataset

The USGS National Hydrography Dataset (NHD) is a collection of geospatial datasets representing surface water and hydrologic unit mapping across the United States. Three main NHD products are analyzed in this study including the Watershed Boundary Dataset (WBD), NHDPlus Medium Resolution (MR), and NHDPlus High Resolution (HR). The NHD WBD is a national hydrologic unit dataset representing regions of terrain that drain to segments of the stream network (United States Geological Survey, 2020). The NHDPlus MR geospatial datasets were mapped at a scale of 1:100,000 for the conterminous US (United States Geological Survey, 2020). The NHDPlus HR geospatial datasets were mapped at a scale of 1:24,000 or better (United States Geological Survey, 2020). The USGS NHDPlus geospatial datasets integrate the NHD vector stream network and WBD hydrologic unit boundaries with the USGS National Elevation Dataset NED gridded land surface. The hydrologically-conditioned surface enables the delineation of catchments for each NHD stream segment. A catchment on this scale is defined as the local drainage area for each stream segment. The NHDPlus vector stream network provides value-added attributes such as reach slope and Strahler stream order. Parameters such as stream flow can be estimated by associating precipitation, temperature, and runoff with the NHDPlus catchments.

NHDPlus MR geospatial datasets were downloaded from the National Flood Interoperability Experiment (NFIE) HydroShare repository (Fagan, 2015a; Fagan, 2015b). Brazos, Colorado, Harris, Jefferson, Mitchell, and Uvalde counties were entirely contained by the "NFIE-Geo Texas Gulf-Region" dataset (Fagan, 2015a). Young county included data from "NFIE-Geo Texas-Gulf Region" and "NFIE-Geo

Mississippi Region" (Fagan, 2015a; Fagan, 2015b). NHDPlus MR subwatershed, catchment, and flowline feature layers were used in this study.

### 3.4 National Water Model Forecasts

The National Water Model (NWM) is a hydraulic modelling framework that simulates observed and forecast streamflows for 2.7 million stream reaches across the continental United States (Office of Water Prediction, 2020). The NWM Standard Analysis and Assimilation streamflows used for this study are generated from self-cycling 3-hour look-back simulations. Each NWM Standard Analysis and Assimilation streamflow is associated with a corresponding NHDPlus MR stream segment.

The NWM streamflows in this study were determined by sampling the maximum streamflow for each stream segment between August 18, 2017 and September 4, 2017. The purpose was to simulate a "worst case scenario" for fluvial flooding during the 2017 Hurricane Harvey event. The NWM Standard Analysis and Assimilation archived outputs were downloaded from a Hurricane Harvey HydroShare repository (National Water Center, 2020).

### 3.5 Federal Emergency Management Agency Harvey Flood Depths Grid

The Federal Emergency Management Agency (FEMA) Harvey Flood Depths Grid is a 3-meter horizontal resolution dataset of gridded depth. The FEMA Harvey Flood Depths Grid was originally published on Novermber 15, 2017 as an Environmental Systems Research Institute (ESRI) ArcGIS geodatabase. The FEMA

3-meter inundation depth and extent maps utilized a Triangulated Irregular Network (TIN) interpolation informed by USGS Hurricane Harvey High Water Marks and observed water levels at stream gauges interpolated along rivers. The TIN included four quality assurance measures including identifying; dips, spikes, duplication, and inaccurate/unrealistic measurements. Inundation extents were validated with remote sensing. Elevation data was generated by mosaicking 3-meter resampled elevations from 1-meter and 3-meter LiDAR and Interferometric Synthetic Aperture Radar (IfSAR) data. The FEMA Harvey Flood Depths Grid is shown in Figure 3.9 with Colorado, Harris, and Jefferson county boundaries.

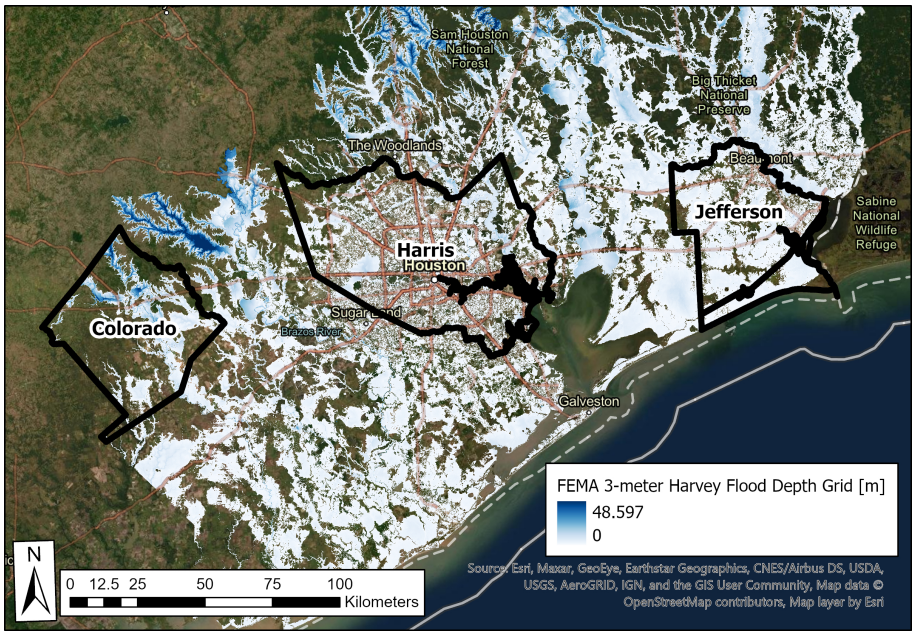


Figure 3.9: FEMA Harvey Flood Depths Grid is used to quantify the performance of the 1-meter GeoFlood and 10-meter HAND inundation maps. The black solid polygons indicate the boundaries of Colorado, Harris, and Jefferson counties.

The FEMA 3-meter Harvey Flood Depths Grid was used as an extent and depth reference to compare the 1-meter and 10-meter inundation simulations. The Federal Emergency Management Agency FEMA Harvey Flood Depths Grid was

downloaded from a Hurricane Harvey HydroShare repository (Federal Emergency Management Administration, 2020a).

### 3.6 United States Geological Survey Hurricane Harvey High Water Marks

During and after Hurricane Harvey, the USGS surveyed 2123 High Water Marks (HWMs) among 1258 sites in southeast Texas (Watson et. al., 2018). HWMs are physical demarcations of the peak flood water level and are used to make informed analysis of flood events (Koenig et. al., 2016). Evidence of these inundation depths may include vegetation and seed lines, debris and mud deposits, and stain lines on building walls. HWMs provide valuable information for flood frequency analysis studies, damage assessment reports, and inundation mapping models (Watson et. al., 2018).

Of the 2123 USGS HWMs collected, 310 selected USGS HWMs intersected the study area. Of the selected USGS HWMs, 220 lie within the Harris County study area and 90 lie within the Jefferson County study area. The selection criteria includes three main components. First, the spatial references must be North American Datum of 1983 (NAD83) and North American Vertical Datum of 1988 (NAVD88). Second, the USGS HWMs must have one of the following quality codes; excellent (+/- 0.05 feet), good (+/- 0.10 feet), or fair (+/- 0.20 feet). Of the selected USGS HWMs, 111 were excellent quality, 109 were good quality, and 90 were fair quality. USGS HWMs with the quality codes; poor (+/- 0.40 feet), very poor ($>$ 0.40 feet), or unknown/historical were excluded from the analysis. Third, the surveyed height above ground for each selected USGS HWM must not be zero or blank. The USGS HWMs were used to evaluate the GeoFlood inunda-

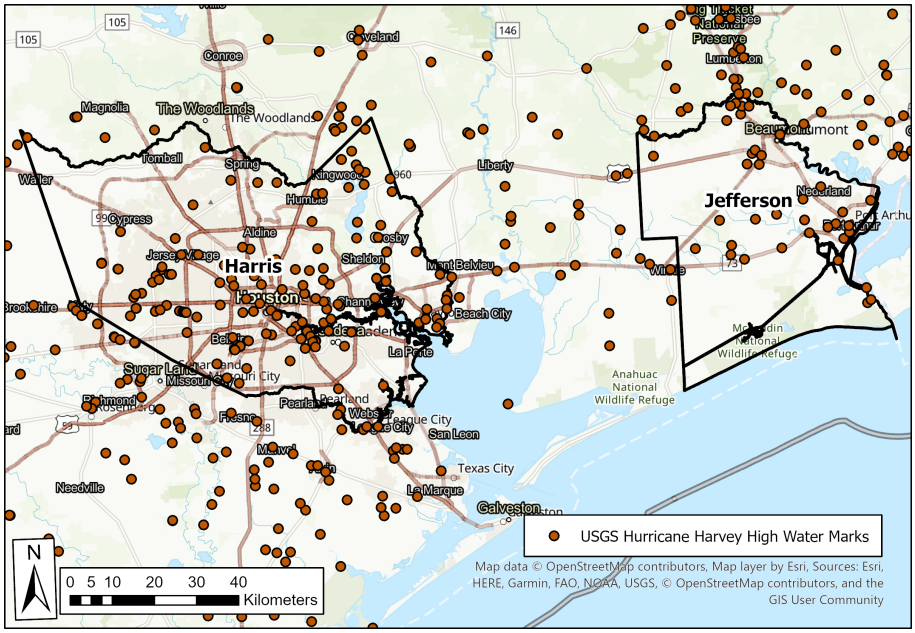


Figure 3.10: Selected USGS Hurricane Harvey High Water Marks. The USGS Hurricane Harvey High Water Marks are used to quantify the depth performance of the 1-meter GeoFlood and 10-meter HAND inundation mapping simulations. The black solid boundaries indicate the extents of Harris and Jefferson counties.

tion depths. Therefore, USGS HWMs with a height above ground equal to zero, thus indicating a flood extent boundary, were removed from the USGS HWM selection for this study.

---

# Chapter 4: Methodology

## 4.1 DEM Processing and Mosaicking

The GeoFlood and HAND processes can be applied to a variety of geospatial scales including catchments, drainage basins, NOAA Hydrologic Unit Codes (HUCs), political boundaries, or simply user-defined regions of interest. Both workflows work best in study areas defined by scaled watershed boundaries since hydraulic geometries are derived from drainage areas. Since NOAA analysis are frequently performed on the HUC12 geospatial scale, we conducted our analysis on the same scale in order to preserve continuity across projects. The processing and mosaicking of the workflow input data are detailed in the following steps:

(i) HUC12s are defined as hydrologic units with 12 digits from the National Hydrography Dataset NHD databases. All HUC12s that intersect or were fully contained within a county were selected for processing. The Texas County Boundaries dataset was retrieved from the Texas Department of Transportation (TxDOT) Transportation Planning and Programming (TPP) Open Data Portal (Texas Department of Transportation, 2019).

(ii) A "select by location" process was used to determine the flowline selection for each HUC12. NHDPlus MR flowlines were selected if their geometric centroids were within their respective HUC12.

(iii) The selected HUC12s for each county were then dissolved into a single shapefile. For situations where the selected NHDPlus MR flowlines extended beyond the boundaries of the dissolved HUC12 shape, individual catchments were

appended to the dissolved shape. The appended catchments were appended on a case-by-case basis depending on whether the catchment could fully contain the extended NHDPlus MR flowlines. The appended catchments were dissolved into the HUC12 shapefile.

(iv) The previously defined individual HUC12 geometric boundary shapes were then buffered by 500 meters. A 500 meter geodesic buffer allowed the spatial computations to have an extent of overlap between the HUC12 scale of analysis. Inundation maps computed with non-buffered or less than 500 meter buffered HUC12s showed erroneous extent and depth at the boundaries (Carruthers, 2020). Inundation maps computed for HUC12s with buffers greater than 500 meters showed little extent and depth improvement at the cost of increased computational time and HUC12 file size (Carruthers, 2020).

(v) The LiDAR panels were selected by spatial union with the buffered HUC12 shapefile. LiDAR panels were prioritized by most recent collection date. The selected LiDAR panel names were stored in a .csv file. TACC's database of LiDAR panels for Texas, the USGS The National Map's (TNM) 3D Elevation Program (3DEP), and the Texas Natural Resources Information System (TNRIS) StratMap were queried to extract the selected DEM datasets (The National Map 3D Elevation Program, 2020; Texas Natural Resources Information System, 2020).

(vi) The selected LiDAR panels for each HUC12 were then mosaicked into a continuous DEM raster. The mosaicked DEM was clipped to the associated buffered HUC12 shapefile. LiDAR panels were first mosaicked by individual flight mission, then different flight missions were mosaicked together to cover the HUC12 where applicable. The most recent flight mission was chosen where LiDAR panel overlap occurred.

Figure 4.1 shows the 1-meter high-resolution terrain for HUC 120200070201. This 146 km$^2$ HUC12 is located in northwest Jefferson county. The sinuous, low relief Pine Island Bayou runs from west to east through the upper portion of the HUC12. Smaller streams originating from the bottom portion of the HUC12 flow toward the northeast to join the Pine Island Bayou. The NHDPlus MR catchment boundaries represent the drainage areas for each NHDPlus MR flowline. The 1.9 gigabyte DEM extends 500 meters beyond the extent of the HUC12 boundary as seen in Figure 4.1.

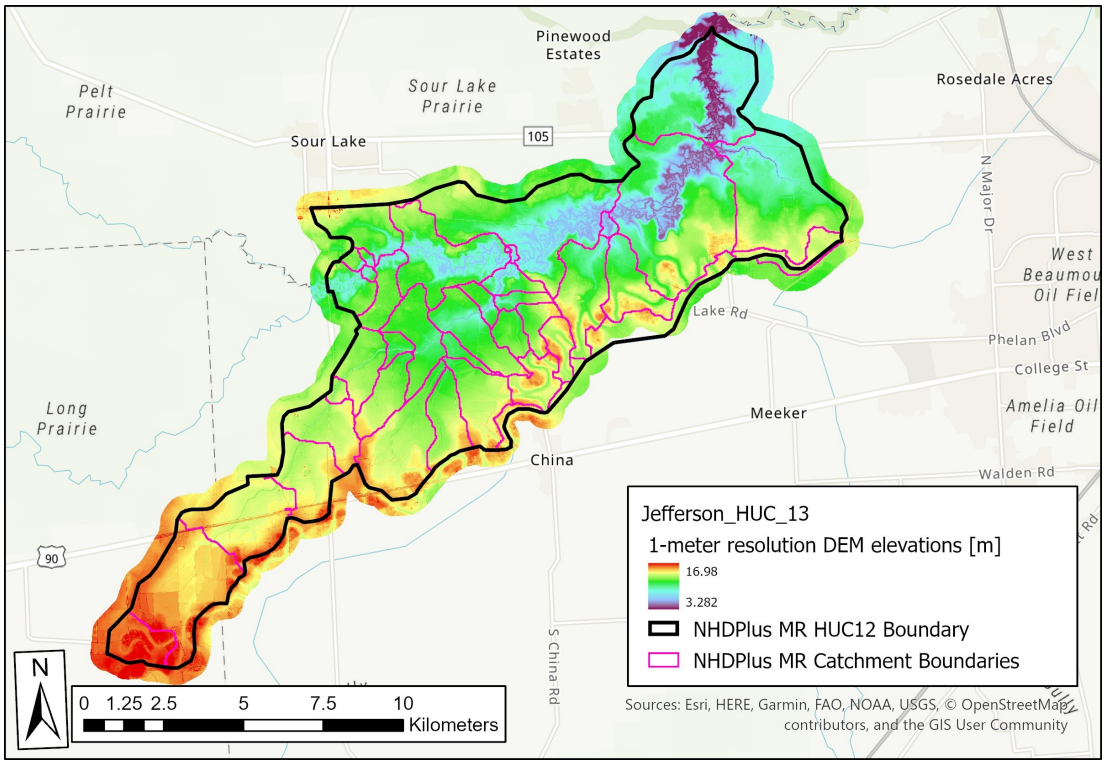


Figure 4.1: 1-meter resolution DEM for HUC 120200070201 located in northwest Jefferson county. The black solid boundary represents the extent of the NHDPlus MR HUC12. The magenta solid boundary represents the extents for each NHDPlus MR catchment. Jefferson_HUC_13 references the HUC12 numbering scheme developed for the data management portion of the project.

## 4.2 Channel Network Extraction

GeoNet, part of the GeoFlood workflow, extracts the channel networks from high-resolution terrain through the following operations: (i) nonlinear filtering smooths the high-resolution terrain, (ii) slope, curvature, watershed delineation, flow accumulation, and flow directions rasters are generated and used for channel feature identification, (iii) a least-cost path is determined for channel network identification.

First, an anisotropic diffusion filter is applied to the high-resolution terrain. GeoNet implements the Perona-Malik nonlinear filter defined as:

$$\frac{\partial h(x,y,t)}{\partial t} = \nabla \cdot [c(x,y,t)\nabla h] \tag{4.1}$$

where t is the iteration time step and c is the diffusion coefficient. The diffusion coefficient can be represented as:

$$c = \frac{1}{1 + \left(\frac{|\nabla h|}{\lambda}\right)^2} \tag{4.2}$$

where $|\nabla h|$ is the absolute value of the elevation gradient at location (x,y) and $\lambda$ is the smoothing quantile of the gradient distribution (Perona and Malik, 1990).

The nonlinear filter removes noise and enhances topographic features that are critical to channel network extraction (Passalacqua et. al., 2010; Perona and Malik, 1990). Three adjustable Perona-Malik nonlinear filter parameters are defined and are discussed below.

The diffusion coefficient allows for preferential DEM smoothing as a function

of gradients. Feature boundaries of interest in channel network definition are likely to have high gradients. Therefore, smoothing should be applied within feature boundaries and penalized across feature boundaries in order to preserve exact feature boundary locations. The smoothing quantile ($\lambda$), or edge stopping threshold, defines the range of slope gradients the Perona-Malik nonlinear filter evaluates and smooths. The smoothing quantile parameter is computed as the 90th quantile of the curvature gradient distribution (Perona and Malik, 1990).

The iteration parameter controls the number of times the Perona-Malik nonlinear filter is applied to a defined range of slope gradients. Increasing the number of iterations may cause excessive smoothing of the DEM and unnecessary computational cost. Decreasing the number of iterations may retain excessive noise in the DEM and cause difficulties in detecting features of interest. Each DEM in the study area is filtered with 50 iterations as recommended by Sangireddy et. al. (2016).

Two definitions of curvature are used within GeoNet. The Laplacian curvature $\gamma$ is computed as the second derivative of the elevation gradient $\nabla$h.

$$\gamma = \nabla^2 h \tag{4.3}$$

The Laplacian curvature method is best suited for engineered terrain with man-made features such as ditches and roads (Passalacqua et. al., 2012). The geometric curvature $\kappa$ normalizes the elevation gradient by its magnitude.

$$\kappa = \nabla \cdot (\nabla h / |\nabla h|) \tag{4.4}$$

The geometric curvature method is effective for identifying features in nat-

ural terrain (Passalacqua et. al., 2012). The geometric curvature calculation method was selected due its ability to capture subtle feature boundaries.

Second, the smoothed DEM was used to generate slope and curvature rasters. The software GRASS GIS 7.8 utilizes the slope and curvature rasters to determine the drainage basins, flow accumulation, flow direction, and drainage outlets (GRASS GIS 7.8, 2021). The GeoNet workflow uses the curvature and flow accumulation rasters to define likely channelized pixels as a binary skeleton raster. The likelihood of a channel being defined in the binary skeleton raster is a combination of positive curvature and contributing flow area. The flow threshold parameter defines the regions where flow accumulation is appreciable. The flow threshold acts as a thinning parameter to exclude small areas in the binary skeleton raster. The flow threshold was set to 500 for all study areas. Please refer to GRASS GIS 7.8 (2021) software documentation, Sangireddy et. al. et. al. (2016), and Passalacqua et. al. et. al. (2010) for specific information regarding the generation of the intermediary rasters noted above.

Lastly, the channel network is determined using geodesic minimization principles (Passalacqua et. al., 2010). The pixels corresponding to the first and last vertices of the NHDPlus MR flowline geometry attribute are taken as the start and end points. The cost function $\psi$ connects the start and end points through geodesic curves. The cost function assigns a cost for each pixel in the DEM. The cost function penalizes paths where the drainage area does not have substantial flow accumulation and curvature is not sufficient compared to the surrounding points. The purpose of the cost function and geodesic least-cost principles is to delineate the natural channel thalweg while crossing man-made boundaries such as roads, culverts, and bridges.

The first cost function, called the *General Cost Function* for this study, utilizes three main parameters and a cost threshold:

$$\psi = \frac{1}{\alpha A + \delta\kappa + 0.75 * NegativeHand} \begin{cases} \psi = \psi \ for \ \psi \ \leq \ \psi^{-1}(p) \\ \psi = 100,000 \ for \ \psi \ > \ \psi^{-1}(p) \end{cases} \tag{4.5}$$

where $\kappa$ is the normalized curvature, A is the normalized flow accumulation and contributing area, and both $\alpha$ and $\delta$ are weighting coefficients used to solve the dimensionality of $\psi$ and adjust the magnitude between $\kappa$ and A. The parameter $\psi^{-1}(p)$ represents the quantile threshold for cost.

The *NegativeHand* binary raster is a function of the elevation difference between the NHDPlus MR flowlines and neighboring pixels. A pixel in the *NegativeHand* binary raster is assigned a one if the neighboring pixels to the NHDPlus MR flowline are lower or equal in elevation (Zheng et. al., 2018a). The *NegativeHand* binary raster was added to the cost function in order to improve the channel network extraction near roads, culverts, and bridges (Zheng et. al., 2018a). The *NegativeHand* component of the cost function receives a 0.75 multiplier in order to balance its impact relative to the other parameters in the expression.

The quantile threshold for cost greatly improved network extraction in sinuous, meandering channels within low relief terrain. Cost functions without the quantile threshold allowed the geodesic least-cost path to cross roads, culverts, and bridges as well as sinuous, meandering bends in flat terrain. The quantile threshold increases the penalty for natural channel bend short-cutting while retaining a low penalty for the crossing of man-made features (Carruthers, 2020).

The result of the *General Cost Function* extracted channel network as compared to the NHDPlus MR flowlines are shown in Figure 4.2. Deviations between the GeoNet extracted channel network and NHDPlus MR flowlines occur more frequently in low relief, sinuous, and braided channel networks. The deviations between the GeoNet extracted channel network and NHDPlus MR flowlines occur within the floodplain of the low slope Pine Island Bayou as shown in Figure 4.2. With the exception of one localized area, the GeoNet extracted channel network and NHDPlus MR flowlines are well correlated across the higher relief topography outside the flat Pine Island Bayou floodplain where detailed feature information is available.

The second cost function, called the *Specialized Cost Function* for this study, was implemented on a case-by-case basis. The *Specialized Cost Function* included the binary raster *HRarray*:

$$\psi = \frac{1}{\alpha A + \delta\kappa + 0.75 * NegativeHand + HRarray} \begin{cases} \psi = \psi \ for \ \psi \ \leq \ \psi^{-1}(p) \\ \psi = 100,000 \ for \ \psi \ > \ \psi^{-1}(p) \end{cases} \tag{4.6}$$

The *Specialized Cost Function* enhancement was needed in exceptionally flat areas where elevation differences were within the error tolerance of the vertical resolution. The *HRarray* was created by converting the NHDPlus HR flowlines into a binary skeleton raster. Pixels in the *HRarray* that intersect the NHDPlus HR flowline geometries were assigned a one and zero elsewhere. The cost function raster and GeoNet outputs are used in the following processes to derive the Height Above Nearest Drainage (HAND) raster.

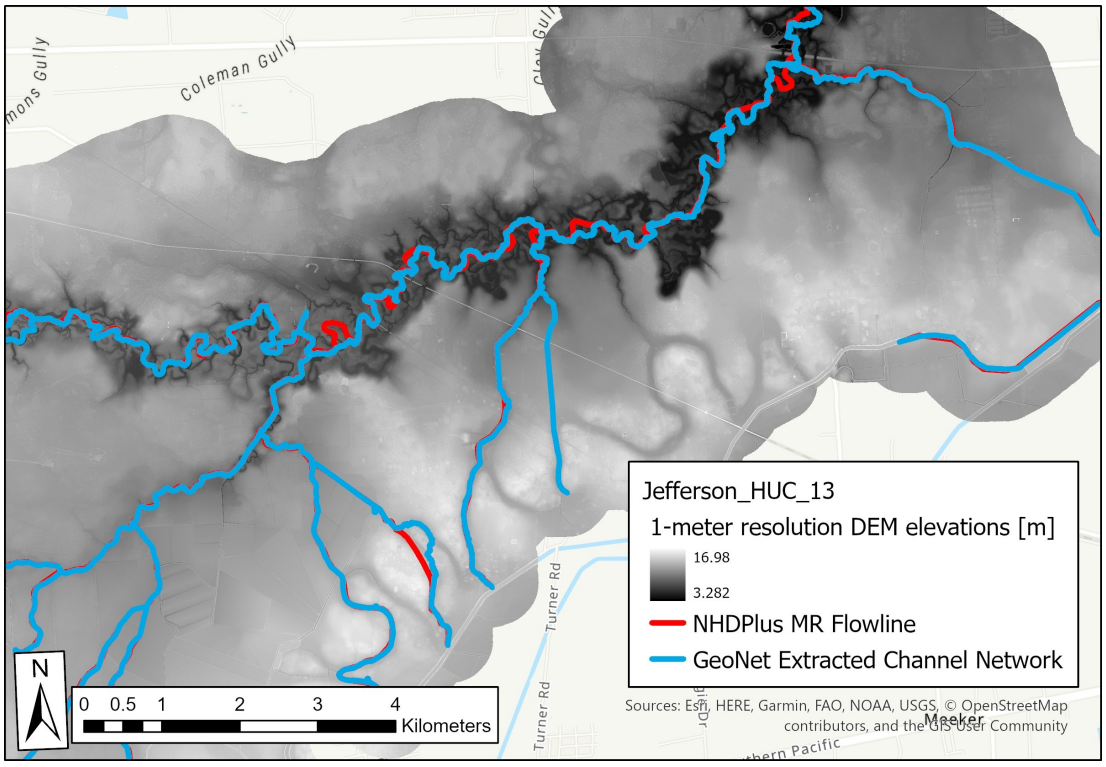


Figure 4.2: The blue solid lines are the GeoNet extracted channel network derived from the HUC 120200070201 1-meter resolution terrain. The red solid lines are the NHDPlus MR flowlines. The 1-meter DEM terrain emphasizes the deviations and correlations between the GeoNet extracted channel network and NHDPlus MR flowlines.

### 4.3 Channel Hydraulic Properties

Channel hydraulic properties are estimated using the outputs of the GeoNet workflow. The GeoFlood workflow, including functions from the Terrain Analysis Using Digital Elevation Models (TauDEM), produces the channel hydraulic properties. TauDEM is a suite of DEM tools for the extraction and analysis of hydrologic information from topography (Tarboton, 1997). The TauDEM operations included in the GeoFlood workflow are:

(1) Pits in the raw DEM are filled using the TauDEM tool called *PitRemove*. Pits, also known as depressions or sinks, are low relief areas contained within a DEM that are completely surrounded by higher relief terrain on all edges. DEM flow routing algorithms are not computationally efficient when computing within pits because drainage directions are limited or nonexistent. *PitRemove* identifies pits in the DEM and raises their elevation to the level of the lowest pour point around their edge (Tarboton, 2015).

(2) Flow directions are computed across the pit-filled DEM using the D-infinity flow directions (*Dinf*) tool. Flow directions are assigned based on the steepest downward slope of a planar triangular facet on a block-centered grid (Tarboton, 1997). The flow direction is represented as an angle in radians between zero and two times pi.

(3) The extracted channel geometries are segmented into lengths of 1000 meters (Godbout et. al., 2019). Longer channel segments may lead to inaccurate hydraulic geometry generalizations. Shorter channel segments may increase the likelihood of hydraulic geometry and slope calculation issues. Elevation differences within the vertical error tolerance of the DEM are more likely with shorter channel

segments.

(4) The Height Above Nearest Drainage (HAND) raster is computed using the pit-filled DEM, D-infinity flow directions rasters, and a *path* binary raster representing the GeoNet extracted channel network. The *path* binary raster assigns a value of one to pixels intersecting the GeoNet extracted channel network and zero elsewhere. The GeoNet extracted channel network serves as the nearest drainage path. The HAND method estimates the vertical height of any pixel in the DEM relative to the nearest drainage path. The HAND raster for HUC 120200070201 is shown in Figure 4.3 as an example.

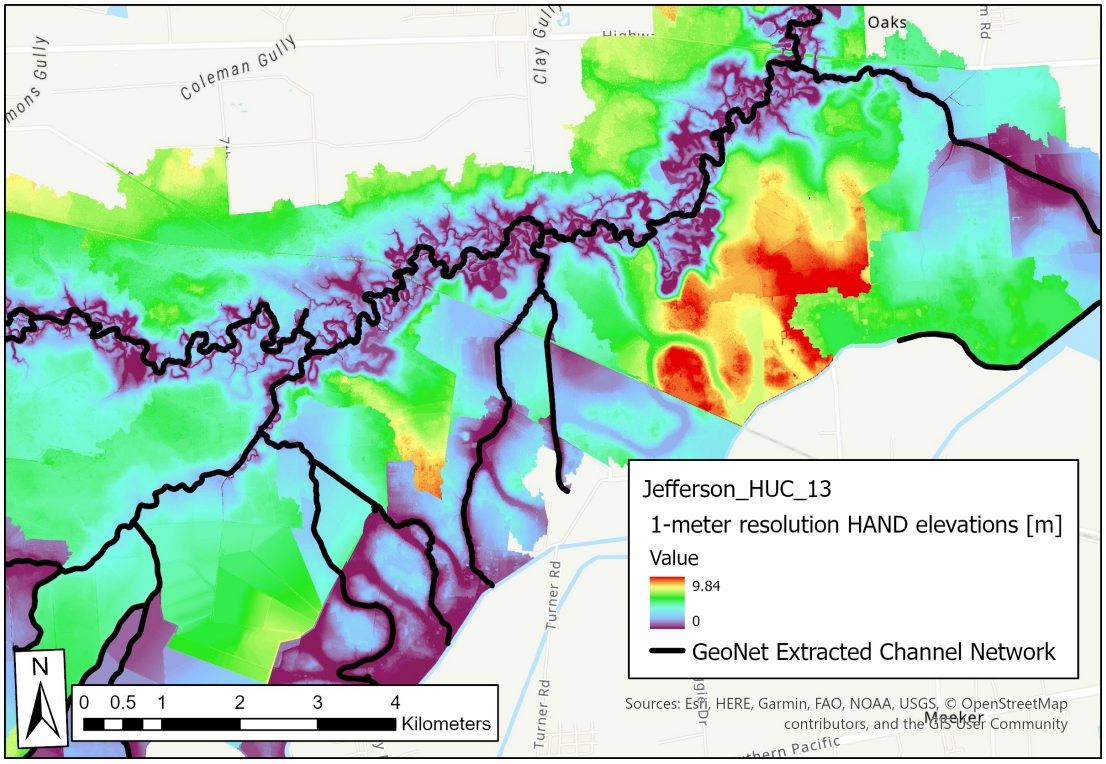


Figure 4.3: 1-meter resolution Height Above Nearest Drainage HAND raster for HUC 120200070201 in northwest Jefferson county. The black solid lines represents the GeoNet extracted channel network derived from 1-meter resolution terrain. The HAND values are determined using the segmented GeoNet extracted channel network as the nearest drainage path.

(5) The channel hydraulic properties can be determined from the HAND raster by calculating the water surface area, channel bed area, and inundation volume of the inundated zone at stage heights from 0 meters to 20 meters in increments of 0.1 meters. Details regarding the following estimation of channel hydraulic properties can be found in Zheng et. al. (2018b).

(i) A uniform reach-average water level $y$ is applied to each river reach along the channel network segment. An inundation depth raster can be computed across the inundated area $I(y)$ within the local catchment draining to the channel network segment:

$$d_{pixel}(y) = \begin{cases} y - HAND_{pixel} & if\ HAND_{pixel} \leq y\ (inundated,\ pixel \in I(y)) \\ 0 & if\ HAND_{pixel} > y\ (not\ inundated,\ pixel \notin I(y)) \end{cases} \tag{4.7}$$

where the water depth at any pixel $d_{pixel}(y)$ is the difference between the reach-averaged water level $y$ and the $HAND_{pixel}$.

(ii) The water surface area of the inundated area at a water depth of $y$, $A_{surface}(y)$, can be computed as:

$$A_{surface}(y) = \sum_{pixel\ \in\ I(y)} A_{pixel} \tag{4.8}$$

where $A_{pixel}$ is the area of the pixel.

(iii) The channel bed area of the inundated area at a water depth of $y$,

$A_{channel\ bed}(y)$, can be computed as:

$$A_{channel\ bed}(y) = \sum_{pixel\ \in\ I(y)} A_{pixel}\sqrt{(1 + (S_{pixel})^2)} \tag{4.9}$$

where $S_{pixel}$ is the inverse tangent of the slope angle.

(iv) The inundation volume of the inundated zone $V(y)$ at a water depth of $y$ can be computed as:

$$V_{inundation}(y) = \sum_{pixel\ \in\ I(y)} A_{pixel} d(y)_{pixel} \tag{4.10}$$

(v) The reach-average channel width at a water depth of $y$, $W(y)$, can be computed as:

$$W(y) = A_{surface}(y)/L \tag{4.11}$$

(vi) The reach-average cross-sectional area $A_{cross-section}(y)$ can computed as:

$$A_{cross-section}(y) = V_{inundation}(y)/L \tag{4.12}$$

(vii) The reach-average cross-sectional wetted perimeter $P(y)$ can be computed as:

$$P(y) = A_{channel\ bed}(y)/L \tag{4.13}$$

(viii) The reach-average cross-sectional hydraulic radius $R(y)$ can be com-

puted as:

$$R(y) = A_{cross-section}(y)/P(y) \tag{4.14}$$

The determined channel hydraulic properties can then be used to derive inundation and extent maps with a known discharge.

## 4.4 Inundation Extent and Depth Maps

The Manning's equation can be applied to relate a discharge $Q(y)$ to a corresponding water depth of $y$ at uniform flow. The Manning's equation in metric units is written as:

$$Q(y) = \left(\frac{1.00}{n}\right) A_{cross-section}(y) R(y)^{\frac{2}{3}} (S_{channel\ bed})^{\frac{1}{2}} \tag{4.15}$$

where $n$ is the Manning's roughness coefficient, $A_{cross-section}(y)$ is the reach-average cross-sectional area, $R(y)$ is the reach-average cross-sectional hydraulic radius, and $S_{channel\ bed}$ is the slope of the channel network segment. A synthetic rating curve can be calculated by computing discharge $Q(y)$ along incremental stage heights. Additionally, water depths can be computed as a function of discharge $y(Q)$. For this analysis, the National Water Model NWM forecasted discharges and HAND methods are used to generate inundation maps for seven Texas counties. The discharges used in this study are the maximum NWM streamflows sampled throughout the 2017 Hurricane Harvey event.

The 1-meter GeoFlood inundation depth map for HUC 120200070201 in northwest Jefferson county is shown in Figure 4.4. Depths are greatest within the channel and normally dissipate as a function of distance from the channel

centerline. In general, lower flowrates are associated with channels that originate within the HUC12. Higher flowrates, such as those assigned to Pine Island Bayou, are attributed to larger rivers that flow into and out of the HUC12 boundaries. Therefore, larger inundation depths are correlated with higher flowrates.

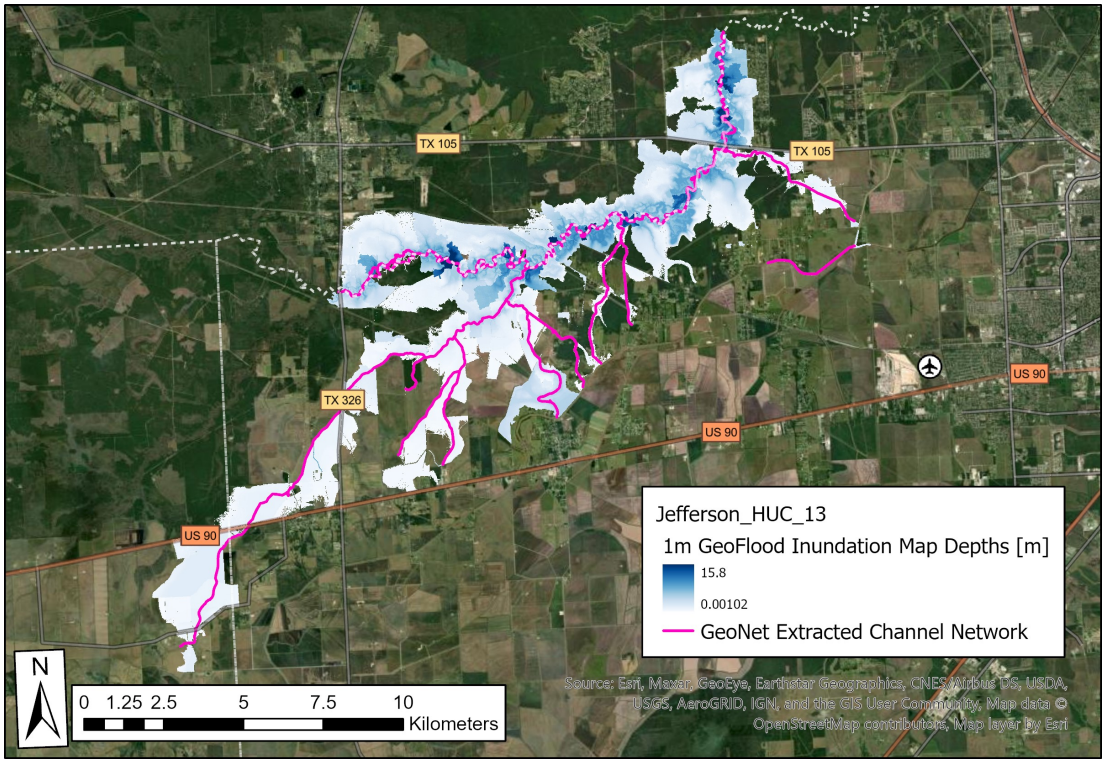


Figure 4.4: 1-meter resolution GeoFlood inundation map for HUC 120200070201 in northwest Jefferson county. The Pine Island Bayou flows from west to east through the upper portion of the inundated area.

## 4.5 Statistical Analysis

A copy of the raster comparison and statistical analysis script is provided in Appendix A.

### 4.5.1 Inundation Map Extent Comparisons

To compare inundation extent, the HAND at 10-meter, GeoFlood 1-meter, and FEMA 3-meter maps are converted to binary rasters, intersected, and categorized into four classes as seen in Table 4.1.

| **Inundation Extent Comparison Matrix** | **Wet (Inundated)** | **Dry (Not Inundated)** |
|---|---|---|
| **Wet** | WW | WD |
| **Dry** | DW | DD |

Table 4.1: Nomenclature for inundation extent comparison statistics.

The "W" refers to a wet, inundated pixel whereas the "D" refers to a dry, not inundated pixel. The first letter in each class refers to the condition of the pixel in the inundation binary extent raster $a$ while the second letter refers to the condition of the pixel in the inundation binary extent raster $b$. The rasters $a$ and $b$ may refer to the GeoFlood 1-meter, HAND 10-meter, or FEMA 3-meter inundation binary extent rasters depending on the analysis. Descriptors in the results section will clearly differentiate the model or reference being compared.

Figure 4.5 shows the binary extent conversion of the 1-meter GeoFlood inundation map for HUC 120200070201 in northwest Jefferson county. All inundated (wet) pixels in the 1-meter GeoFlood inundation map are assigned a value of one and zero elsewhere. The binary extent conversion was applied to the GeoFlood 1-meter, HAND 10-meter, and FEMA 3-meter datasets.

Figure 4.6 represents the comparison between the GeoFlood 1-meter and HAND 10-meter inundation maps for HUC 120200070201 in northwest Jefferson county. The ArcGIS Pro *conditional evaluation* tool downsamples the larger resolution inundation binary extent raster to the smallest resolution pixel size of the

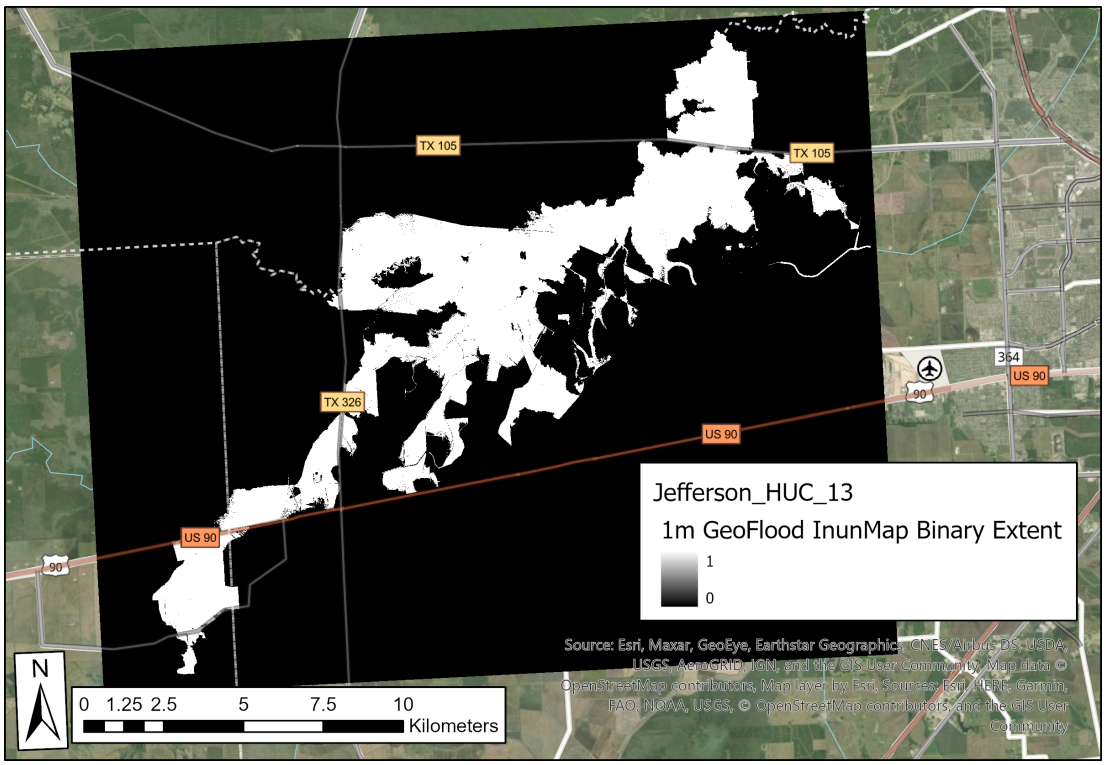


Figure 4.5: 1-meter resolution GeoFlood binary inundation extent map representing inundated and noninundated pixels of HUC 120200070201 in northwest Jefferson county. Inundated pixels are white and noninundated pixels are black.

input rasters. Wet-wet pixels tend to be near the channel centerlines whereas wet-dry and dry-wet pixels are often located near the outer boundaries of the inundation extents.

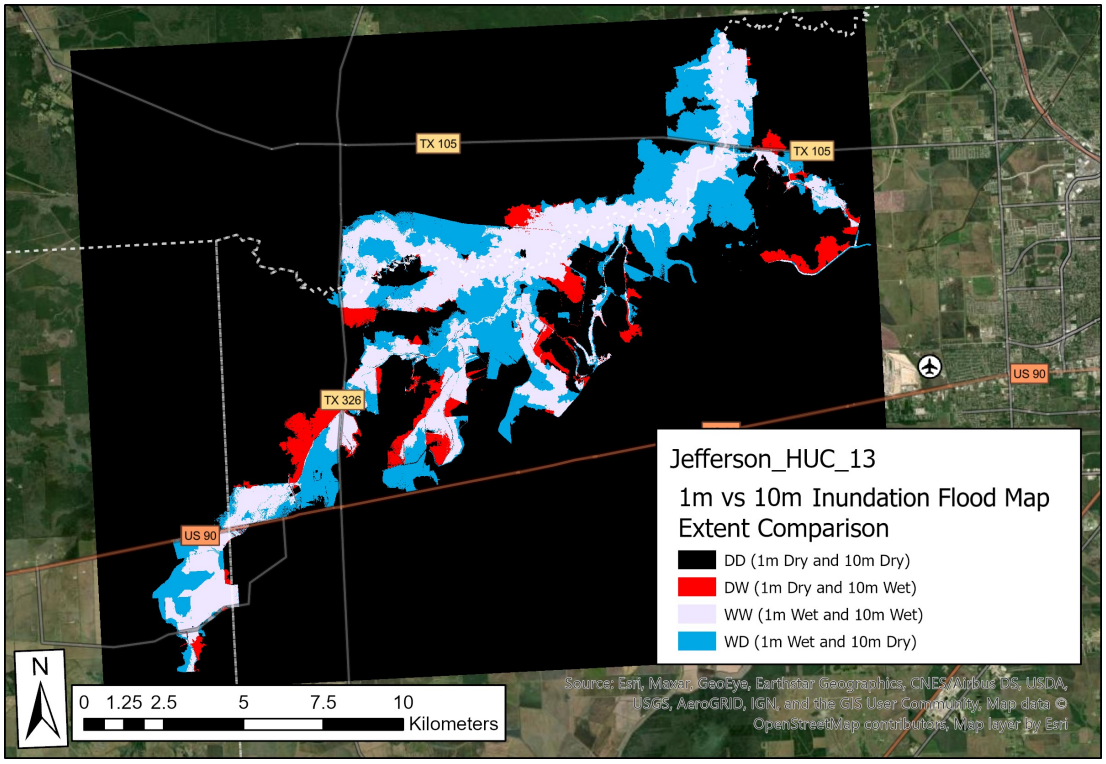


Figure 4.6: GeoFlood 1-meter versus HAND 10-meter resolution inundation extent comparison for HUC 120200070201 in northwest Jefferson county. 1-meter inundated pixels and 10-meter noninundated pixels are blue. 1-meter and 10-meter inundated pixels are light purple. 1-meter noninundated pixels and 10-meter inundated pixels are red. 1-meter and 10-meter noninundated pixels are black.

Four metrics, inundation area ratio, accuracy, underestimation, and overestimation, are used in the inundation extent comparisons. These metrics were adapted from the flood inundation mapping statistical analysis conducted by Johnson et. al. (2019).

The inundation area ratio ($IAR$) compares the total area of binary inundation regardless of spatial accuracy as seen in Equation 4.16. An inundation area

ratio of one indicates that the compared inundation maps have equal inundation area coverage regardless of inundation depth. A value greater than 1 in a GeoFlood 1-meter to HAND 10-meter comparison indicates that the inundation area of the GeoFlood 1-meter model is greater than the inundation area of the HAND 10-meter model. A value less than 1 in a GeoFlood 1-meter to FEMA 3-meter comparison indicates that the inundation area of the GeoFlood 1-meter model is less than the inundation area of the FEMA 3-meter reference.

$$Inundation\ Area\ Ratio\ (IAR) = \frac{total\ wet\ pixels\ from\ a}{total\ wet\ pixels\ from\ b} \tag{4.16}$$

Accuracy for inundation extent comparisons can be computed as the total number of intersecting wet pixels ($W_aW_b$) divided by the total number of all intersecting pixels with at least one pixel being wet ($W_aW_b$, $W_aD_b$, and $D_aW_b$). Accuracy is computed using Equation 4.17 shown below. Results from the accuracy computation are between zero and one. An accuracy of one means the compared inundation binary extent rasters have perfect correlation. Conversely, the compared inundation binary extent rasters have no correlation with an accuracy of zero. An accuracy between one and zero represents the percentage of corresponding inundated pixels in $a$ and $b$ relative to the total number of all intersecting pixels excluding $D_aD_b$ pixels.

$$Accurate\ (A)\ =\ \frac{W_aW_b}{W_aW_b + W_aD_b + D_aW_b} \tag{4.17}$$

The underestimation of inundation is computed using Equation 4.18.

$$Underestimate\ (U)\ = \frac{D_a W_b}{W_a W_b + W_a D_b + D_a W_b} \tag{4.18}$$

The overestimation of inundation is computed using Equation 4.19.

$$Overestimate\ (O)\ = \frac{W_a D_b}{W_a W_b + W_a D_b + D_a W_b} \tag{4.19}$$

The summation of the Accurate, Underestimate, and Overestimate statistics equals one. The extent comparison statistics are used to determine the performance of the GeoFlood workflow versus the HAND 10-meter and the FEMA 3-meter reference flood inundation maps.

### 4.5.2 Inundation Map Depth Comparisons

The difference in water surface elevations (WSEs) is computed between inundation depth rasters or points $a$ and $b$. Similar to the extent statistical comparisons, $a$ and $b$ may refer to the GeoFlood 1-meter, HAND 10-meter, FEMA 3-meter, or USGS HWM inundation depths depending on the analysis. The WSE differences are analyzed using the Root Mean Square Error (4.20), Mean Absolute Error (4.21), and Mean Error (4.22) inundation depth comparison metrics.

$$Root\ Mean\ Square\ Error\ (RMSE) = \sqrt{\frac{\sum_{n=1}^{N}(Z_a - Z_b)^2}{N}} \tag{4.20}$$

$$Mean\ Absolute\ Error\ (MAE) = \frac{\sum_{n=1}^{N}|Z_a - Z_b|}{N} \tag{4.21}$$

$$Mean\ Error\ (ME) = \frac{\sum_{n=1}^{N}(Z_a - Z_b)}{N} \tag{4.22}$$

The WSEs $Z_a$ and $Z_b$ are the intersecting pixels corresponding to the inundation depths of $a$ and $b$, respectively. The total number of intersecting $W_a W_b$ pixels is computed as $N$. The inundation depth comparison is only computed on pixels that are flooded in both inundation depth rasters or points $a$ and $b$.

Figure 4.7 shows the results of the ArcGIS Pro *minus* function. The 10-meter HAND inundation depth raster is subtracted from the 1-meter GeoFlood inundation depth raster where both pixels are inundated. The ArcGIS Pro *minus* function downsamples the larger resolution inundation depth raster to the smallest resolution pixel size of the raster inputs.

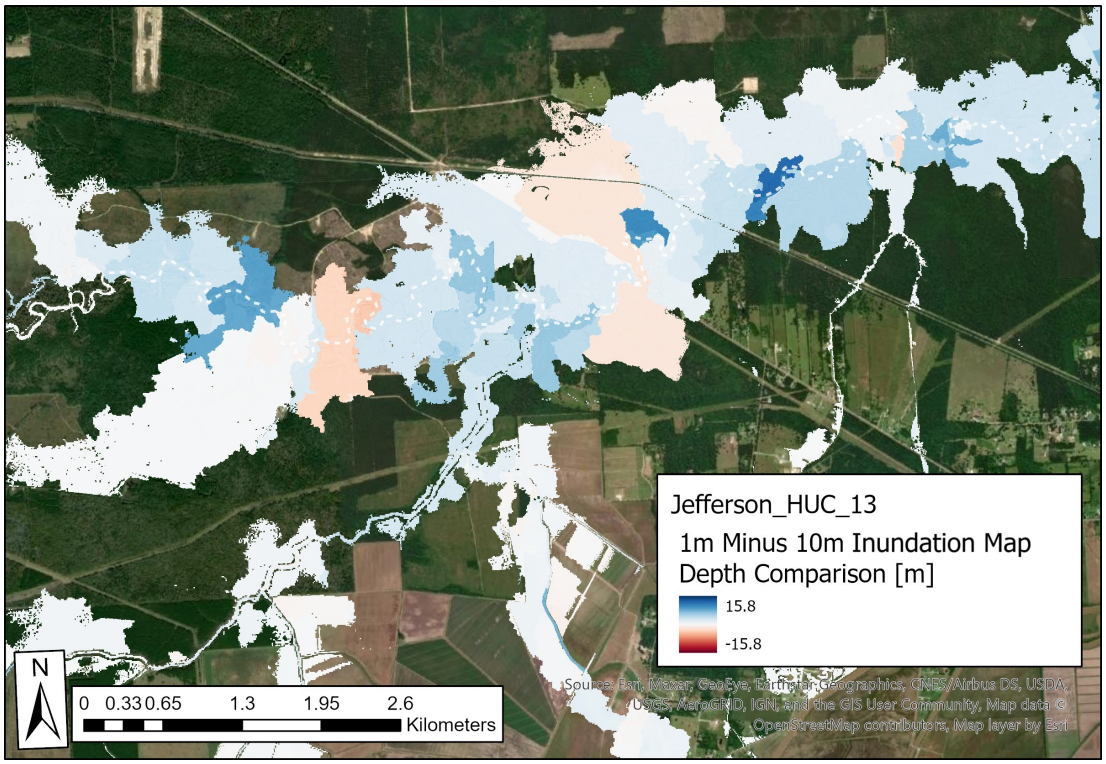


Figure 4.7: GeoFlood 1-meter versus HAND 10-meter resolution inundation depth comparison for HUC 120200070201 in northwest Jefferson county. Differences in depth are represented by a divergent color scale. Pixels with a blue hue show that the 1-meter GeoFlood inundation depth was greater than the 10-meter HAND inundation depth. Pixels with a red hue show that the 10-meter HAND inundation depth was greater than the 1-meter GeoFlood inundation depth. Larger differences in depth are correlated with a darker color in the divergent color scheme.

# Chapter 5: Results

## 5.1 Comparison of Model to Model

The inundation extent coverages as a percentage of NHD catchment area were determined for each of the selected Texas counties. Figures 5.1 and 5.2 show the percent of NHD catchment inundated box plots for the GeoFlood 1-meter and HAND 10-meter models, respectively. Uvalde county had the lowest medians at 1.13% and 1.02%, respectively. The effects of flooding were less significant in Mitchell, Uvalde, and Young counties because they were far away from Hurricane Harvey's center. Jefferson county has the highest medians at 57.8% and 48.5%, respectively. The results from this analysis reinforce the tremendous amounts of Hurricane Harvey precipitation and inundation observations in the southeastern Texas counties Brazos, Colorado, Harris, and Jefferson.

### 5.1.1 Inundation Extent Comparison

The inundation extent comparison boxplot for Inundation Area Ratio (IAR) between the 1-meter and 10-meter models is shown in Figure 5.3. An IAR greater than one indicates the GeoFlood 1-meter model has a larger inundation extent than the HAND 10-meter model. The median IAR is greater than one for all seven Texas counties. Based on the median IAR, the 1-meter model simulates a greater inundation extent than the 10-meter model irrespective of NHD catchment scale terrain and channel characteristics. The average IAR is 127% greater for Brazos, Colorado, Harris, and Jefferson counties at 3.38 versus Mitchell, Uvalde, and

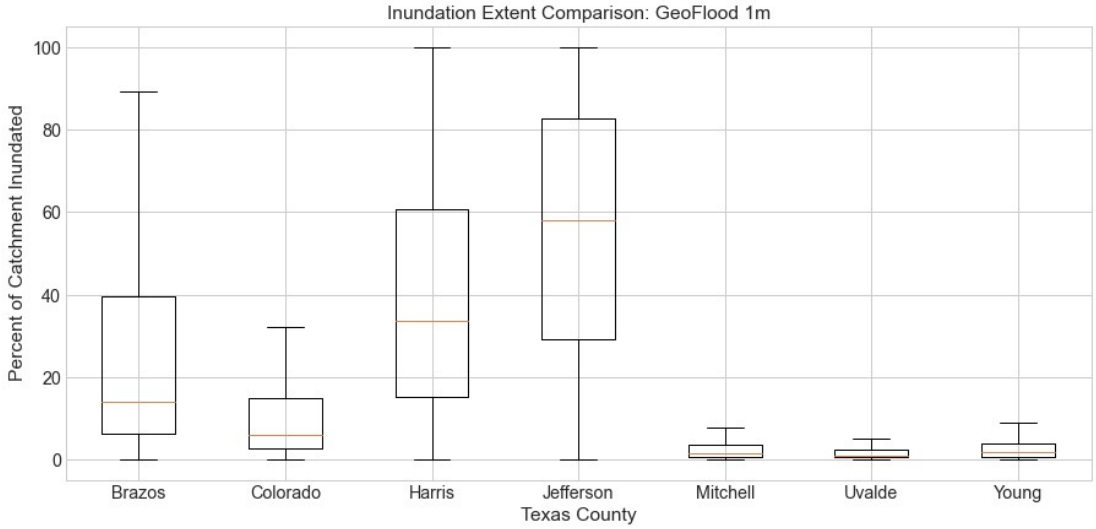


Figure 5.1: Inundation extent coverage as a percentage of NHD catchment area for the Geoflood 1-meter model.

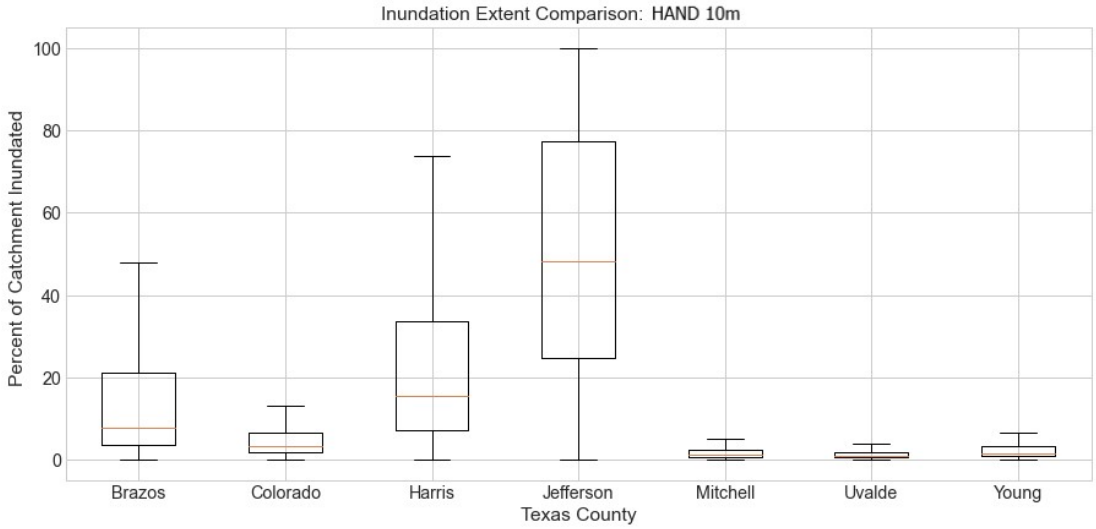


Figure 5.2: Inundation extent coverage as a percentage of NHD catchment area for the HAND 10-meter model.

Young counties at 1.49. The distinct contrast in average IAR may indicate that IAR differences increase in low terrain relief counties containing many sixth-order streams with high flowrates. The greatest IAR variance occurs in Harris county which may suggest that IAR variance increases in regions with high density development and man-made infrastructure. The lowest median IAR occurs in Young county. Young county received lesser amounts of precipitation from Hurricane Harvey, therefore, differences in inundation extent for the 1-meter and 10-meter models are diminished due to the lack of appreciable inundation. The lowest IAR variance is attributed to Uvalde county which has the highest terrain relief relative to the selected counties in this study.

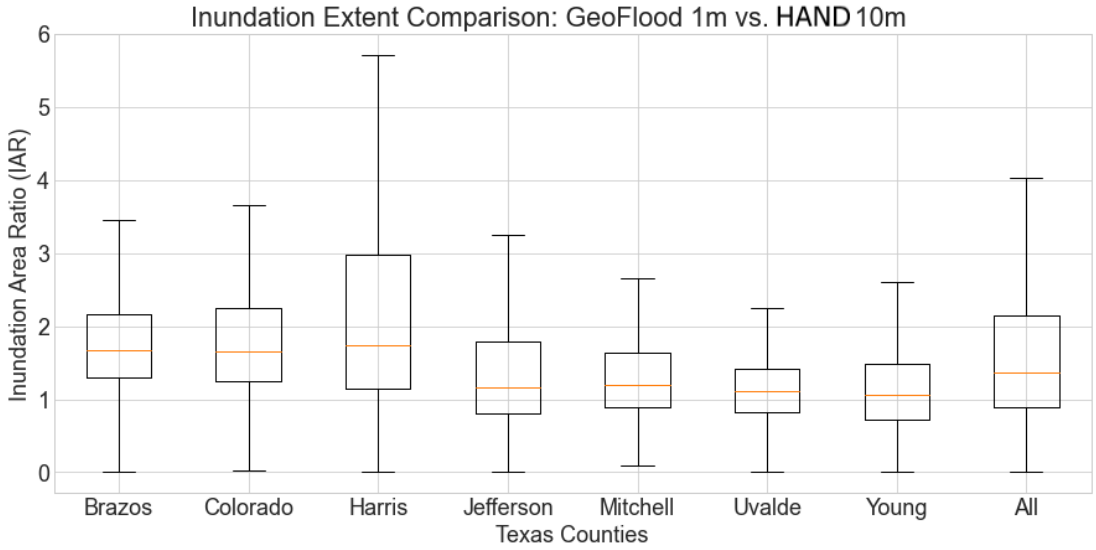


Figure 5.3: Inundation extent comparison boxplot for Inundation Area Ratio (IAR). GeoFlood 1-meter inundated area is divided by the HAND 10-meter inundated area within the NHD catchment. IARs over one indicates the GeoFlood 1-meter model has a greater inundated area, while below one suggests a lesser inundated area.

Figure 5.4 shows the accurate inundation extent statistic boxplots comparing the 1-meter model to the 10-meter model. An accuracy nearer to one indicates

greater inundation extent overlap, whereas lesser overlap is represented by an accuracy closer to zero. The median accuracy for all counties is 0.370, while the lowest median accuracy is 0.218 in Uvalde county and the highest median accuracy is 0.476 in Jefferson county. Accuracy is likely a function of total inundation extent among other factors, where counties with large 1-meter and 10-meter inundation extents experience greater median accuracy. Jefferson county has the greatest median accuracy as well as minimum and maximum whisker range. Substantial inundation from Hurricane Harvey, low-relief terrain, and lower slope may contribute to both the high median accuracy and high interquartile range in Jefferson county. The average accuracy for Brazos, Colorado, Harris, and Jefferson counties is 31.5% greater than for Mitchell, Uvalde, and Young counties. The increase in accuracy for low relief counties near the Gulf of Mexico can likely be attributed to greater precipitation from Hurricane Harvey, thereby increasing the total inundation extent.

Summary inundation extent comparison statistics for each of the seven Texas counties are provided in Table 5.1. Underestimation for the GeoFlood 1-meter model is likely more frequent in regions with high relief, high slopes, and lesser flowrates. Young county has both the greatest interquartile range for inundation extent underestimation and the lowest total inundation. GeoFlood 1-meter overestimation versus the HAND 10-meter model is relatively similar for all counties except Jefferson. Jefferson county has both the lowest median overestimation and highest interquartile range. Similar to the previously discussed trend; greater inundation, lower slope, and low-relief terrain may contribute to Jefferson county's atypical overestimate statistics.

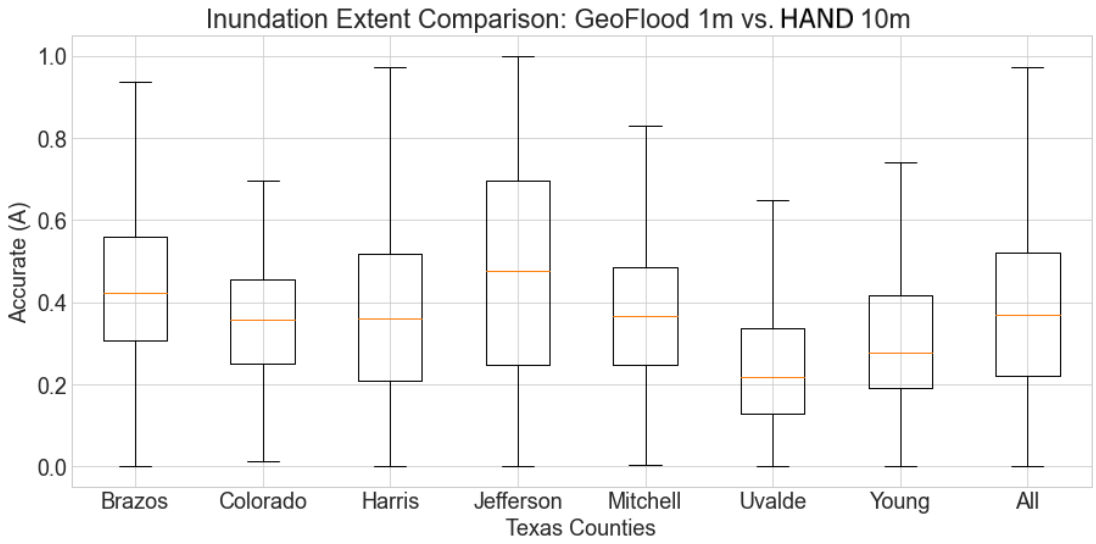


Figure 5.4: Inundation extent comparison boxplot for Accurate (A). The accurate metric is the percentage of intersecting GeoFlood 1-meter and HAND 10-meter inundated area divided by the total inundated area. Accuracy nearer to one indicates greater inundation extent overlap, while accuracy nearer to zero means lesser overlap.

| | Brazos | | Colorado | | Harris | | Jefferson | | Mitchell | | Uvalde | | Young | |
|---|---|---|---|---|---|---|---|---|---|---|---|---|---|---|
| Stat | Med | IQR | Med | IQR | Med | IQR | Med | IQR | Med | IQR | Med | IQR | Med | IQR |
| IAR | 1.67 | 0.87 | 1.66 | 1.00 | 1.75 | 1.84 | 1.16 | 0.98 | 1.19 | 0.74 | 1.12 | 0.59 | 1.05 | 0.76 |
| A | 0.42 | 0.25 | 0.36 | 0.20 | 0.36 | 0.31 | 0.48 | 0.45 | 0.37 | 0.24 | 0.22 | 0.21 | 0.28 | 0.22 |
| U | 0.06 | 0.13 | 0.11 | 0.19 | 0.06 | 0.17 | 0.10 | 0.30 | 0.23 | 0.31 | 0.34 | 0.25 | 0.30 | 0.36 |
| O | 0.46 | 0.25 | 0.49 | 0.23 | 0.48 | 0.39 | 0.25 | 0.44 | 0.37 | 0.20 | 0.40 | 0.18 | 0.34 | 0.23 |

Table 5.1: GeoFlood 1-meter versus HAND 10-meter inundation extent comparison statistic summary. Med is the median descriptive statistic. IQR is the interquartile range descriptive statistic. IAR, A, U, and O are the inundation area ratio, accurate, underestimate, and overestimate inundation extent comparison metrics, respectively.

### 5.1.2 Inundation Depth Comparison

The Root Mean Squared Error (RMSE) in meters for the inundation depth comparison between the GeoFlood 1-meter and HAND 10-meter models is shown in Figure 5.5. A larger RMSE corresponds to a greater difference in inundation depth between the 1-meter and 10-meter models. The median RMSE for Brazos, Colorado, Harris, and Jefferson counties at 1.34 is 326% greater than for Mitchell, Uvalde, and Young counties at 0.314. The larger RMSE is likely attributed to greater overall inundation depths for both models. Uvalde county has the lowest median RMSE and interquartile range as well as the highest relief relative to the seven Texas county study area. Jefferson, the county with the greatest inundation and lowest relief, has the highest median RMSE and interquartile range.

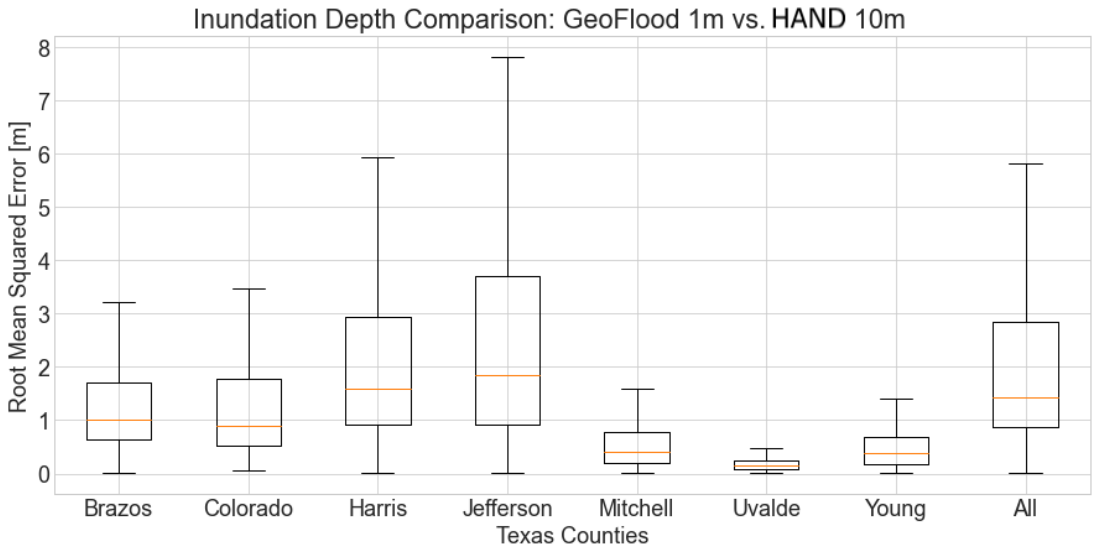


Figure 5.5: Inundation depth comparison boxplot for Root Mean Squared Error (RMSE). RMSE measures the average magnitude of the errors using the quadratic scoring rule. A greater RMSE indicates larger variance in inundation depth, whereas smaller RMSEs are associated with lesser depth variance.

Figure 5.6 shows the mean error (ME) boxplot for the GeoFlood 1-meter to

HAND 10-meter inundation depth comparison. The median ME is greater than zero for all counties, which indicates that the GeoFlood 1-meter model tends to simulate greater inundation depth than the HAND 10-meter model irrespective of NHD catchment scale terrain and channel characteristics. Since Harris county has the highest median ME, mean error between the 1-meter and 10-meter models may be greatest for regions with widespread man-made infrastructure and high density development. Jefferson county has the largest interquartile range for ME likely due to the greater inundation and lower relief relative to the study area.

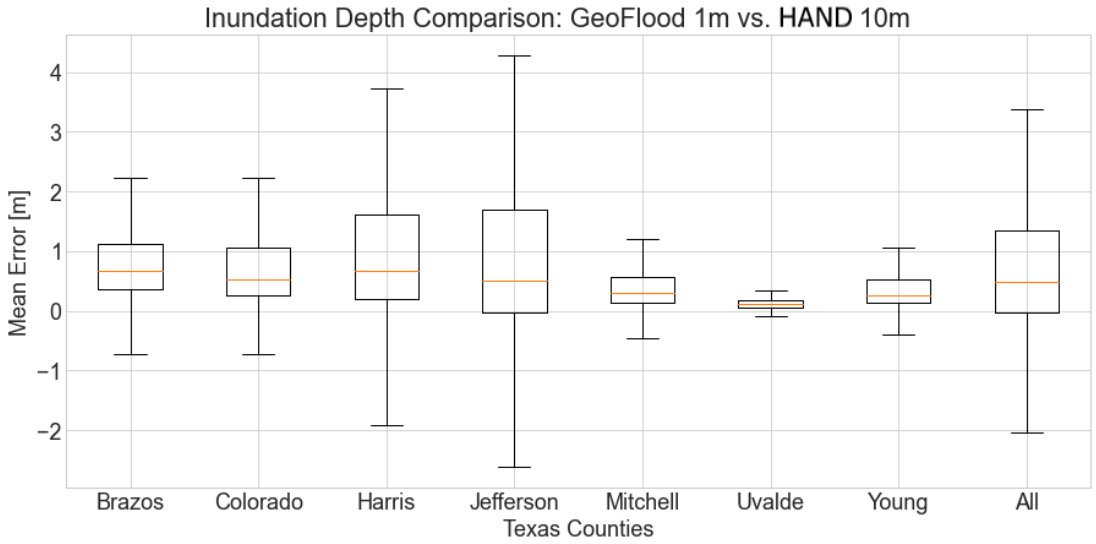


Figure 5.6: Inundation depth comparison boxplot for Mean Error (ME). Mean error calculates the average error while retaining their sign. A positive ME means the 1-meter model tends to overestimate, while a negative sign suggests underestimation.

Summary inundation depth comparison statistics for each of the seven Texas counties are provided in Table 5.2. Mean average error (MAE) is greater than zero for all counties suggesting a tendency for greater inundation depths for the GeoFlood 1-meter model versus the HAND 10-meter model. As a stipulation, this

analysis is comparing model to model, therefore, depth comparisons are relative to the simulations and not whether a model is more accurate as compared to an established reference. Comparisons of the models against the FEMA Harvey flood depths grid and USGS high water mark references are shown in Section 5.2.

| | Brazos | | Colorado | | Harris | | Jefferson | | Mitchell | | Uvalde | | Young | |
|---|---|---|---|---|---|---|---|---|---|---|---|---|---|---|
| Stat | Med | IQR | Med | IQR | Med | IQR | Med | IQR | Med | IQR | Med | IQR | Med | IQR |
| RMSE [m] | 1.01 | 1.06 | 0.91 | 1.24 | 1.59 | 2.03 | 1.85 | 2.80 | 0.41 | 0.58 | 0.15 | 0.16 | 0.39 | 0.51 |
| MAE [m] | 0.79 | 0.81 | 0.71 | 1.01 | 1.18 | 1.74 | 1.38 | 2.42 | 0.34 | 0.48 | 0.13 | 0.13 | 0.32 | 0.44 |
| ME [m] | 0.67 | 0.77 | 0.52 | 0.80 | 0.66 | 1.42 | 0.50 | 1.73 | 0.31 | 0.43 | 0.11 | 0.11 | 0.26 | 0.39 |

Table 5.2: GeoFlood 1-meter versus HAND 10-meter inundation depth comparison statistic summary. Med is the median descriptive statistic. IQR is the interquartile range descriptive statistic. RMSE, MAE, and ME are the root mean squared error, mean absolute error, and mean error inundation depth comparison metrics, respectively. RMSE, MAE, and ME are computed in meters.

### 5.1.3 Terrain Characteristics

Various terrain characteristics were examined to determine correlations with GeoFlood 1-meter improvements. The terrain characteristics included topographical relief in the form of slope elevation difference, distance to the Gulf of Mexico, catchment area, stream length, and choropleth maps for general spatial trends. The most prominent correlations are presented below.

A strong downward sloping relationship exists between the root mean squared error inundation depth metric and the NHD catchment's topographical relief. Figure 5.7 shows the relationship between inundation depth difference and topographical relief as quantified by median RMSE and median relief. Relief was computed as the vertical distance between the NHD flowline's starting and ending points. The inundation depth differences are greater in counties with low relief, in contrast to inundation depth differences being lower in high relief counties. Jefferson

county shows the greatest median RMSE and lowest relief, while Uvalde county shows the opposite RMSE trend and terrain characteristics.

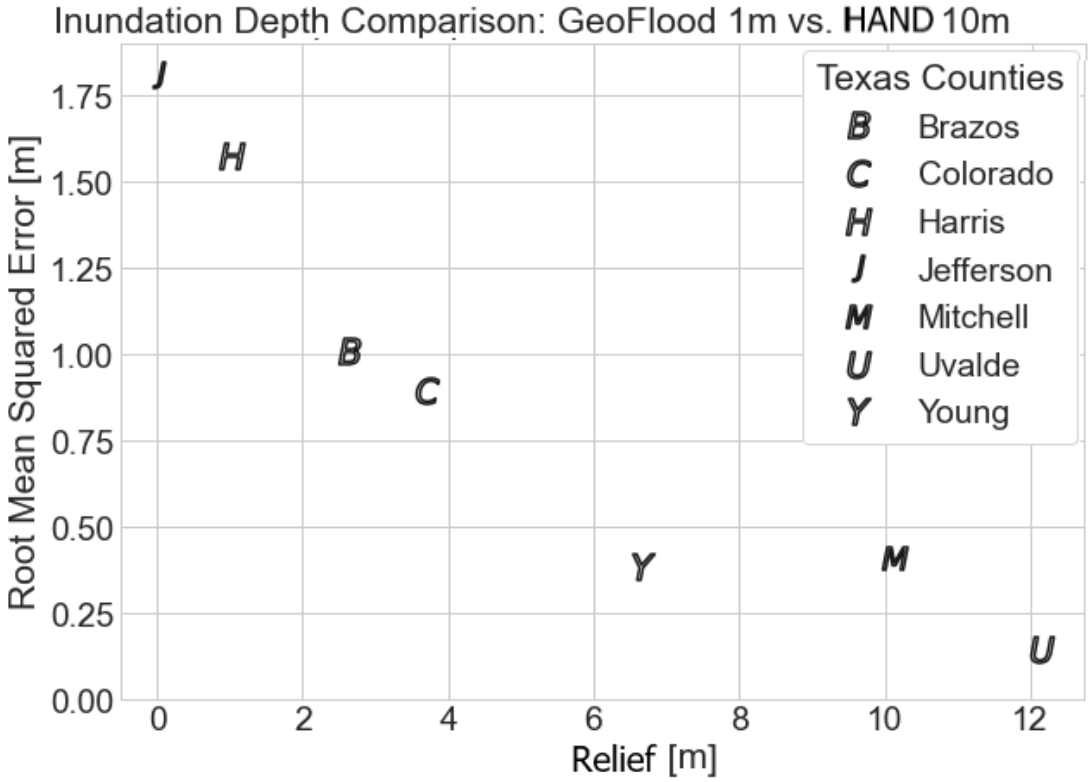


Figure 5.7: Median root mean squared error (RMSE) inundation depth comparison versus median relief between the GeoFlood 1-meter and HAND 10-meter models. Relief is computed as the vertical distance between the beginning and end points of the NHDPlus MR flowline.

Similar to the previous relationship, the RMSE versus stream length comparison shows a downward sloping trend. The correlation between the median RMSE and median stream length is shown in Figure 5.8. For this analysis, the stream length represents the length of each NHD flowline per NHD catchment. The trend suggests counties with shorter stream lengths experience greater inundation depth differences. Concurrently, the relationship indicates that counties with shorter stream lengths have smaller NHD catchment areas, which is congruent

with the NHD catchment area boxplot displayed in Figure 3.8.

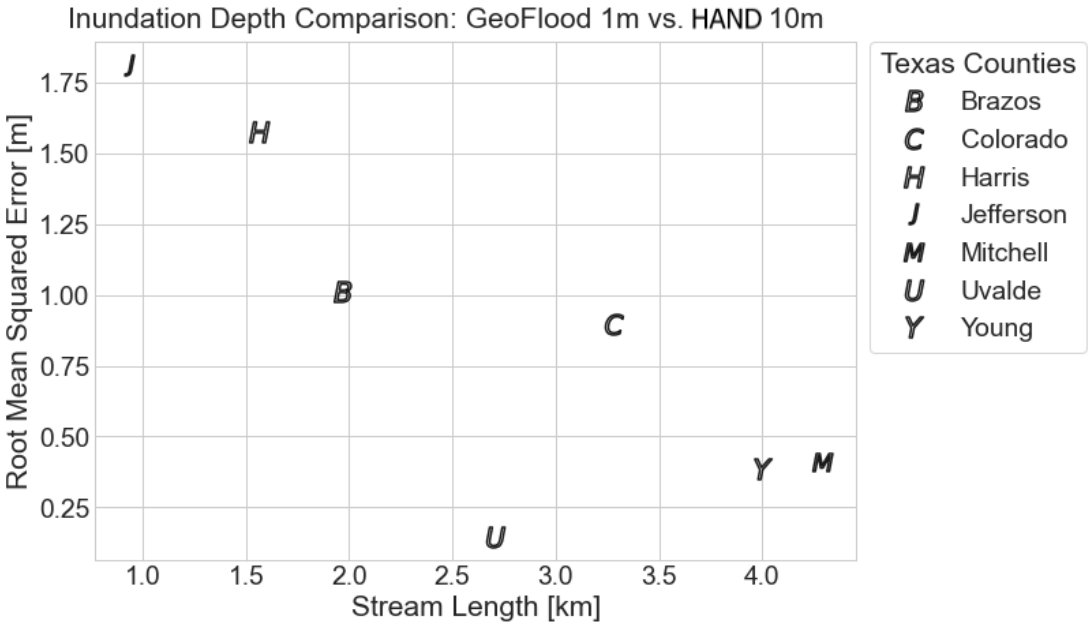


Figure 5.8: Median root mean squared error (RMSE) inundation depth comparison versus median NHDPlus MR flowline length between the GeoFlood 1-meter and HAND 10-meter models.

Figure 5.9 shows the accuracy inundation extent metric choropleth map for Mitchell County. Darker green colors indicate higher accuracy between the GeoFlood 1-meter and HAND 10-meter inundation extents. Flowing from north to south, the larger Colorado river joins western flowing Beals Creek near the center of Mitchell County. Inundation extent overlap, as measured by the accuracy metric, appears to be concentrated near the higher stream order channels. In contrast, overlap is generally lower within NHD catchments containing channel heads.

A terrain slope and underestimate inundation extent metric choropleth map is shown in Figure 5.10. Greater propensity for the GeoFlood 1-meter model to underestimate inundation extent versus the HAND model is shown with darker shading of the NHD catchments. The boundary between the high slope canyon-

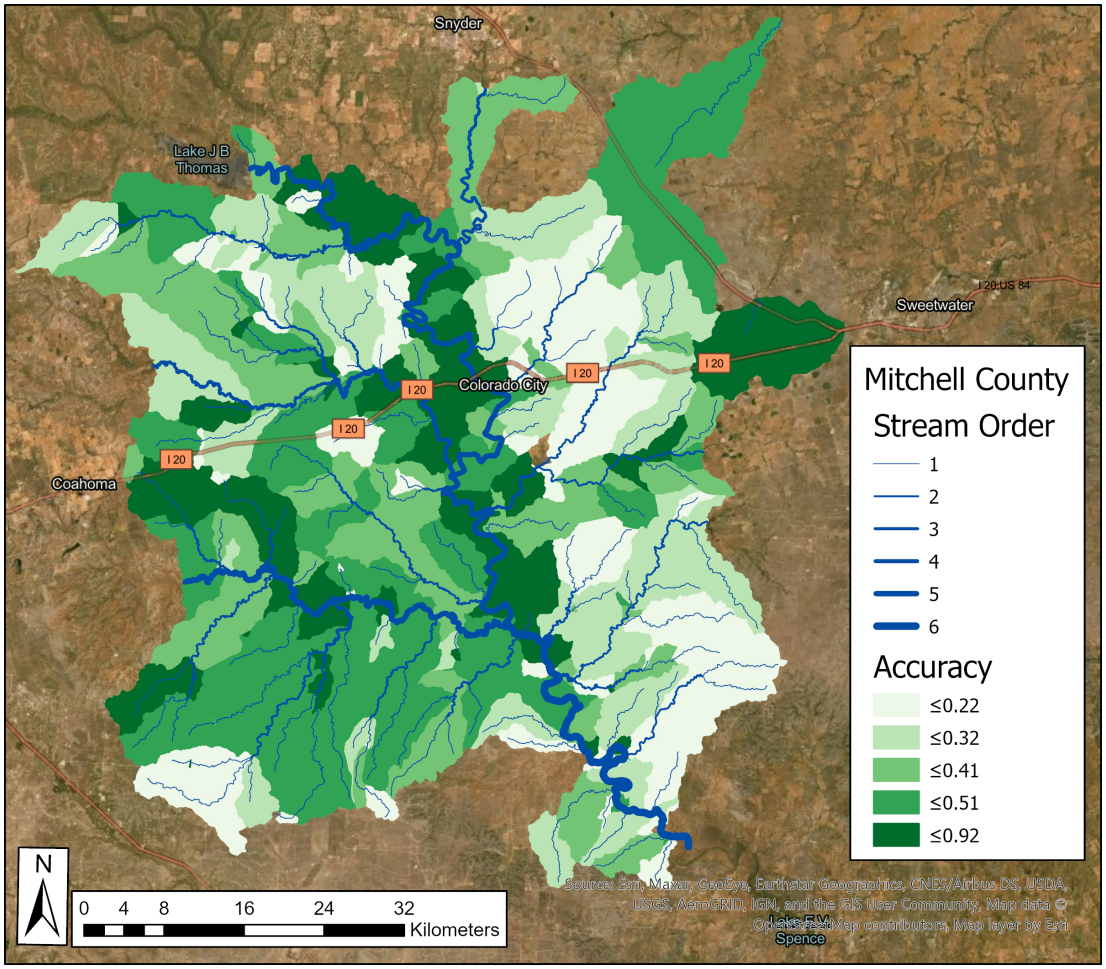


Figure 5.9: GeoFlood 1-meter versus HAND 10-meter accuracy choropleth map for Mitchell County. Strahler stream orders are represented by blue graduated NHDPlus MR flowlines.

lands of the Balcones Escarpment and lower relief plains is delineated by a solid black curve. Uvalde county provided a unique comparison between naturally adjacent high and low relief terrain characteristics. As shown in Figure 5.10, the 1-meter model underestimates inundation extent versus the 10-meter model more frequently in higher relief terrain. In contrast, the Geoflood 1-meter model transitions to higher accuracy and a tendency to overestimate versus the 10-meter model in lower relief terrain.

In relationship to the underestimation inundation extent metric, the mean error inundation depth metric shows similar trends in Uvalde county. Figure 5.11 shows the terrain slope and mean error inundation depth metric choropleth map. Darker shaded NHD catchments represent higher mean error between the GeoFlood 1-meter and HAND 10-meter inundation depth maps. Greater mean error is correlated with the steeply sloped Balcones escarpment in contrast to the low, rolling terrain of southern Uvalde county. Inundation depth differences are greater in higher relief terrain for the 1-meter versus 10-meter resolution models.

### 5.1.4 Channel Characteristics

Channel characteristics analyzed for this study included Strahler stream order, stream slope, and mean annual flow. Stream slope was the best indicator for GeoFlood 1-meter improvement versus the HAND 10-meter models. The most significant relationships for channel characteristics are detailed below.

The accurate inundation extent metric versus NHD flowline slope showed a general, down-sloping trend in Figure 5.15. The accurate metric and NHD flowline slopes represent the medians for each respective county. Similar to the relief terrain characteristic, Jefferson county has the greatest median inundation

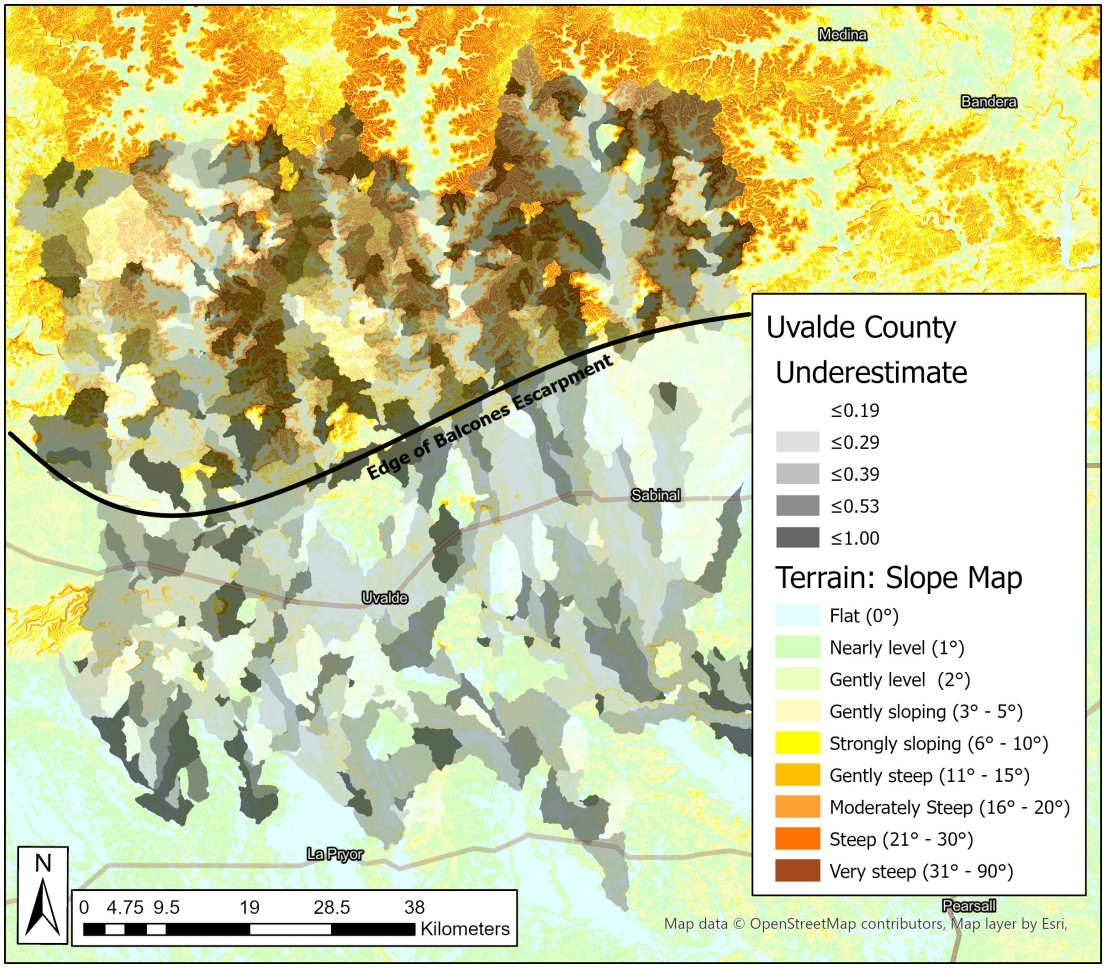


Figure 5.10: GeoFlood 1-meter versus HAND 10-meter underestimate choropleth map for Uvalde County. The underestimate metric describes the tendency for the 1-meter model to underestimate inundation extent versus the 10-meter model. Missing catchment data occurs where either the 1-meter or 10-meter models are not inundated.

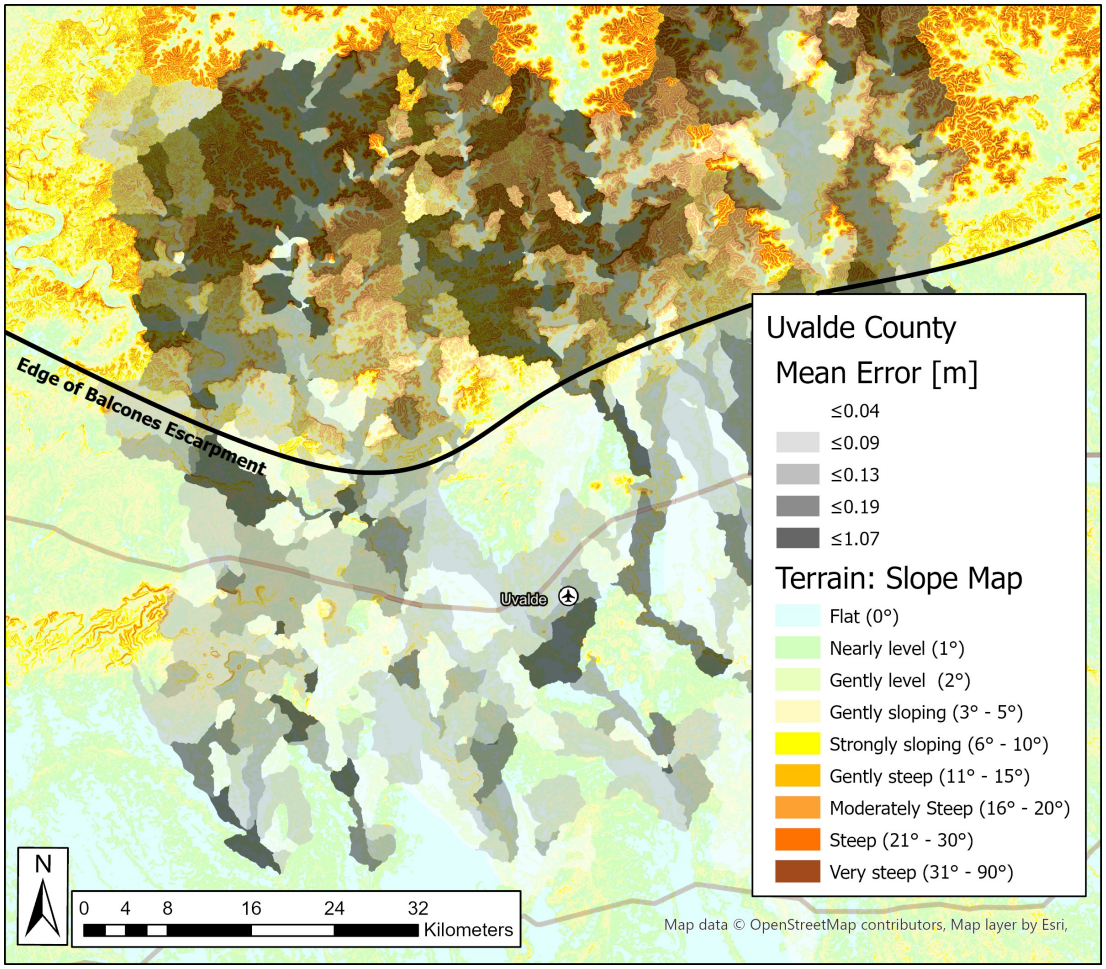


Figure 5.11: GeoFlood 1-meter versus HAND 10-meter mean error choropleth map for Uvalde County. Missing catchment data occurs where either the 1-meter or 10-meter models are not inundated.

extent accuracy and lowest median slope, while high relief Uvalde county displays an opposing relationship. This may suggest inundation extent overlap between the 1-meter and 10-meter models is highest in low slope regions.

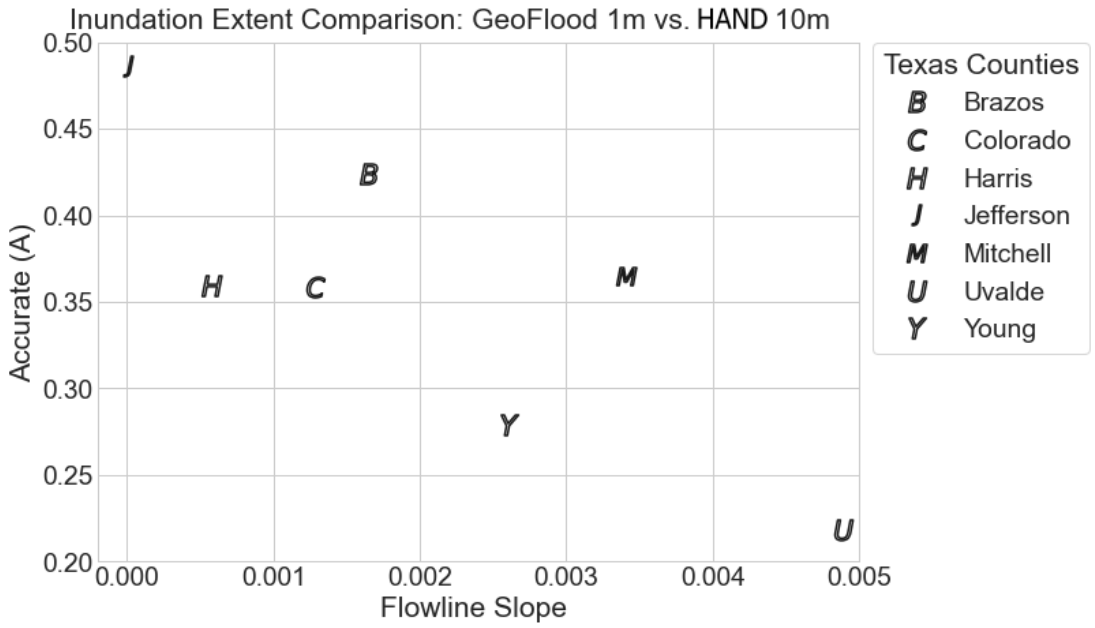


Figure 5.12: Median accurate inundation extent metric versus median NHD flowline slope between GeoFlood 1-meter and HAND 10-meter models.

Figure 5.13 shows the relationship between the accurate inundation extent metric and Strahler stream order. This box plot reinforces many hypotheses previously discussed. First, median 1-meter to 10-meter inundation extent overlap peaks for stream orders four and five. Second, the HAND at 10-meter model tends to overestimate in lower stream orders and underestimate in higher stream orders versus the GeoFlood model. The transition between overestimation and underestimation between the 1-meter and 10-meter models likely occurs near stream orders four and five where accuracy is greatest. Accuracy is reduced for lower and higher stream orders because increasingly larger areas of compared inundation ex-

tent are classified as overestimated or underestimated, respectively. Overall, this infers that the high resolution terrain improvements are most impactful for regions with high or low Strahler stream orders.

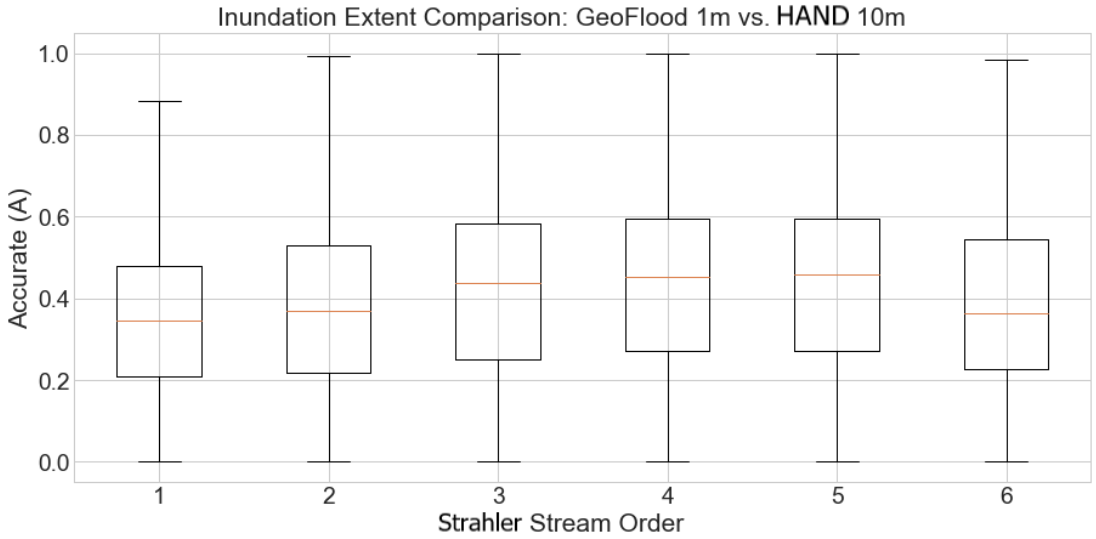


Figure 5.13: Box plot for accurate inundation extent metric versus Strahler stream order between GeoFlood 1-meter and HAND 10-meter models.

An up-sloping trend best defines the relationship between the underestimate inundation extent metric and NHD flowline slope. Figure 5.14 shows the median underestimate metrics plotted against the median NHD flowline slopes for each Texas county. Counties in the south-southeastern Coastal physiographic provinces including Jefferson, Colorado, Harris, and Brazos are grouped separately from Mitchell, Uvalde, and Young counties of the north-northwestern Plains physiographic provinces. Terrains with flatter slopes experience lower rates of GeoFlood 1-meter underestimation versus the HAND 10-meter model. In contrast, GeoFlood 1-meter underestimation occurs with higher frequency in counties with steeper slopes.

A significant downward trend exists for the relationship between the root

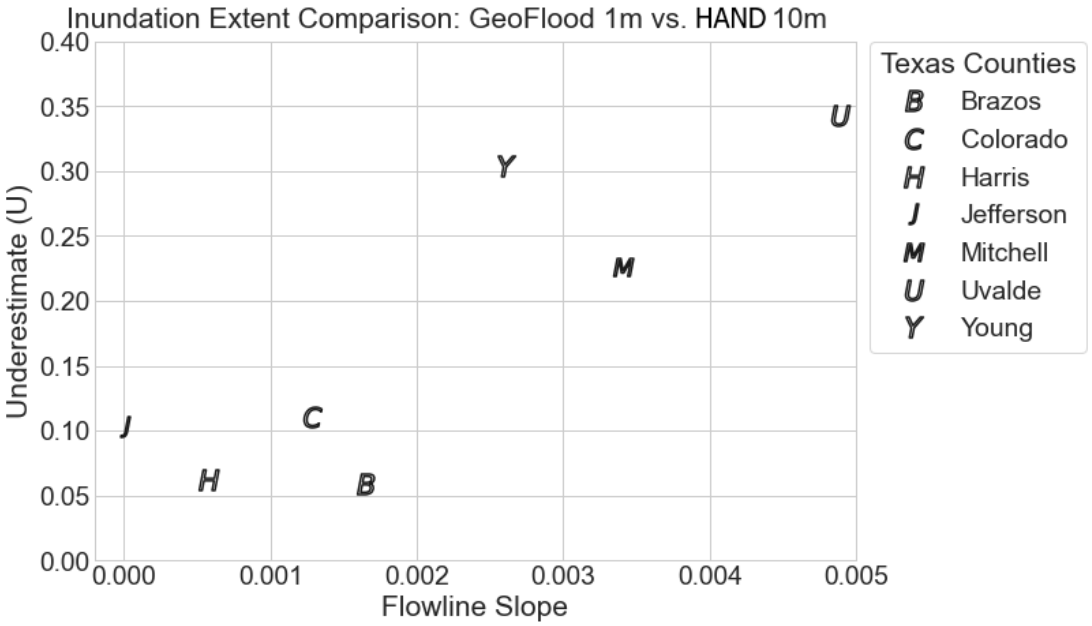


Figure 5.14: Median underestimate inundation extent metric versus median NHD flowline slope between GeoFlood 1-meter and HAND 10-meter models. The underestimate metric describes the tendency for the 1-meter model to underestimate inundation extent versus the 10-meter model.

mean squared error inundation depth metric and NHD flowline slope. The relationship between median RMSE and median NHD flowline slope is shown in Figure 5.15. Inundation depth difference is greater for counties with higher channel slopes, while the difference is lesser for lower channel slopes. Similar to the findings for inundation extent accuracy, the differences for inundation depth are strongly correlated with channel slope.

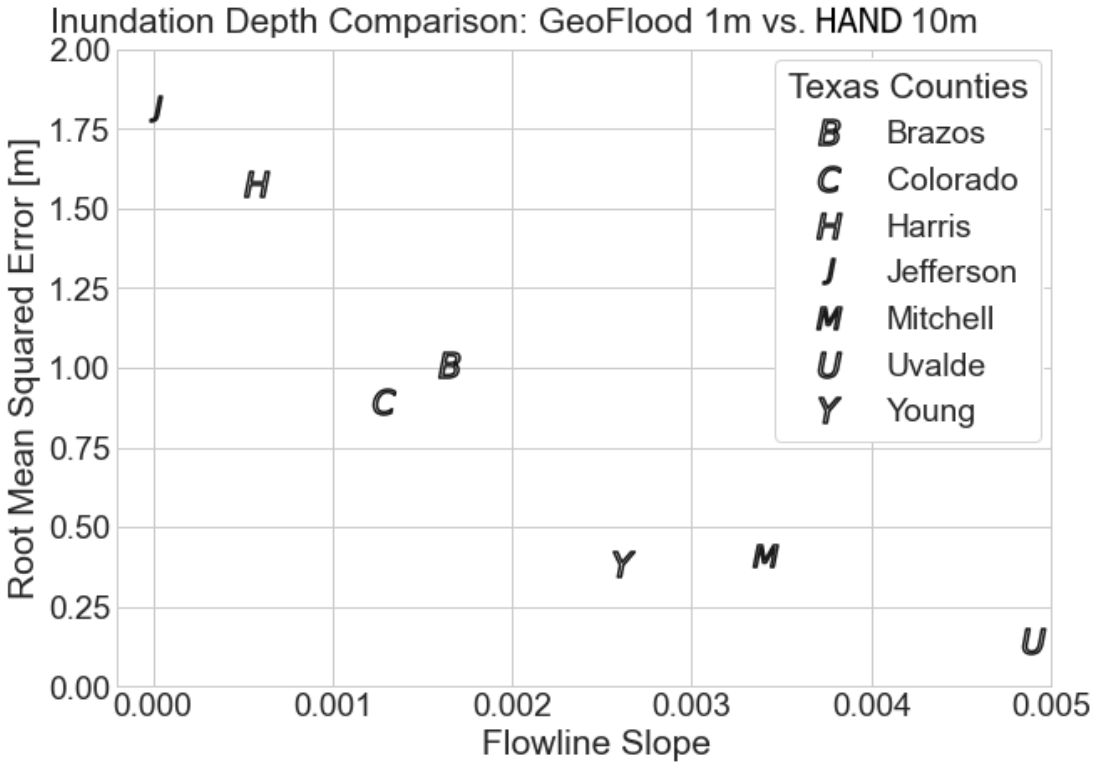


Figure 5.15: Median root mean squared error [m] RMSE inundation depth comparison versus median NHD flowline slope between the GeoFlood 1-meter and HAND 10-meter models.

Figure 5.16 shows the root mean squared error choropleth map for Colorado county. The blue NHD flowlines are graduated by Strahler stream order. The darker red NHD catchments represent a greater difference in inundation depth

between the GeoFlood 1-meter and HAND 10-meter simulations. As shown in Figure 5.16, the darker red coloration follows closely along the north to south flowing Colorado River. This indicates inundation depth differences are greatest near channels with higher stream orders.

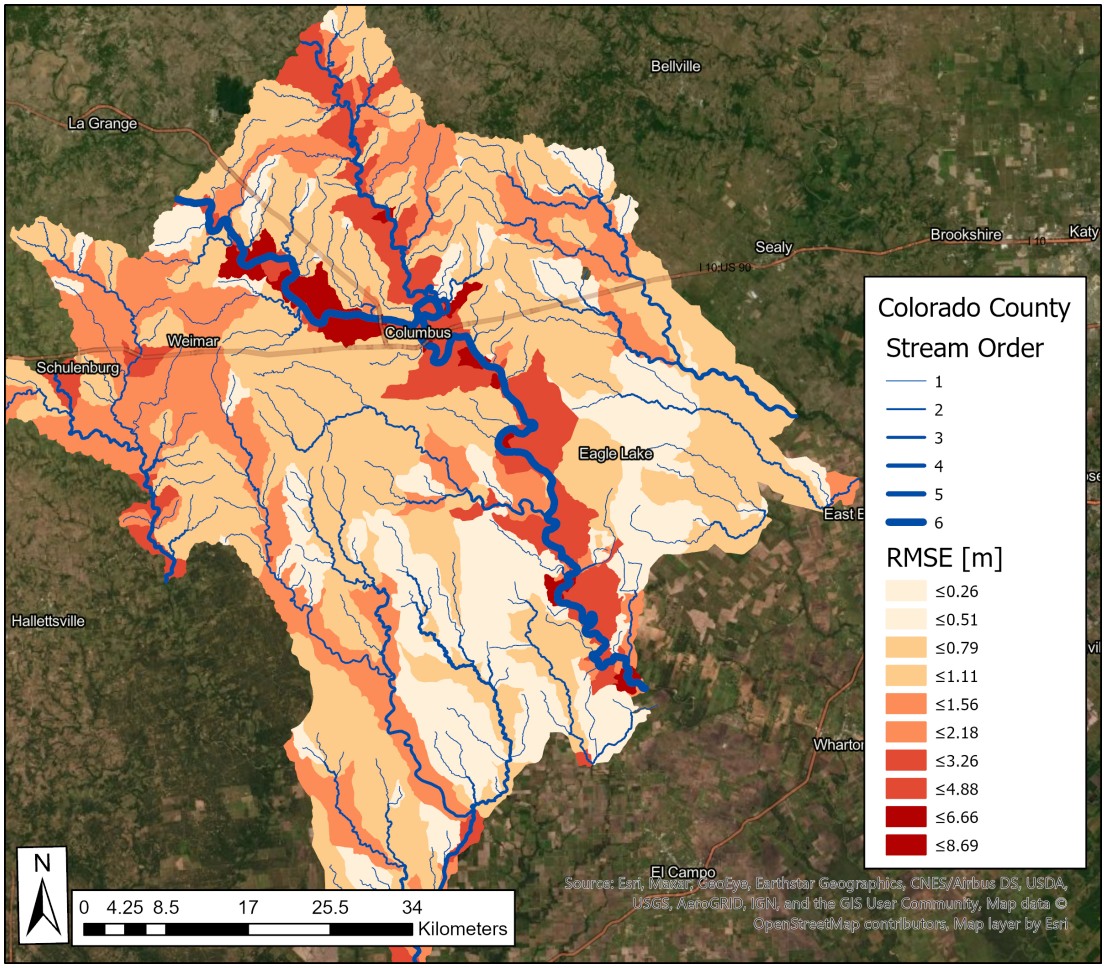


Figure 5.16: GeoFlood 1-meter versus HAND 10-meter root mean square error choropleth map for Colorado County. Stream orders represented by blue graduated NHD flowlines.

## 5.2 Comparison of Models to References

### 5.2.1 Inundation Extent Comparison

Figures 5.17 and 5.18 show the inundation area ratio (IAR) for GeoFlood 1-meter and HAND 10-meter inundation extents versus the FEMA Harvey flood depths grid reference, respectively. Inundation area ratios closer to one indicate greater inundation extent correlation with the FEMA reference. The median IARs are less than one for both the 1-meter and 10-meter models suggesting an inclination for both workflows and resolutions to underestimate inundation extent. The GeoFlood 1-meter median IARs for Colorado, Harris, and Jefferson counties are 126%, 95.5%, and 13.7% greater than HAND 10-meter median IARs, respectively. Greater GeoFlood 1-meter inundation extent correlation with the FEMA 3-meter reference is likely the result of increased inundation extent versus the HAND 10-meter model as shown in Section 5.1. The GeoFlood 1-meter IAR interquartile ranges for Colorado, Harris, and Jefferson counties are 68.4%, 45.8%, and -5.13% different than the HAND 10-meter IAR interquartile ranges, respectively. Generally, increasing the resolution of terrain data may increase both the inundation extent coverage and variance.

The accurate inundation depth comparison metrics for the GeoFlood 1-meter and HAND 10-meter model versus the FEMA 3-meter reference are shown in Figures 5.19 and 5.20, respectively. Accuracy closer to one indicates greater inundation extent overlap, while accuracy nearer to zero suggest lesser overlap. The GeoFlood 1-meter median accuracies for Colorado, Harris, and Jefferson counties are 56%, 62.4%, and 12.5% greater than HAND 10-meter median accuracies, respectively. Similar to the inferences made from the IAR metric, the GeoFlood

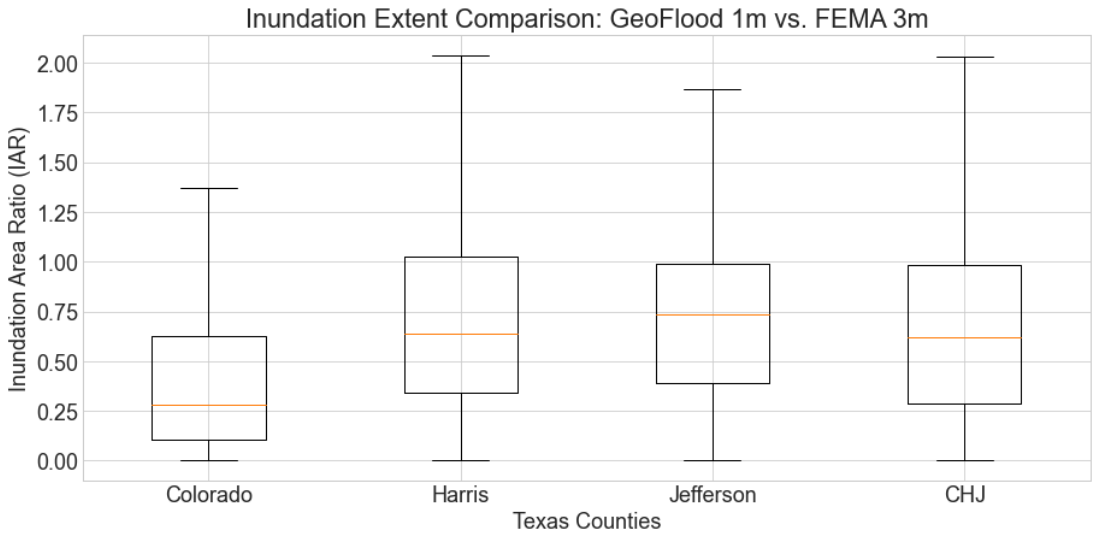


Figure 5.17: Inundation extent comparison boxplot for Inundation Area Ratio (IAR). GeoFlood 1-meter inundated area is divided by the FEMA 3-meter inundated area within the NHD catchment. IARs below one indicates the GeoFlood 1-meter model has a lesser inundated area, while above one suggests a greater inundated area.

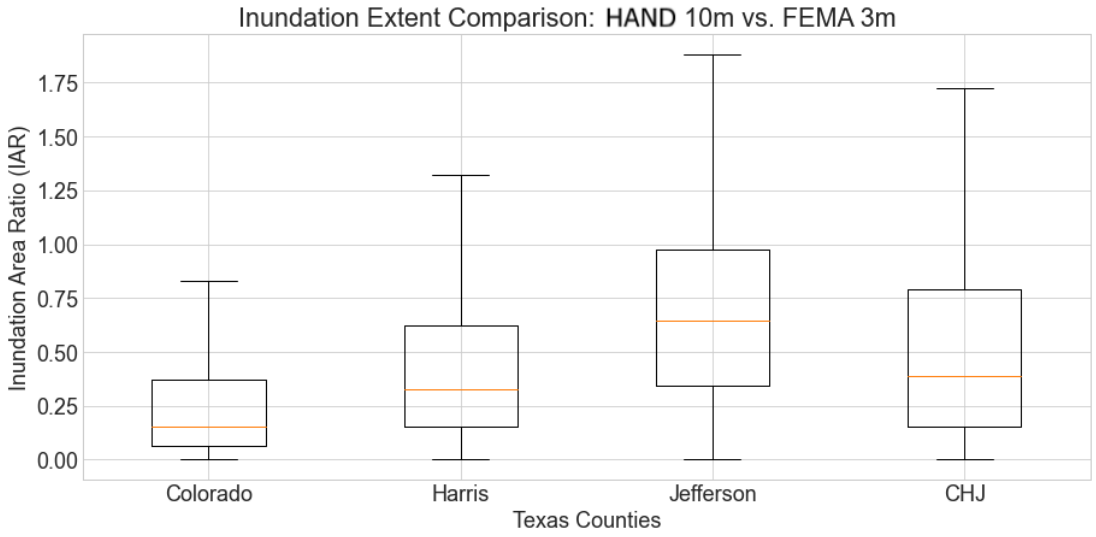


Figure 5.18: Inundation extent comparison boxplot for Inundation Area Ratio (IAR). HAND 10-meter inundated area is divided by the FEMA 3-meter inundated area within the NHD catchment. IARs below one indicates the 10-meter model has a lesser inundated area, while above one suggests a greater inundated area.

1-meter model is likely better correlated to the FEMA 3-meter reference than the HAND 10-meter model due to the increased inundation extent and depth performance provided by high-resolution terrain. The GeoFlood 1-meter accurate metric interquartile ranges for Colorado, Harris, and Jefferson counties are 74.7%, 25.4%, and 1.25% greater than the HAND 10-meter IAR interquartile ranges, respectively. In congruence with previous findings, the improvement in GeoFlood accuracy may also increase the variance in inundation extent correlation with reference datasets.

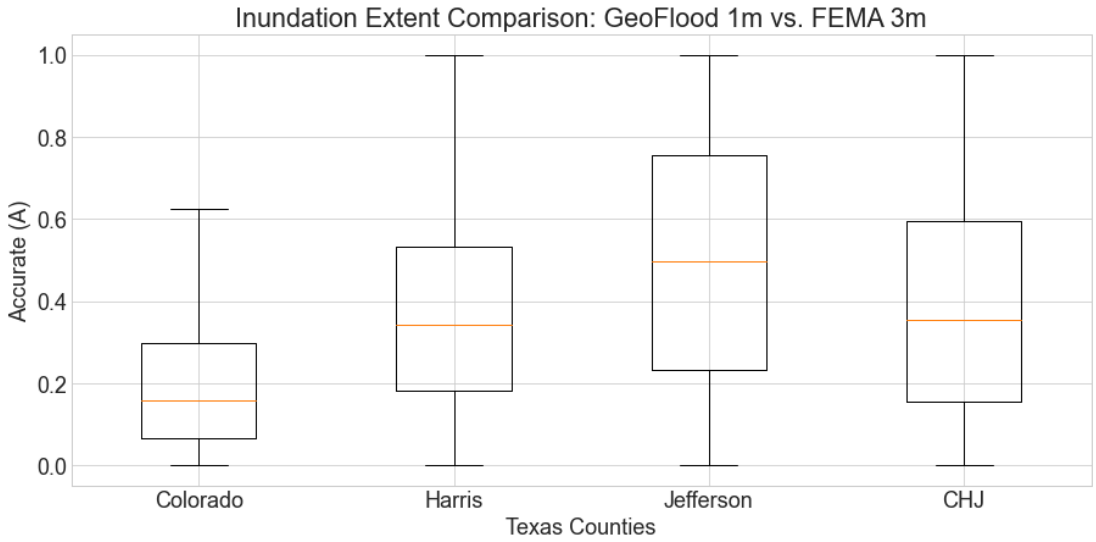


Figure 5.19: Inundation extent comparison boxplot for Accurate (A). The accurate metric is the percentage of intersecting GeoFlood 1-meter and FEMA 3-meter inundated area divided by the total inundated area. Accuracy nearer to one indicates greater inundation extent overlap, while accuracy nearer to zero means lesser overlap.

Summary inundation extent statistics for GeoFlood 1-meter versus FEMA 3-meter and HAND 10-meter versus FEMA 3-meter are provided in Tables 5.3 and 5.4, respectively. A quantification of the GeoFlood model inundation extent improvement is provided in the comparison statistics Table 5.5. GeoFlood model improvements are noted in Colorado, Harris, and Jefferson counties for median

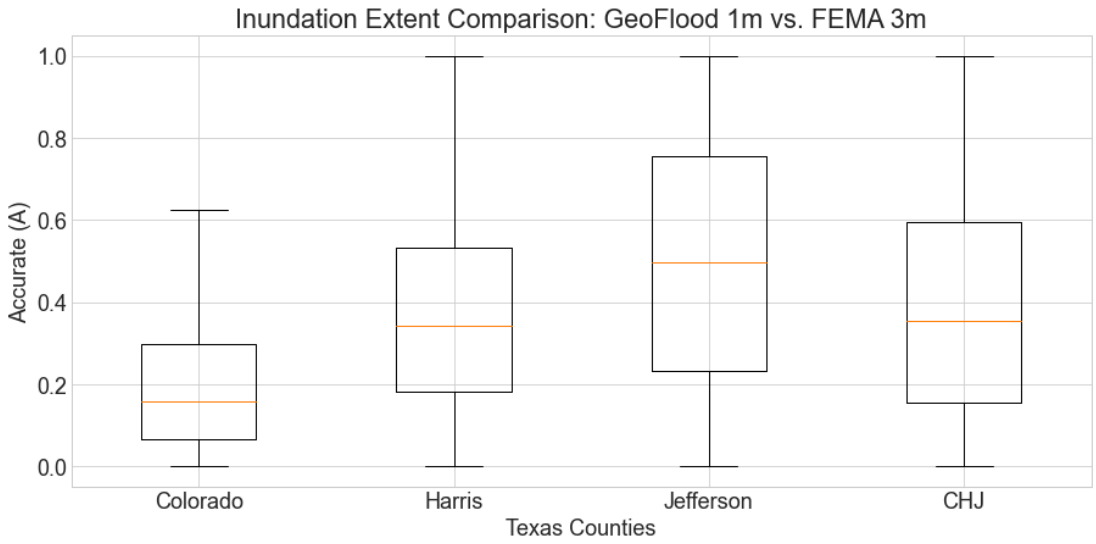


Figure 5.20: Inundation extent comparison boxplot for Accurate (A). The accurate metric is the percentage of intersecting HAND 10-meter and FEMA 3-meter inundated area divided by the total inundated area. Accuracy nearer to one indicates greater inundation extent overlap, while accuracy nearer to zero means lesser overlap.

inundation area ratio (IAR) and accuracy (A). The underestimation reduction and relatively no change in overestimation by the GeoFlood model may imply that a majority of the inundation extent changes are directly correlated with an increase in accuracy, rather than underestimation becoming overestimation and vice versa. Harris county incurred the greatest GeoFlood inundation extent comparison statistics differences versus the FEMA 3-meter reference. Therefore, the GeoFlood workflow improvements, most notably enhancements from the GeoNet extracted channel network, may lead to greater GeoFlood inundation extent performance especially in highly developed regions like Harris county. In contrast, the interquartile ranges for most inundation extent comparison metrics were greater for the GeoFlood 1-meter than the HAND 10-meter model versus the FEMA 3-meter reference. While LiDAR availability and the GeoFlood approach may improve

performance on average, variance may cause better or worse performance on a smaller than NHD catchment scale.

| | Colorado | | Harris | | Jefferson | |
|---|---|---|---|---|---|---|
| Stat | Median | IQR | Median | IQR | Median | IQR |
| Inundation Area Ratio (IAR) | 0.28 | 0.52 | 0.64 | 0.68 | 0.74 | 0.60 |
| Accurate (A) | 0.16 | 0.23 | 0.34 | 0.35 | 0.50 | 0.52 |
| Underestimate (U) | 0.74 | 0.44 | 0.45 | 0.51 | 0.31 | 0.52 |
| Overestimate (O) | 0.01 | 0.11 | 0.10 | 0.24 | 0.01 | 0.14 |

Table 5.3: GeoFlood 1-meter versus FEMA 3-meter inundation extent comparison statistic summary. IQR is the interquartile range descriptive statistic.

| | Colorado | | Harris | | Jefferson | |
|---|---|---|---|---|---|---|
| Stat | Median | IQR | Median | IQR | Median | IQR |
| Inundation Area Ratio (IAR) | 0.15 | 0.31 | 0.33 | 0.47 | 0.65 | 0.63 |
| Accurate (A) | 0.10 | 0.13 | 0.21 | 0.28 | 0.44 | 0.52 |
| Underestimate (U) | 0.85 | 0.26 | 0.69 | 0.40 | 0.40 | 0.55 |
| Overestimate (O) | 0.00 | 0.07 | 0.03 | 0.12 | 0.01 | 0.12 |

Table 5.4: HAND 10-meter versus FEMA 3-meter inundation extent comparison statistic summary. IQR is the interquartile range descriptive statistic.

### 5.2.2 Inundation Depth Comparison

Inundation depth comparisons for root mean squared error (RMSE) and mean error (ME) between the GeoFlood 1-meter model and FEMA 3-meter reference are provided in Figure 5.21 and Figure 5.22, respectively. The medians and interquartile ranges for the depth comparison statistics are shown in Table 5.6 for GeoFlood 1-meter and Table 5.7 for HAND 10-meter. The higher relief terrain and relatively steeper slopes of Colorado county may contribute to its greater median RMSE and RMSE interquartile range versus Harris, and Jefferson counties. Concurrently, similar trends may explain the higher median mean error and mean

| | Colorado | | Harris | | Jefferson | |
|---|---|---|---|---|---|---|
| abs(Stat Difference) | Median | IQR | Median | IQR | Median | IQR |
| Inundation Area Ratio (IAR) | **0.13** | *0.21* | **0.31** | *0.22* | **0.09** | **0.03** |
| Accurate (A) | **0.06** | *0.10* | **0.13** | *0.07* | **0.06** | *0.01* |
| Underestimate (U) | **0.11** | *0.18* | **0.25** | *0.11* | **0.09** | **0.02** |
| Overestimate (O) | 0.00 | *0.04* | *0.07* | *0.12* | 0.00 | *0.02* |

Table 5.5: GeoFlood 1-meter versus FEMA 3-meter inundation extent comparison statistics minus HAND 10-meter versus FEMA 3-meter inundation extent comparison statistics. IQR is the interquartile range descriptive statistic. **Bold** statistical difference values indicate HRT performance improvements, while *italic* values suggest a reduction in performance from the HRT model. All values reported as absolute value of the statistical differences.

error interquartile range for Colorado county versus Harris and Jefferson counties. Median mean errors for the GeoFlood 1-meter model versus the FEMA 3-meter reference are near zero for Harris county at -0.22 meters and Jefferson county at 0.05 meters. Median mean errors near zero are significant because this may indicate satisfactory inundation depth performance for the GeoFlood 1-meter workflow.

| | Colorado | | Harris | | Jefferson | |
|---|---|---|---|---|---|---|
| Stat | Median | IQR | Median | IQR | Median | IQR |
| RMSE [m] | 3.10 | 4.83 | 1.54 | 1.88 | 1.70 | 2.39 |
| MAE [m] | 2.74 | 4.76 | 1.14 | 1.67 | 1.40 | 2.10 |
| ME [m] | -2.56 | 5.01 | -0.22 | 1.46 | 0.05 | 2.23 |

Table 5.6: GeoFlood 1-meter versus FEMA 3-meter inundation depth comparison statistic summary. RMSE, MAE, and ME are the root mean squared error, mean absolute error, and mean error inundation depth comparison metrics, respectively. RMSE, MAE, and ME are computed in meters.

GeoFlood 1-meter and HAND 10-meter models versus the FEMA 3-meter reference inundation depth comparative performance improvements are shown in Table 5.8. The GeoFlood workflow improves average inundation depth performance by 20.5% for median RMSE and 17.2% for median MAE in Colorado and

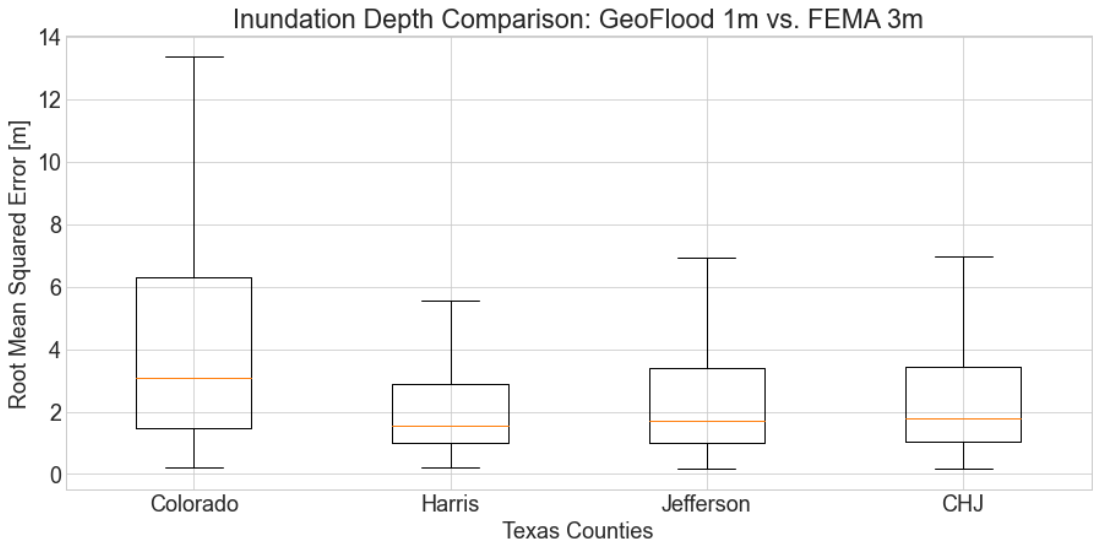


Figure 5.21: Inundation depth comparison boxplot for Root Mean Squared Error (RMSE) for GeoFlood 1-meter versus FEMA 3-meter. RMSE measures the average magnitude of the errors using the quadratic scoring rule. A greater RMSE indicates larger variance in inundation depth, whereas smaller RMSEs are associated with lesser depth variance. CHJ refers to the aggregate results from Colorado, Harris, and Jefferson county. RMSE, MAE, and ME are the root mean squared error, mean absolute error, and mean error inundation depth comparison metrics, respectively. RMSE, MAE, and ME are computed in meters.

| | Colorado | | Harris | | Jefferson | |
|---|---|---|---|---|---|---|
| Stat | Median | IQR | Median | IQR | Median | IQR |
| RMSE [m] | 3.90 | 6.07 | 1.86 | 2.08 | 1.50 | 1.81 |
| MAE [m] | 3.67 | 5.85 | 1.49 | 2.03 | 1.26 | 1.65 |
| ME [m] | -3.57 | 5.82 | -0.85 | 2.00 | -0.47 | 1.72 |

Table 5.7: HAND 10-meter versus FEMA 3-meter inundation depth comparison statistic summary. RMSE, MAE, and ME are the root mean squared error, mean absolute error, and mean error inundation depth comparison metrics, respectively. RMSE, MAE, and ME are computed in meters.

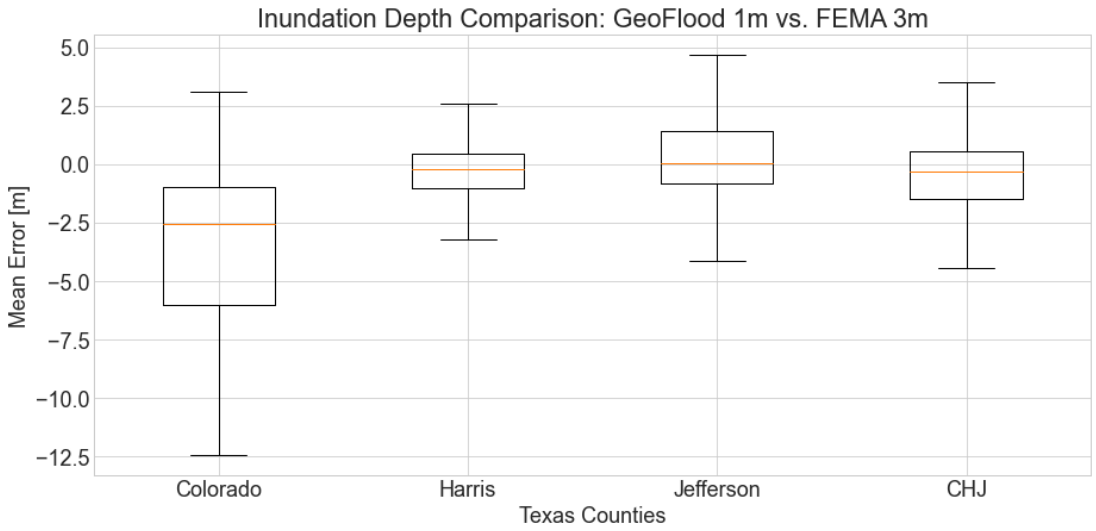


Figure 5.22: Inundation depth comparison boxplot for Mean Error (ME) for GeoFlood 1-meter versus FEMA 3-meter. Mean error calculates the average error while retaining their sign. A positive ME means the GeoFlood 1-meter model tends to overestimate, while a negative sign suggests underestimation. A ME near zero indicates negligible deviance in inundation depth when averaged across the NHD catchment. CHJ refers to the aggregate results from Colorado, Harris, and Jefferson county. RMSE, MAE, and ME are the root mean squared error, mean absolute error, and mean error inundation depth comparison metrics, respectively. RMSE, MAE, and ME are computed in meters.

Harris counties, respectively. The GeoFlood 1-meter workflow shows a 13.3% and 11.1% decrease in performance for the RMSE and MAE inundation depth metrics for Jefferson county. Median mean error was reduced by 28.3%, 75.1%, and 89.4% for Colorado, Harris, and Jefferson counties, respectively. The general decreases in RMSE, MAE, and ME may imply that the GeoFlood workflow offers significantly better inundation depth performance versus conventional HAND methods. The interquartile range narrowed across all inundation depth comparison metrics for Colorado and Harris counties. This may suggest that the GeoFlood workflow offers better performance via lower inundation depth variance in counties with appreciable relief and dense development. Jefferson county shows an overall increase in interquartile range for the GeoFlood model in all inundation depth comparison metrics. The higher medians and widened IQRs for Jefferson county may be attributed to the greater inundation and lower relief relative to Harris and Colorado counties. Colorado county has the highest median RMSE and RMSE interquartile range for both the 1-meter and 10-meter model comparisons against the FEMA 3-meter Harvey flood depths grid. This may imply that GeoFlood underestimates inundation depth in counties with relatively higher relief and steeper slopes.

The inundation depth comparisons against the USGS Hurricane Harvey High Water Marks (HWMs) are shown in Table 5.9 for the FEMA 3-meter reference, HAND 10-meter model, and GeoFlood 1-meter model. Of the 831 USGS HWMs selected for analysis, 36.8% locations were inundated with either the FEMA reference, 10-meter model, or 1-meter model. A "hit" is a point location with an inundation depth from the USGS HWM and the reference or model. The percentage of hits for the FEMA 3-meter reference, HAND 10-meter model, and GeoFlood 1-meter model were 27.9%, 15.9%, and 21.2%, respectively. This suggests that

| | Colorado | | Harris | | Jefferson | |
|---|---|---|---|---|---|---|
| abs(Stat Difference) | Median | IQR | Median | IQR | Median | IQR |
| RMSE [m] | **0.80** | **1.24** | **0.32** | **0.20** | *0.20* | *0.59* |
| MAE [m] | **0.93** | **1.08** | **0.34** | **0.36** | *0.14* | *0.45* |
| ME [m] | **1.01** | **0.82** | **0.63** | **0.53** | **0.52** | *0.51* |

Table 5.8: GeoFlood 1-meter versus FEMA 3-meter inundation depth comparison statistics minus the HAND 10-meter versus FEMA 3-meter inundation depth comparison statistics. IQR is the interquartile range descriptive statistic. **Bold** statistical difference values indicate GeoFlood performance improvements, while *italic* values suggest a reduction in performance. All values reported as absolute value of the statistical differences. RMSE, MAE, and ME are the root mean squared error, mean absolute error, and mean error inundation depth comparison metrics, respectively. RMSE, MAE, and ME are computed in meters.

the GeoFlood 1-meter workflow provides inundation extent performance improvements versus the HAND 10-meter workflow. Of the 306 selected HWM points, 36.9% were inundated by both workflows, while 20.5% were inundated only with the GeoFlood 1-meter model and 6.21% were inundated only with the HAND 10-meter model. In congruence with previous analysis, this shows that the GeoFlood model may improve inundation extent performance.

However, the GeoFlood model shows decreased performance for all inundation depth comparison metrics in both counties analyzed. The root mean squared error and mean error was 60.4% and 147% greater, respectively, for the GeoFlood 1-meter model versus the HAND 10-meter model comparison. Figure 5.23 shows the Kernel Density Estimate (kde) plots for the FEMA 3-meter reference, HAND 10-meter model, and GeoFlood 1-meter inundation depth comparisons versus the USGS HWMs. The FEMA 3-meter inundation depths appear to be better correlated with the USGS HWMs than the GeoFlood and HAND workflows. The spread of the GeoFlood 1-meter inundation depth kde plot is greater than the HAND 10-

meter. Why inundation depth performance may have declined in the comparison against the USGS HWMs in contrast to the FEMA 3-meter comparison will be explored in Section 5.3.

| | Harris County | | | Jefferson County | | |
|---|---|---|---|---|---|---|
| | FEMA 3m | HAND 10m | GF 1m | FEMA 3m | HAND 10m | GF 1m |
| RMSE [m] | 0.77 | 1.85 | 2.41 | 0.92 | 1.51 | 3.72 |
| MAE [m] | 0.42 | 1.26 | 1.80 | 0.58 | 1.21 | 2.10 |
| ME [m] | 0.25 | 0.86 | 1.69 | 0.30 | 0.25 | 1.53 |

Table 5.9: Inundation depth comparison statistics versus the USGS Hurricane Harvey high water marks (HWMs). FEMA 3m refers to the FEMA 3-meter Harvey flood depths grid reference. HAND 10m refers to the HAND 10-meter model. GF 1m refers to the GeoFlood 1-meter model. RMSE, MAE, and ME are the root mean squared error, mean absolute error, and mean error inundation depth comparison metrics, respectively. RMSE, MAE, and ME are computed in meters.

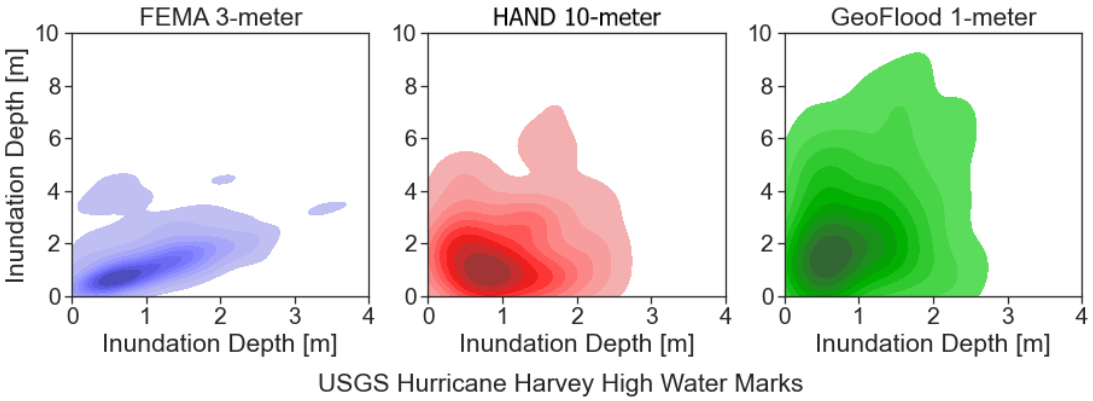


Figure 5.23: Kernel Density Estimate plots for FEMA 3-meter, HAND 10-meter, and GeoFlood 1-meter inundation depths on the ordinates versus the USGS Hurricane Harvey high water marks on the abscissa.

### 5.2.3 Terrain Characteristics

Unlike the previous statistical and geospatial correlations, some relationships are more difficult to discern. Figure 5.24 shows the choropleth map for the GeoFlood

1-meter to FEMA 3-meter accuracy inundation extent comparison metric in Harris county. Previous analysis for the GeoFlood 1-meter to HAND 10-meter model comparison showed higher accuracy near channels with high Strahler stream orders. However, the lack of geospatial relationships for inundation extent comparison metrics are apparent in Harris county. The lack of geospatial patterns may be due to Houston's high-density development including residential and commercial infrastructure, man-made conveyance channels, and abundant roadways. In addition to the lack of geospatial patterns, there was an absence of relationships to terrain characteristics including relief, distance to the Gulf of Mexico, catchment area, and stream length.

### 5.2.4 Channel Characteristics

Figure 5.25 shows the Kernel Density Estimation and histograms for the GeoFlood 1-meter to FEMA 3-meter accuracy inundation extent metric versus the NHD flowline. The accuracy for the inundation extent comparison in Colorado, Harris, and Jefferson counties is centered between 0.1 and 0.5, while the NHD flowline slopes are between 0.00001 and 0.0015. Inundation extent overlap, as quantified by the accurate metric, between the Geoflood 1-meter model and FEMA 3-meter flood depths grid is greatest near a slope of 0.00075.

The Kernel Density Estimation for inundation depth mean error versus NHD flowline slope is shown in Figure 5.26. The inundation depth difference is centered around zero as exhibited by the mean error histogram on the ordinate. The coefficient of skewness of -1.53 indicates a left-tailed distribution of mean errors. The tendency for negative mean errors indicates that the GeoFlood 1-meter model underestimates inundation depth as compared to the FEMA 3-meter

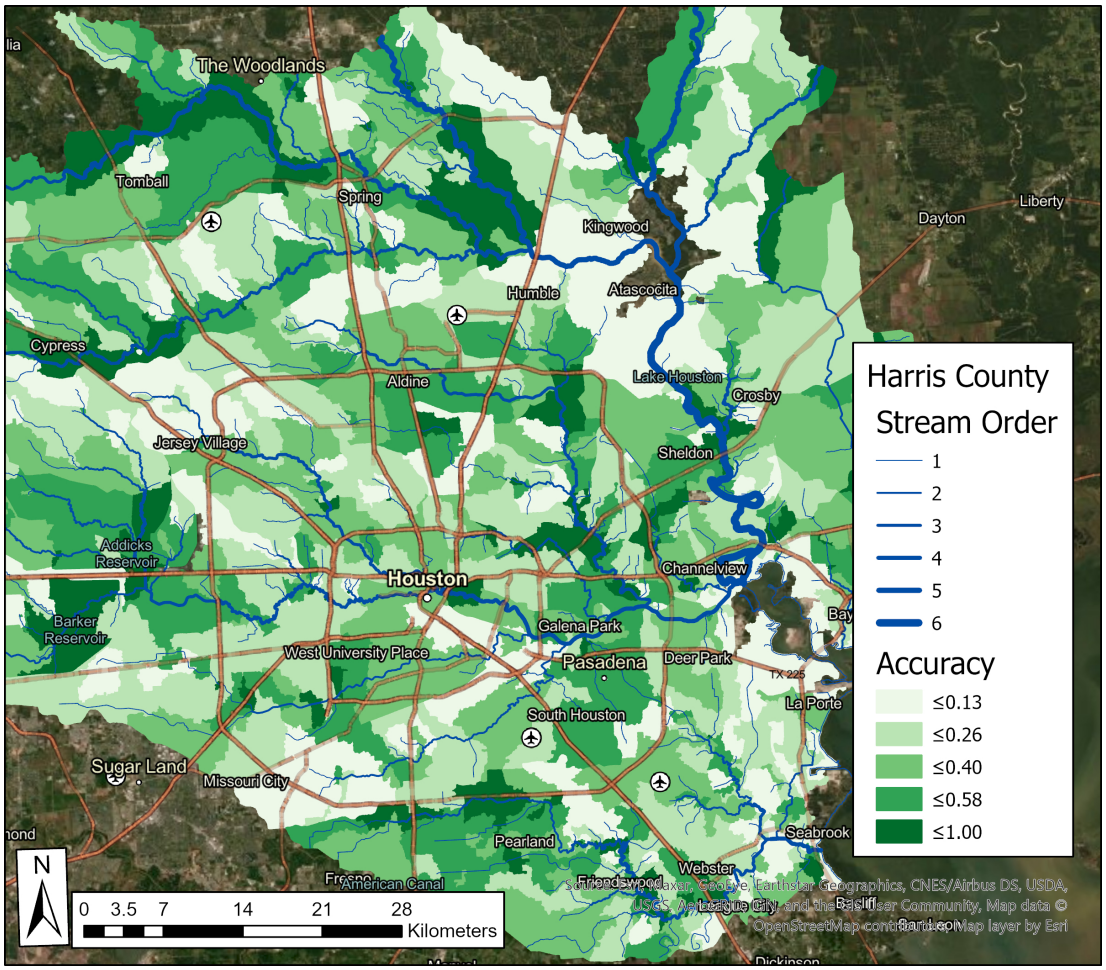


Figure 5.24: GeoFlood 1-meter versus FEMA 3-meter accuracy choropleth map for Harris County. Strahler stream orders represented by blue graduated NHDPlus MR flowlines. Missing catchment data is due to geospatial incompatibilities between the model and reference which may cause errors in the statistical comparison.

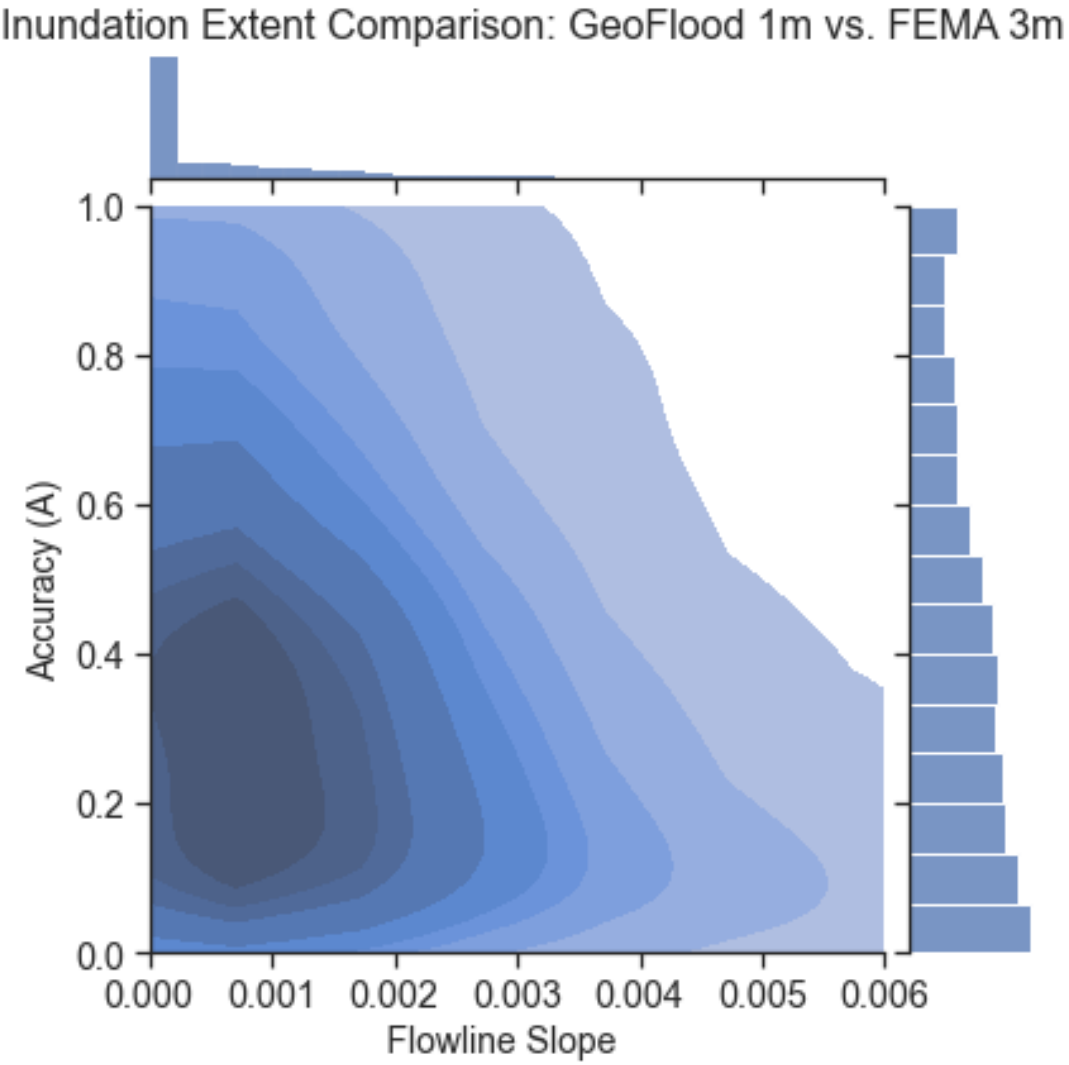


Figure 5.25: Accurate inundation extent comparison metric kernel density estimate and histogram for the GeoFlood 1-meter model versus the FEMA 3-meter reference. The accurate metric is the percentage of intersecting GeoFlood 1-meter and FEMA 3-meter inundated area divided by the total inundated area. Accuracy nearer to one indicates greater inundation extent overlap, while accuracy nearer to zero means lesser overlap.

reference. However, most of the negative mean errors occur in Colorado county as shown in Table 5.6.

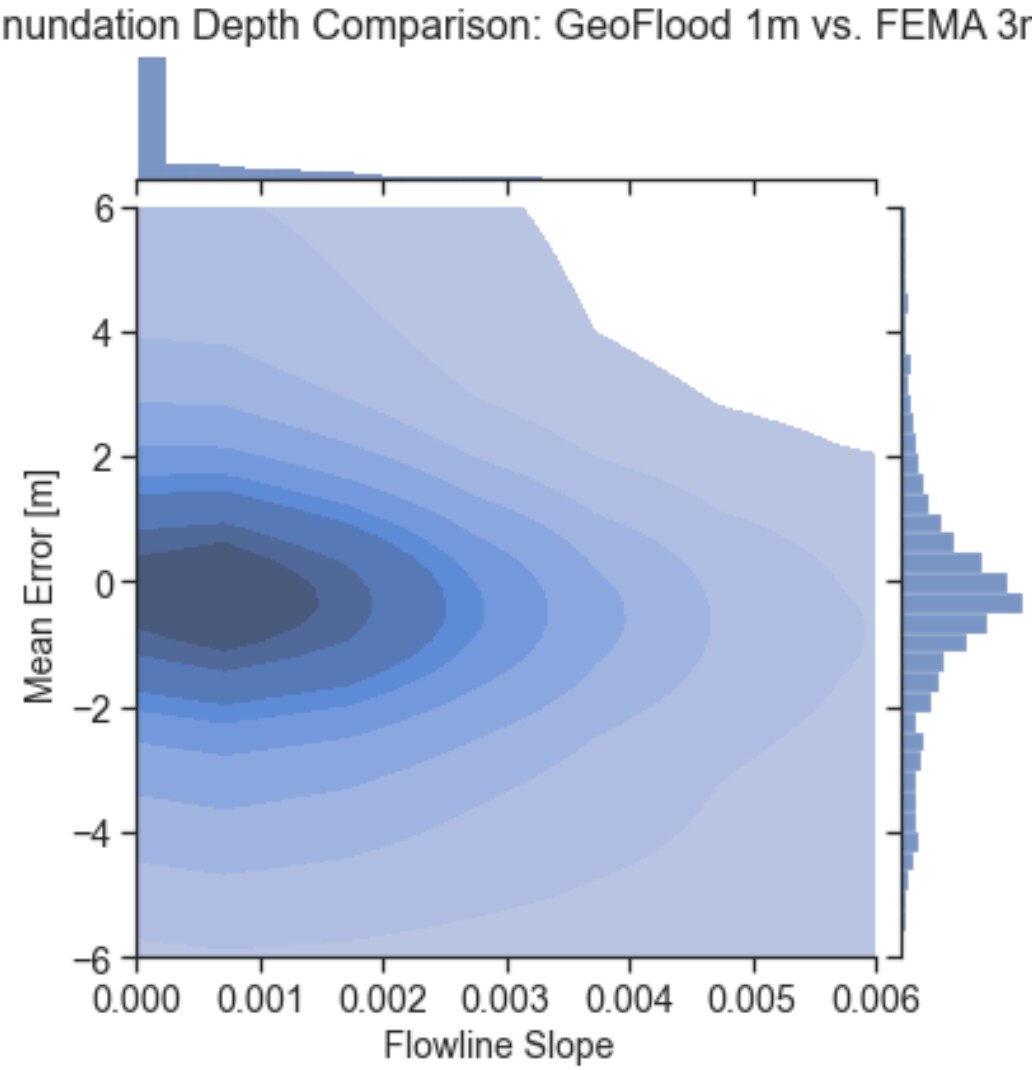


Figure 5.26: Mean error inundation depth comparison versus NHD flowline slope between GeoFlood 1-meter model and FEMA 3-meter flood depths grid.

The GeoFlood 1-meter to FEMA 3-meter root mean squared error choropleth map for Jefferson county is shown in Figure 5.27. Similar to the Colorado county inundation depth comparison between GeoFlood 1-meter and HAND

10-meter, inundation depth differences appear to gravitate toward high Strahler stream order channels. Additionally, RMSE appears to be lower in NHD catchments with channel heads. RMSE is particularly high along the Neches River, Taylor Bayou, and in the flat coastal region of south western Jefferson county. High RMSEs appear to be correlated with regions labeled as NHD waterbodies.

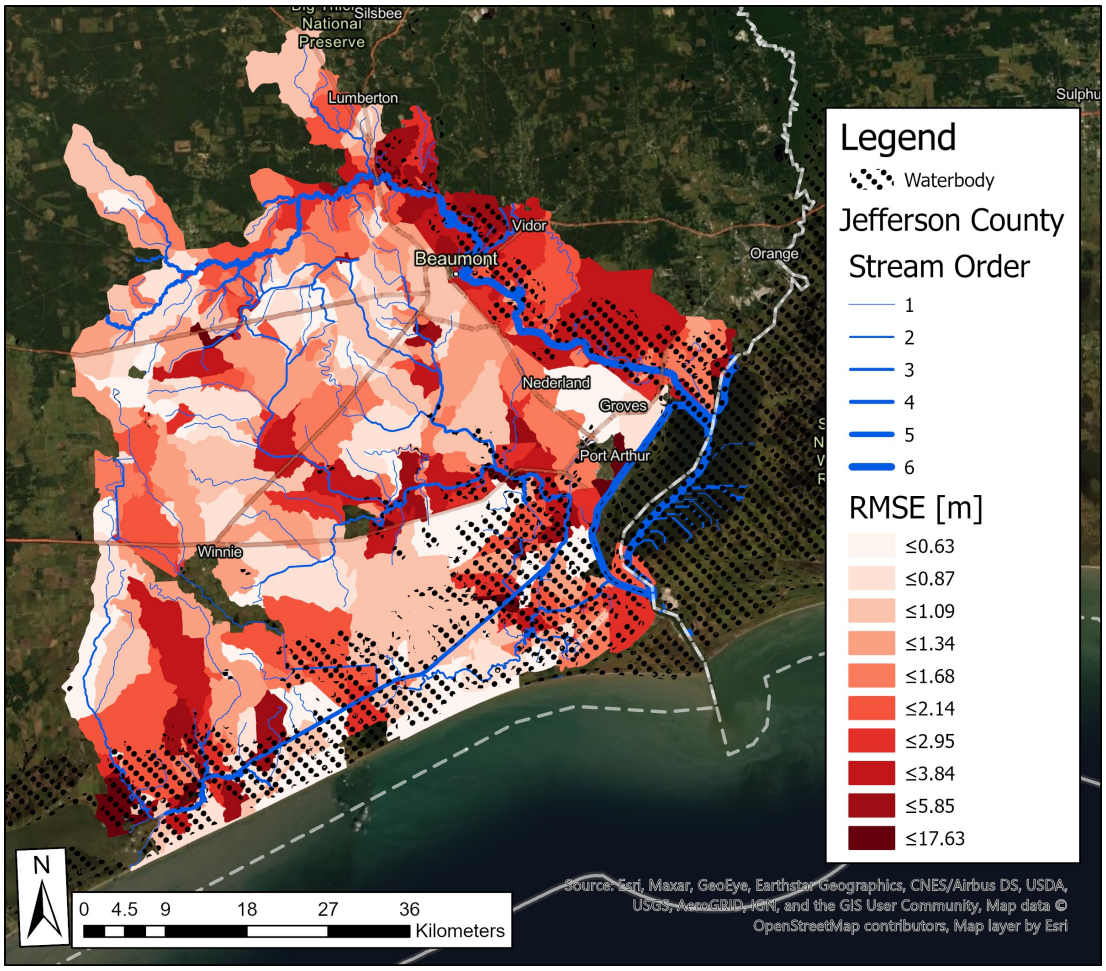


Figure 5.27: GeoFlood 1-meter versus FEMA 3-meter root mean square error choropleth map for Jefferson County. Strahler stream orders are represented by blue graduated NHDPlus MR flowlines. NHD designated waterbodies are shown as a black hatched dot pattern. Missing catchment data is due to geospatial incompatibilities between the model and reference which may have caused errors in the statistical comparison.

## 5.3 GeoFlood Limitations

### 5.3.1 Segment Catchment Filling

An infrequent issue with the hydraulic geometry estimation and segment catchment area has been identified in both the GeoFlood 1-meter and HAND 10-meter workflows. A segment catchment is the local drainage basin for each channel segment. The channel hydraulic geometry and synthetic rating curve are derived from the segment catchment scale. In some cases, the accuracy of the hydraulic geometry is limited by the overall size of the segment catchment. Hydraulic geometry values begin repeating, simulating a "bathtub" effect, once the surface area of the segment catchment area has been maximized. The hydraulic geometry is considered accurate up to the maximum surface area threshold as indicated by italicized data row in 5.10. Stage heights above this maximum threshold will inaccurately predict inundation depth within the segment catchment.

Figure 5.28 shows an example filled segment catchment in Jefferson county HUC12 120200070201. The maximum Hurricane Harvey flowrate of 1991 $m^3/s$ was assigned to the 350 meter channel segment in HYDROID 36. The discharge of 1991 cubic meters per second corresponds to the stage height of 14.12 meters in the hydraulic geometry table, shown as bold text in Table 5.10. The "bathtub" effect is apparent in Figure 5.28 where all inundation depths inside the segment catchment are the maximum 14.12 meters and adjacent pixels just outside the filled segment catchment show depths between 2 and 4 meters.

Segment catchment filling occurs more frequently in the GeoFlood 1-meter workflow due to increased terrain resolution. A greater number of segment catchments are generated at finer spatial resolution. This suggests higher resolution

terrains can more accurately represent subtle drainage basin features that were unrecognizable in the medium resolution workflow. The increased number of drainage basins is a response to the increased density of high resolution features. Additionally, channel segments less than 1000 meters in length may contribute to a higher percentage of filled segment catchments. Shorter channel segments are correlated with smaller segment catchments. Some channel segments less than 1000 meters are NHD flowlines that were not segmented.

| **Stage [m]** | **Surface Area [$m^2$]** | **Inun Area Ratio** | **Discharge [$m^3/s$]** |
|---|---|---|---|
| 1.8 | 77065 | 0.999715 | 25.71 |
| 1.9 | 77084 | 0.99996 | 30.24 |
| *2* | *77087* | *1.0* | *35.05* |
| 2.1 | 77087 | 1.0 | 40.15 |
| ... | ... | ... | ... |
| **14.12** | **77087** | **1.0** | **1991** |

Table 5.10: Hydraulic geometry table for segment catchment HYDROID 36 in Jefferson HUC12 120200070201. Stage, surface area, and discharge are measured in meters, square meters, and cubic meters per second, respectively. The three dots represent a break in the incremental dataset.

Figure 5.29 shows USGS High Water Mark ID 22280 located within a GeoFlood 1-meter filled segment catchment. The inundation depth difference is 18 times greater for the GeoFlood 1-meter model versus the HAND 10-meter model. The HAND 10-meter model segment catchment area for this channel segment was large enough to accurately estimate the hydraulic geometry for a discharge of 351 $m^3/s$. Unfortunately, the hydraulic geometry for the GeoFlood 1-meter model simulated the "bathtub" effect for the selected discharge and corresponding stage height of 13.20 meters. Artificial ponding behind the roadway, a short channel segment, and corresponding small segment catchment area are the likely causes for this scenario's "bathtub" effect. The filled segment catchments, especially for

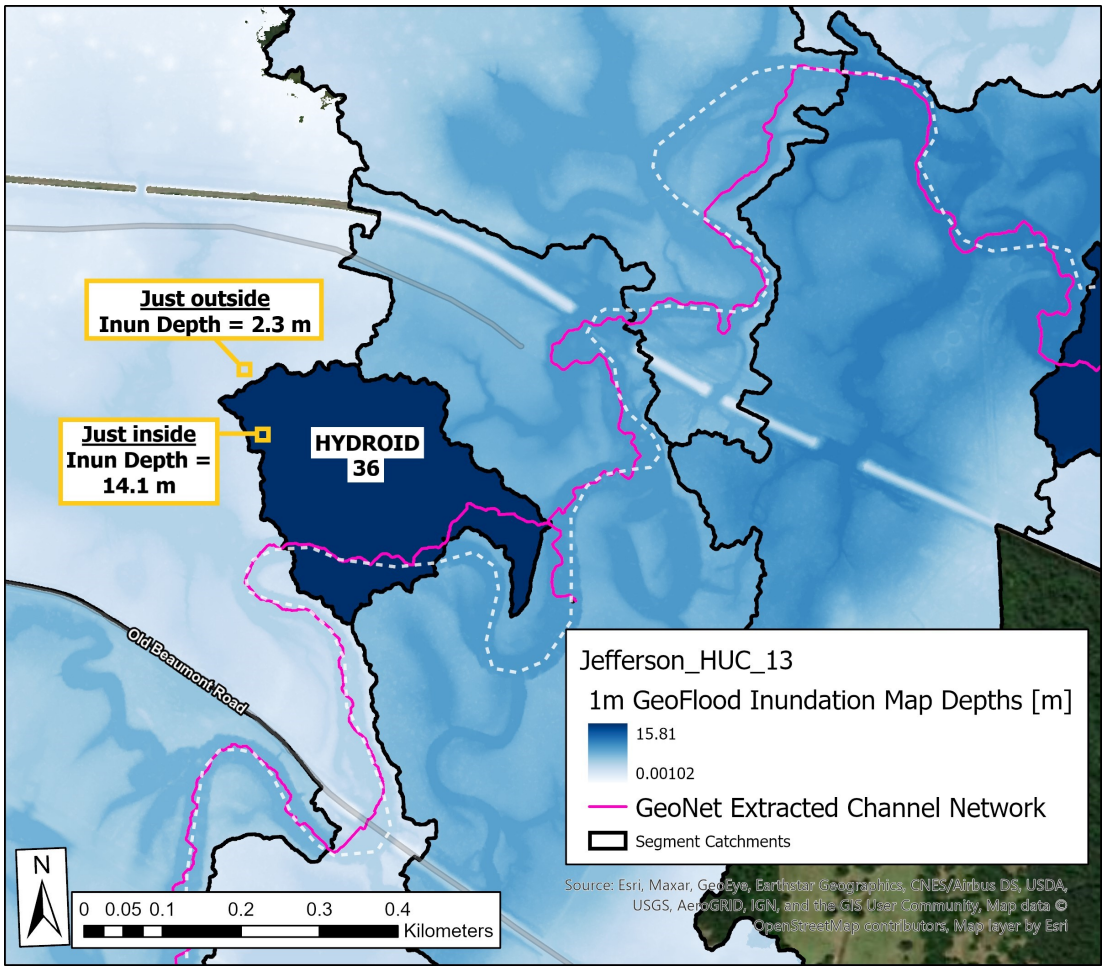


Figure 5.28: Filled segment catchment HYDROID 36 in Jefferson HUC12 120200070201. COMID for the channel segment is 1523925. Differences between 1-meter GeoFlood inundation depth are extreme at the edge of the filled catchment.

the GeoFlood model, frequently intersect the USGS HWMs, thus causing inflated inundation depths. Filled segment catchments likely skewed the inundation depth metric comparisons against the USGS Hurricane Harvey High Water Marks. The bias caused by the filled segment catchments likely caused the observed decrease in inundation depth performance at 1-meter resolution as shown in Table 5.9.

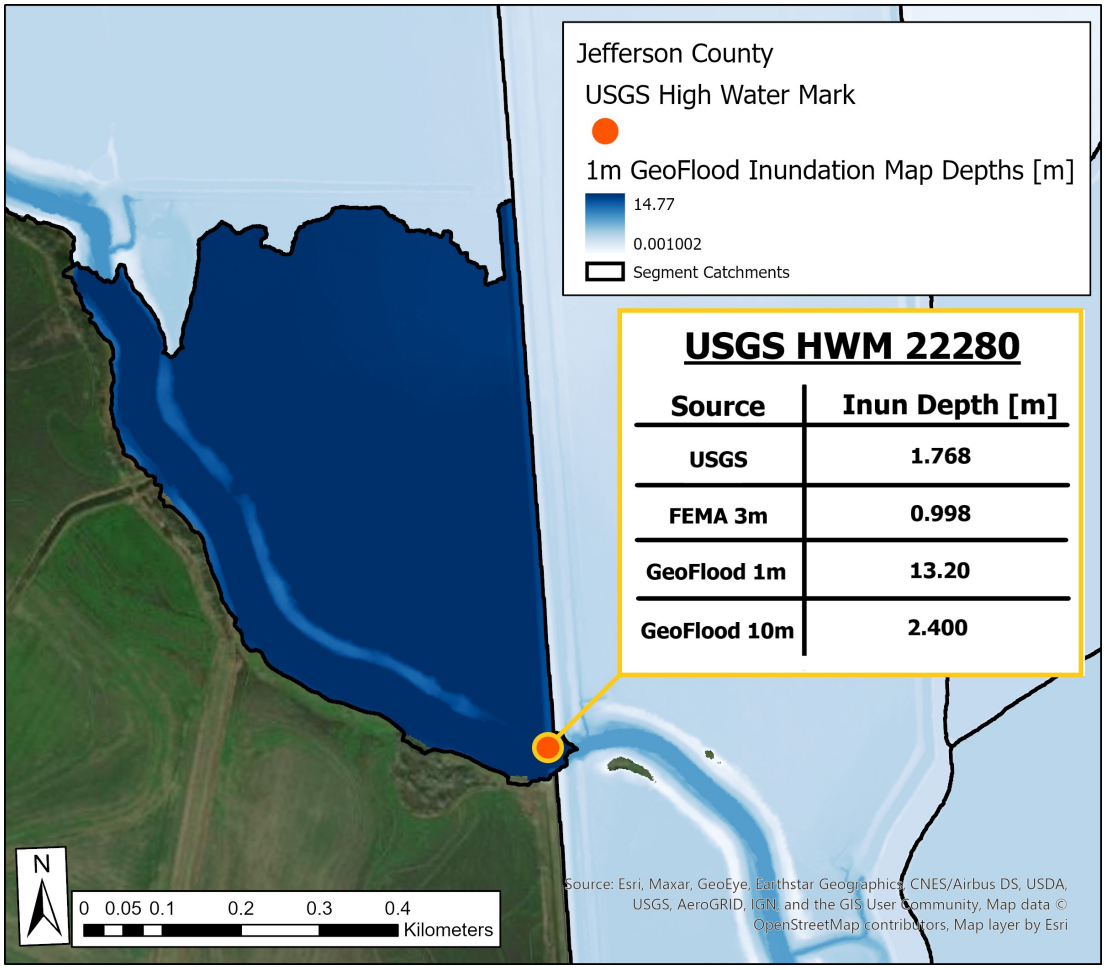


Figure 5.29: USGS Hurricane Harvey High Water Mark within filled segment catchment in Jefferson HUC12 120402020300.

### 5.3.2 Pluvial and Coastal Flooding

The HAND-NWM model structure as presented in this study is only capable of simulating fluvial flood hazard. Compound flood hazards from precipitation and storm surge, otherwise known as pluvial and coastal flooding, are not captured. Hurricane Harvey was predominantly a pluvial event where flood rise was attributed to intense local rainfall, rather than flooding from riverbank overtopping. A two-dimensional hydrodynamic model with fluvial, pluvial, and coastal flood components simulated 78% of the Hurricane Harvey benchmark flood extent and was within 1 meter of the USGS observed HWMs (Wing et. al., 2019). While the GeoFlood model takes only seconds to compute with NWM forecasted outputs, computationally intensive 2D hydrodynamic models often outperform in flood inundation extent and depth simulations. Additionally, increasing hurricane intensity from climate change and sea level rise from global warming may emphasize the importance of compound fluvial, pluvial, and coastal modeling of flood hazards.

# Chapter 6: Discussion

The following chapter will address the research questions proposed in Section 1.

## 6.1 *Which terrain characteristics significantly impact GeoFlood's performance?*

The most significant terrain characteristic impacting Geoflood's performance was topographic relief. A majority of inundation extent and depth improvements were strongly correlated to terrain relief. For example, inundation area ratios and accuracy inundation extent metrics for the GeoFlood 1-meter to HAND 10-meter model comparison were greater and had higher variance in low relief counties. The GeoFlood 1-meter inundation extent is less extensive than HAND 10-meter in areas with high relief. Since 1-meter DEMs more correctly depict the terrain, especially in high relief regions, streamflows are more confined to the channel. In contrast, terrain relief was less significant for GeoFlood 1-meter to HAND 10-meter inundation depth comparisons. Workflow errors such as the "bathtub" effect may limit our ability to make definitive conclusions about inundation depth comparisons. The Root Mean Squared Errors (RMSEs), Mean Average Errors (MAEs), and Mean Errors (MEs) show greater overall GeoFlood 1-meter inundation depths versus HAND 10-meter for all counties, irrespective of NHD catchment scale terrain relief. The GeoFlood 1-meter to HAND 10-meter RMSE versus relief analysis reinforced the hypothesis that inundation depth differences are greatest in counties with low relief and intense fluvial flooding.

The stream length terrain characteristic suggests that regions with shorter lengths experience greater depth differences. Geospatially, overlap between the GeoFlood and HAND models was greatest near channels with higher Strahler stream orders, while overlap was lower in NHD catchments containing channel heads.

When the scope of focus is reduced to a single county, like Uvalde, statistical comparisons are less likely to be skewed by the magnitude of flowrates due to a specific storm event. Therefore, Uvalde county shows an unencumbered view of geospatial trends for the Geoflood 1-meter versus HAND 10-meter comparison. Inundation extent and depth analysis conducted in Uvalde county showed geospatial patterns as a function of terrain slope. The HAND 10-meter model overestimates inundation extent more frequently in the higher relief terrain of northern Uvalde county whereas higher accuracy and HAND underestimation were more significant in the lower relief region of southern Uvalde county. Additionally, inundation depth differences are greater in the high relief terrain of Uvalde county versus the rolling, hilly terrain of southern Uvalde.

High-resolution terrain and GeoNet extracted network performance enhancements were supported by the GeoFlood model versus FEMA reference statistical comparison results. For example, accuracy improvements for the GeoFlood model translated to greater inundation extent overlap versus the FEMA Harvey flood depths grid. The inundation extent improvements brought by the GeoFlood model were greatest in Harris county, which may suggest that GeoFlood 1-meter performance is better than HAND 10-meter in low relief, highly developed regions with abundant man-made infrastructure. While median inundation extent performance metrics improved overall, often the variance of these same metrics increased with

the introduction of LiDAR and the GeoFlood workflow.

Inundation depth comparison metrics showed a similar performance improvement trend. The RMSEs, MAEs, and MEs showed improvement in Colorado and Harris county, as well as for the mean error in Jefferson county. Colorado county, with the highest relief relative to Harris and Jefferson, showed the greatest RMSE, MAE, and ME versus the FEMA 3-meter reference. The higher relief terrain of Colorado county may have caused increased underestimation by both Geoflood and HAND models. However, Colorado county also showed the greatest inundation depth performance improvement at 1-meter resolution. Geospatial patterns of terrain characteristic correlations were difficult to ascertain. High-density development including residential and commerical infrastructure, roadways, bridges, and conveyance channels appeared to reduce the significance of terrain correlations with inundation extent and depth comparison metrics.

Although computed and analyzed, relationships to the catchment area and distance from the Gulf of Mexico were less significant. Relief was a better substitute for the distance from the Gulf of Mexico, while stream length was better represented by the NHD catchment area. Future work might explore the relationship of distance from the inundated pixel to its nearest drainage path.

## 6.2 *Which channel characteristics significantly impact GeoFlood's performance?*

The channel characteristic with the most significant correlation to GeoFlood's improvement were flowline slope and Strahler stream order. Similar to the previous analysis, the inundation area ratio had the highest variance in regions with low slope. Inundation extent overlap, in terms of GeoFlood 1-meter to HAND 10-

meter accuracy, decreases as channel slope increases. Congruently, overstimation by the HAND model versus the GeoFlood model increases with increasing NHD flowline slope. Median accuracy is greatest for Strahler stream orders four and five, while lesser for the remaining stream orders. The relationship between accuracy, underestimation, and overestimation is exemplified by the relationship between median accuracy and Strahler stream order. As a reminder, the accurate (A), underestimate (U), and overestimate (O) metrics sum to one. Therefore, if each metric shows an increasing or decreasing trend versus channel slope, there must be a point at which they cross each other. The intersection point indicates the channel slope (0.00075), and stream orders (4 and 5), at which GeoFlood 1-meter to HAND 10-meter accuracy is maximized while underestimation and overestimation are minimized. The reduction in median accuracy for stream order six is due to the increase in HAND 10-meter underestimation as compared to the GeoFlood 1-meter model. In contrast, the decreasing median accuracy from stream orders three to one indicates an increasing tendency for HAND 10-meter overestimation. Overall, the improvements provided by high-resolution terrain are most significant across the majority of Strahler stream orders.

Inundation depth differences between the GeoFlood 1-meter and HAND 10-meter models are strongly correlated to channel slope. The RMSE versus NHD flowline slope relationship shows a significant downsloping trend meaning regions with lower slopes tend to have increased inundation depth difference. However, inundation depth metrics between the GeoFlood and HAND models may be poor indicators of GeoFlood performance against the reference. For example, a GeoFlood 1-meter model with a high RMSE versus the HAND 10-meter model may provide better performance because the inundation depth differences are greater. Suppose

a HAND 10-meter model shows poor depth performance versus the FEMA 3-meter reference, while the the GeoFlood 1-meter model shows good depth performance. The RMSE model-to-model comparison metric may be high in this scenario because the GeoFlood 1-meter inundation depth performance was better due to its increased depth difference from the HAND 10-meter model. This is especially significant when considering improvements from the extracted channel network. The improvements from the GeoFlood extracted channel network likely means that the channel centerline more accurately represents the channel thalweg. Therefore, the extracted channel network lies at a lower elevation in the channel bottom versus the NHDPlus MR flowlines. Additionally, the 1-meter resolution DEMs experience lesser smoothing than the 10-meter DEMs. Lesser DEM smoothing leads to lower channel thalweg elevations. The channel centerline elevation differences cause the inundation depth metrics to increase within and near channels, which are reinforced in the statistical analysis as well as geospatial observations. In conclusion, the RMSE versus NHD flowline slope relationship reinforces greater inundation depth performance in lower relief regions at 1-meter resolution.

Geospatially, inundation depth differences between the GeoFlood model and FEMA flood depths grid are greatest near high Strahler stream order channels and lower near channel heads. Additionally, high RMSEs are often associated with regions intersected by NHD designated waterbodies. This may be due to the difficulty of extracting channel networks within hydroflattened waterbodies.

Relationships to the mean annual flow channel characteristic were less significant. Strahler stream order was determined to be a better proxy for mean annual flow correlations.

## 6.3 *Where does high-resolution terrain improve inundation mapping performance using the GeoFlood workflow?*

High resolution terrain (HRT) most notably improves flood inundation mapping across a majority of Strahler stream orders, as well as in low relief, low slope, and densely developed NHD catchments. Inundation extent and depths metrics, including inundation area ratio, accuracy, RMSE, MAE, and ME indicate GeoFlood performance improvement versus the HAND 10-meter model when compared against the FEMA Hurricane Harvey flood depths grid. Inundation extent performance enhancements had greater significance in the low relief, low slope, and high-density development regions in Harris county. The greatest inundation depth performance increase was in higher relief Colorado county.

Two primary hypothesis may explain why GeoFlood provides increased performance. First, improved terrain resolution provides increased HAND and hydraulic geometry accuracy. Features such as two-lane roadways, culverts, individual residential homes, ditches, and man-made water conveyance features appear in the 1-meter resolution terrain whereas their presence is poorly represented in the 10-meter resolution terrain. As such, the GeoFlood HAND rasters and hydraulic geometry for each channel segment more accurately detect finer scale features. The inundation extent performance increases in Harris county, as displayed in Table 5.5, which bolsters this first hypothesis. Second, the 1-meter GeoNet extracted channel network more accurately represents the channel thalweg. Therefore, in higher relief terrain, elevations differences from the NHDPlus MR flowlines to the GeoNet extract channel network are likely greater, thus, allowing more capacity for improvement. The inundation depth performance increases in Colorado county,

as shown in Table 5.8, support this second hypothesis.

## 6.4 *Where is the HAND approach and related estimation of hydraulic geometry appropriate?*

The HAND approach and estimation of hydraulic geometry approach is most appropriate where high-resolution terrain is available and a sensitivity analysis can be performed on the results. The GeoNet and GeoFlood workflow includes modifiable parameters that affect the final inundation mapping results. This study focused on developing the most robust GeoFlood workflow applied to seven counties, 266 HUC12s, 4999 channels, and 31,938 $km^2$ of study area using a single set of optimized parameters. The median inundation extent accuracy for the GeoFlood comparison versus FEMA 3-meter flood depths grid was 0.353. In contrast, in the GeoFlood performance study conducted by Zheng et. al. (2018a), the study area focused on five creeks within the 892 $km^2$ Onion Creek HUC12 watershed. Zheng et. al. conducted multiple sensitivity analysis on terrain characteristics and roughness coefficients in order to optimize the GeoFlood workflow parameters for the focus area. The fit index used in Zheng et. al. is equivalent to the accurate inundation extent comparison metric in this study. The highest fit index of the GeoFlood extent reached 79% to 87% as compared to the FEMA 100-year floodplain (Zheng et. al., 2018a). Therefore, greater inundation area extent accuracy is probable with study area specific optimization on smaller scales.

Johnson et. al. (2019) tested an unmodified version of a NWM-HAND inundation mapping workflow with NHDPlusV2 medium-resolution flowlines and 10-meter resolution HAND across 54 catchments in eleven US states. Inundation extent accuracy ranged from 19% to 25% when compared against U.S. Flood Inun-

dation Mapping Repository (USFIMR) maps (Johnson et. al., 2019). The roughly equivalent HAND 10-meter workflow in this study showed a median inundation extent accuracy performance of 23.7%, which is congruent with the findings of Johnson et. al. (2019). Additionally, similar hypotheses such as underprediction in lower-order reaches and overprediction in higher-order reaches are shared with this study. Johnson et. al. recommended in the 2019 paper that higher resolution elevation data would produce more sensitive rating curves, especially in areas of low relief. Additionally, spatial misalignment of NHD NHDPlusV2 medium-resolution flowlines can have significant limitations on the accuracy of inundation extent. The inundation extent and depth performance improvements from high-resolution terrain and GeoNet extracted channel network, as shown in this study, reaffirm the conclusions of Johnson et. al..

---

# Chapter 7: Conclusions and Future Work

This study showed that using high resolution terrain data and the GeoFlood workflow improves inundation extent and depth performance. The inundation extent comparison metrics showed a 49% median accuracy performance increase and 30% median underestimation reduction versus the FEMA reference. The RMSE, MAE, and ME inundation depth comparison metrics showed median reductions of 5.3%, 9.2%, and 65% versus the FEMA reference, respectively. The comparison against the USGS HWMs showed opposing trends, however, the segment catchment filling limitation likely biased this inundation depth comparison.

Topographic relief, slope, and Strahler stream order were the most significant indicators for GeoFlood improvement and performance. High resolution terrain improves performance most notably in regions with low slope, low relief, and dense development as well as across a majority of stream orders. Performance improvements from LiDAR data are likely due to enhanced feature detection on finer scales and improved channel centerline delineation. The HAND-NWM inundation mapping approach is most appropriate where high resolution terrain data is available. A sensitivity analysis can be conducted on the modifiable parameters of the GeoFlood workflow to further improve the performance of GeoFlood.

In this study, the GeoFlood workflow changeable parameters, including the roughness coefficients, were optimized for the variety of terrain encountered in the seven Texas counties. Applying this study's exact workflow parameters to create inundation maps in other regions may show roughly equivalent or reduced inundation extent and depth performance.

Future applications of the GeoFlood and NWM integrated workflow should consider the effects of filled segment catchments. A function that identifies filled segment catchments would allow the GeoFlood user to assess the performance of the inundation maps as well as indicate opportunities for parameter optimization. Inundation comparisons from the current 1-meter GeoFlood workflow to a hypothetical workflow with 10-meter HAND and extracted channel networks would separate the effects between channel network improvements and resolution of terrain. Additionally, normalization of precipitation events or reference datasets may improve the comparison significance between distanced regions. The inclusion of pluvial and coastal compound flooding would likely increase GeoFlood's flood inundation extent and depth performance.

Overall, this study supports the integration of high-resolution terrain data into large-scale GeoFlood-NWM applications.

---

# Appendices

# A Raster Comparison Statistics: Code, Examples, and Visualization

## 1-meter vs. 10-meter Inundation Raster Comparison

### Import modules

```
# ArcGIS Pro Arcpy can only be run through the Python installations provided with the ArcGIS Pro license

import arcpy # ArcGIS Pro geographic data analysis, data conversion, data management, and map automation
from arcpy.sa import * # ArcGIS Pro Spatial Analyst
```

```
import numpy as np # Perform numerical operations on multi-dimensional arrays
import pandas as pd # Data analysis
import matplotlib.pyplot as plt # Plotting of rasters and datasets
import matplotlib.patches as pltpatches # Binary legend formatting
import rasterio # Import of geospatial rasters
from osgeo import gdal # Translator library for raster and vector geospatial data formats
import sys # System-specific parameters and functions
import os # Miscellaneous operating system interfaces
import time # Time management
import geopandas as gpd # Geospatial data operations and plotting
import json # Lightweight data interchange format inspired by JavaScript object literal syntax
import folium # Mapping and visualization
import matplotlib.colors as colors # List of named colors supported in matplotlib
```

### ArcGIS Pro: Binary, Conditional, Minus, Diff

```
def BinaryConditionalMinusDiff():
    try:
        # To allow overwriting outputs change overwriteOutput option to True.
        arcpy.env.overwriteOutput = True

        # Check out any necessary licenses.
        arcpy.CheckOutExtension("ImageAnalyst")

        # Letter range
        # [chr(i) for i in range(ord('a'),ord('j'))]

        for Value in range(0,24,1): # define range for HUC12s in County
            arcpy.env.cellSize = "MINOF"
            ProjectName = r"Brazos"
            Mod = r""
            print(ProjectName, Mod, Value)
            InunMapInputDir = r"C:\\Users\\ras6399\\Documents\\NOAA_Research\\Projects\\1mvs10mComparison\\InunMaps"
            BinaryOutputDir = fr"C:\\Users\\ras6399\\Documents\\NOAA_Research\\Projects\\1mvs10mComparison\\Binary\\{ProjectName}"
            ConditionalOutputDir = fr"C:\\Users\\ras6399\\Documents\\NOAA_Research\\Projects\\1mvs10mComparison\\Diff\\DiffExtent\\
            MinusOutputDir = fr"C:\\Users\\ras6399\\Documents\\NOAA_Research\\Projects\\1mvs10mComparison\\Minus\\{ProjectName}"
```

Figure A.1

```
DiffOutputDir = fr"C:\\Users\\ras6399\\Documents\\NOAA_Research\\Projects\\1mvs10mComparison\\Diff\\{ProjectName}"
clip_Value_1m_inunmap_ABSOLUTE_WORST_tif = fr"{InunMapInputDir}\\{ProjectName}_HUC_{Mod}{Value}\\ABSOLUTE_WORST_CASE\\c
print(clip_Value_1m_inunmap_ABSOLUTE_WORST_tif)
clip_Value_10m_absworsttest_tif = fr"{InunMapInputDir}\\{ProjectName}_HUC_{Mod}{Value}\\clip_{Mod}{Value}_10m_absworstt
print(clip_Value_10m_absworsttest_tif)

# Process: Binary
# Convert inundation maps to binary rasters, one for wet pixels, zero for dry pixels
print('Binary started')
outBinary1m = Con(IsNull(Raster(clip_Value_1m_inunmap_ABSOLUTE_WORST_tif)), 0, 1)
outBinary10m = Con(IsNull(Raster(clip_Value_10m_absworsttest_tif)), 0, 1)
print('Binary complete')

Binaryout1m = fr"{BinaryOutputDir}\\clip_{Mod}{Value}_1m_absworst_BinaryExtent.tif"
Binaryout10m = fr"{BinaryOutputDir}\\clip_{Mod}{Value}_10m_absworst_BinaryExtent.tif"
outBinary1m.save(Binaryout1m)
outBinary10m.save(Binaryout10m)
print('Binary saved')

# Process: Conditional
# Convert inundation maps to a combined conditional raster
# 0 = WW, 1 = WD, -1 = DW, -9999 = DD
print('Conditional started')
outConditional = Con((Raster(Binaryout1m) == 1) & (Raster(Binaryout10m) == 1), 0,
                 Con((Raster(Binaryout1m) == 1) & (Raster(Binaryout10m) == 0), 1,
                 Con((Raster(Binaryout1m) == 0) & (Raster(Binaryout10m) == 1), -1,
                 Con((Raster(Binaryout1m) == 0) & (Raster(Binaryout10m) == 0), -9999))))
print('Conditional complete')
conditionalout = fr"{ConditionalOutputDir}\\clip_{Mod}{Value}_absworst_DiffExtent.tif"
outConditional.save(conditionalout)
print('Conditional saved')

# Process: Minus
# 1-meter inundation raster minus 10-meter inundation raster
print('Minus started')
outMinus = Minus(clip_Value_1m_inunmap_ABSOLUTE_WORST_tif, clip_Value_10m_absworsttest_tif)
print('Minus complete')
minusout = fr"{MinusOutputDir}\\clip_{Mod}{Value}_absworst_MinusDepth.tif"
outMinus.save(minusout)
print('Minus saved')

# Process: Diff (Diff)
# Absolute difference between 1-meter inundation map and 10-meter inundation map
print('Diff started')
outDiff = Diff(clip_Value_1m_inunmap_ABSOLUTE_WORST_tif,clip_Value_10m_absworsttest_tif)
print('Diff complete')
diffout = fr"{DiffOutputDir}\\clip_{Value}_absworst_Diff.tif"
outDiff.save(diffout)
print('Diff saved')

print(f'Binary, Conditional, Minus, and Diff complete for {ProjectName} {Mod}{Value}')
```

Figure A.2

```
    except:
        print('Binary, Conditional, Minus, or Diff has failed.')
        print(arcpy.GetMessages())

if __name__ == '__main__':
    # Global Environment settings
    with arcpy.EnvManager(scratchWorkspace=r"C:\Users\ras6399\Documents\ArcGIS\Projects\1mvs10mComparison\1mvs10mComparison.gdb", w
        BinaryConditionalMinusDiff()
```

## Set Directories

### Directories Function

```
def rastercomparisondirectories(county, mod, value, user):
    """
    The Raster Comparison Directories tool takes arguments: county, mod, value, user
    County refers to one of the Texas counties: Brazos, Colorado, Harris, Jefferson, Mitchell, Uvalde, Young
    Mod refers to any modification to the value, can be alphabetic or numeric
    Value refers to the FID number associated with your HUC12 of interest
    User refers to the user who created the directory structure: choose Alec or Robert
    """

    county = county
    mod = mod
    value = value
    project = f'{county}_HUC_{mod}{value}' # Define project name
    basedir = r'C:\Users\ras6399\Documents\NOAA_Research\Projects\1mvs10mComparison' # Define root filepath
    inunmap10m = f'clip_{mod}{value}_10m_absworsttest.tif' # Define 10-meter inundation map filename
    diff = f'clip_{mod}{value}_absworst_Diff.tif' # Define difference map filename
    binary10m = f'clip_{mod}{value}_10m_absworst_BinaryExtent.tif' # Define 10-meter binary map filename
    binary1m = f'clip_{mod}{value}_1m_absworst_BinaryExtent.tif' # Define 1-meter binary map filename
    minus = f'clip_{mod}{value}_absworst_MinusDepth.tif' # Define 1-meter minus 10-meter map filename
    conditional = f'clip_{mod}{value}_absworst_DiffExtent.tif' # Define conditional map filename

    # Path to folders holding inundation maps
    dir_in_10m_inunmap_raster = f'{basedir}\InunMaps\{project}\{inunmap10m}' # Define directory to 10-meter inundation map
    if user == 'Alec': # If Alec setup directory
        inunmap1m = f'clip_{mod}{value}_1m_inunmap_ABSOLUTE_WORST.tif' # Define 1-meter inundation map filename
        dir_in_1m_inunmap_raster = f'{basedir}\InunMaps\{project}\ABSOLUTE_WORST_CASE\{inunmap1m}' # Define directory to 1-meter in
    elif user == 'Robert': # If Robert setup directory
        inunmap1m = f'clip_{mod}{value}_1m_absworst.tif' # Define 1-meter inundation map filename
        dir_in_1m_inunmap_raster = f'{basedir}\InunMaps\{project}\{inunmap1m}' # Define directory to 1-meter inundation map
    else:
         print('User not valid entry')

    # Path to folders holding ArcGIS Pro Diff files
    # dir_in_diff_raster = f'{basedir}\Diff\{county}\{diff}'
    # Removed to save space on desktop, all Diff files in UT BOX
```

Figure A.3

```
    # Path to folders holding ArcGIS Pro Binary InunMap files
    dir_in_10m_binary_raster = f'{basedir}\Binary\{county}\{binary10m}'
    dir_in_1m_binary_raster = f'{basedir}\Binary\{county}\{binary1m}'

    # Path to folders holding ArcGIS Pro Minus InunMap (1m - 10m) files
    dir_in_minus_raster = f'{basedir}\Minus\{county}\{minus}'

    # Path to folders holding Conditional Extent files
    dir_in_conditional_raster = f'{basedir}\Diff\DiffExtent\{county}\{conditional}'

    return dir_in_10m_inunmap_raster, dir_in_1m_inunmap_raster, dir_in_10m_binary_raster, dir_in_1m_binary_raster, dir_in_minus_ras
```

### Display paths

```
dir_in_10m_inunmap_raster, dir_in_1m_inunmap_raster, dir_in_10m_binary_raster, \
dir_in_1m_binary_raster, dir_in_minus_raster, dir_in_conditional_raster \
= rastercomparisondirectories('Brazos', '', '2', 'Alec')

print('Input 10m inunmap\n', dir_in_10m_inunmap_raster,
  '\n\nInput 1m inunmap\n', dir_in_1m_inunmap_raster,
  '\n\nInput 10m Binary raster\n', dir_in_10m_binary_raster,
  '\n\nInput 1m Binary raster\n', dir_in_1m_binary_raster,
  '\n\nInput Minus raster\n', dir_in_minus_raster,
  '\n\nInput Conditional raster\n', dir_in_conditional_raster)
```

```
Input 10m inunmap
 C:\Users\ras6399\Documents\NOAA_Research\Projects\1mvs10mComparison\InunMaps\Brazos_HUC_2\clip_2_10m_absworsttest.tif

Input 1m inunmap
 C:\Users\ras6399\Documents\NOAA_Research\Projects\1mvs10mComparison\InunMaps\Brazos_HUC_2\ABSOLUTE_WORST_CASE\clip_2_1m_inunmap_ABS
OLUTE_WORST.tif

Input 10m Binary raster
 C:\Users\ras6399\Documents\NOAA_Research\Projects\1mvs10mComparison\Binary\Brazos\clip_2_10m_absworst_BinaryExtent.tif

Input 1m Binary raster
 C:\Users\ras6399\Documents\NOAA_Research\Projects\1mvs10mComparison\Binary\Brazos\clip_2_1m_absworst_BinaryExtent.tif

Input Minus raster
 C:\Users\ras6399\Documents\NOAA_Research\Projects\1mvs10mComparison\Minus\Brazos\clip_2_absworst_MinusDepth.tif

Input Conditional raster
 C:\Users\ras6399\Documents\NOAA_Research\Projects\1mvs10mComparison\Diff\DiffExtent\Brazos\clip_2_absworst_DiffExtent.tif
```

## Import and read file metadata using Rasterio

```
# Use rasterio module to read geospatial data

inunmap_10m_dataset = rasterio.open(dir_in_10m_inunmap_raster) # 10-meter inundation raster
inunmap_1m_dataset = rasterio.open(dir_in_1m_inunmap_raster) # 1-meter inundation raster
```

Figure A.4

```
inunmap_10m_binary_dataset = rasterio.open(dir_in_10m_binary_raster) # 10-meter binary raster
inunmap_1m_binary_dataset = rasterio.open(dir_in_1m_binary_raster) # 1-meter binary raster
inunmap_minus_dataset = rasterio.open(dir_in_minus_raster) # 1-meter minus 10-meter raster
inunmap_conditional_dataset = rasterio.open(dir_in_conditional_raster) # Conditional raster
```

## Bands, height, width, and total cell count

```
# Calculate cell count using extracted raster width and height geospatial data
# Cell count = pixel width * pixel height

inunmap_10m_dataset_cellcount = inunmap_10m_dataset.width*inunmap_10m_dataset.height
inunmap_1m_dataset_cellcount = inunmap_1m_dataset.width*inunmap_1m_dataset.height
inunmap_10m_binary_dataset_cellcount = inunmap_10m_binary_dataset.width*inunmap_10m_binary_dataset.height
inunmap_1m_binary_dataset_cellcount = inunmap_1m_binary_dataset.width*inunmap_1m_binary_dataset.height
inunmap_minus_dataset_cellcount = inunmap_minus_dataset.width*inunmap_minus_dataset.height
inunmap_conditional_dataset_cellcount = inunmap_conditional_dataset.width*inunmap_conditional_dataset.height

print('10m inunmap:\n', 'band count =', inunmap_10m_dataset.count, '\n dimensions = cols',
    inunmap_10m_dataset.width, '| rows', inunmap_10m_dataset.height, '\n total cell count =', inunmap_10m_dataset_cellcount)
print('\n1m inunmap:\n', 'band count =', inunmap_1m_dataset.count, '\n dimensions = cols',
    inunmap_1m_dataset.width, '| rows', inunmap_1m_dataset.height, '\n total cell count =', inunmap_1m_dataset_cellcount)
print('\n10m Binary:\n', 'band count =', inunmap_10m_binary_dataset.count, '\n dimensions = cols',
    inunmap_10m_binary_dataset.width, '| rows', inunmap_10m_binary_dataset.height, '\n total cell count =', inunmap_10m_binary_data
print('\n1m Binary:\n', 'band count =', inunmap_1m_binary_dataset.count, '\n dimensions = cols',
    inunmap_1m_binary_dataset.width, '| rows', inunmap_1m_binary_dataset.height, '\n total cell count =', inunmap_1m_binary_dataset_
print('\nMinus:\n', 'band count =', inunmap_minus_dataset_cellcount, '\n dimensions = cols',
    inunmap_minus_dataset.width, '| rows', inunmap_minus_dataset.height, '\n total cell count =', inunmap_minus_dataset_cellcount)
print('\nConditional:\n', 'band count =', inunmap_conditional_dataset_cellcount, '\n dimensions = cols',
    inunmap_conditional_dataset.width, '| rows', inunmap_conditional_dataset.height, '\n total cell count =', inunmap_conditional_d
```

```
10m inunmap:
 band count = 1
 dimensions = cols 1892 | rows 1644
 total cell count = 3110448

1m inunmap:
 band count = 1
 dimensions = cols 18562 | rows 16129
 total cell count = 299386498

10m Binary:
 band count = 1
 dimensions = cols 1892 | rows 1644
 total cell count = 3110448

1m Binary:
 band count = 1
 dimensions = cols 18562 | rows 16129
 total cell count = 299386498

Minus:
```

Figure A.5

```
 band count = 299386498
 dimensions = cols 18562 | rows 16129
 total cell count = 299386498

Conditional:
 band count = 299386498
 dimensions = cols 18562 | rows 16129
 total cell count = 299386498
```

## Cell size & area

```
# Open 10-meter inundation raster using GDAL
inunmap_10m_dataset_gdal = gdal.Open(dir_in_10m_inunmap_raster)

# Extract transform data from 10-meter inundation raster
transform_10m = inunmap_10m_dataset_gdal.GetGeoTransform() # Extract transform data
xOrigin_10m = transform_10m[0] # Extract x-origin
yOrigin_10m = transform_10m[3] # Extract y-origin
pixelWidth_10m = transform_10m[1] # Extract pixel width
pixelHeight_10m = -transform_10m[5] # Extract pixal height

print('10-meter transform data\n', '[x-origin, pixel width, 0.0, y-origin, pixel height, 0.0]\n', transform_10m)

# Open 1-meter inundation raster using GDAL
inunmap_1m_dataset_gdal = gdal.Open(dir_in_1m_inunmap_raster)

# Extract transform data from 1-meter inundation raster
transform_1m = inunmap_1m_dataset_gdal.GetGeoTransform() # Extract transform data
xOrigin_1m = transform_1m[0] # Extract x-origin
yOrigin_1m = transform_1m[3] # Extract y-origin
pixelWidth_1m = transform_1m[1] # Extract pixel width
pixelHeight_1m = -transform_1m[5] # Extract pixel height

print('1-meter transform data\n', '[x-origin, pixel width, 0.0, y-origin, pixel height, 0.0]\n', transform_1m)
```

```
10-meter transform data
 [x-origin, pixel width, 0.0, y-origin, pixel height, 0.0]
 (724453.2398662139, 9.820378318025297, 0.0, 3402017.857872987, 0.0, -9.820378318025304)
1-meter transform data
 [x-origin, pixel width, 0.0, y-origin, pixel height, 0.0]
 (724462.0, 1.0, 0.0, 3402010.0, 0.0, -1.0)
```

## Convert Rasterio datasets to numpy arrays

```
# Convert to numpy array by reading band 1

npband1_10m_inunmap = inunmap_10m_dataset.read(1)
npband1_1m_inunmap = inunmap_1m_dataset.read(1)
npband1_10m_binary = inunmap_10m_binary_dataset.read(1)
npband1_1m_binary = inunmap_1m_binary_dataset.read(1)
```

Figure A.6

```
npMinus = inunmap_minus_dataset.read(1)
npConditional = inunmap_conditional_dataset.read(1).astype(float)

print('10m InunMap Band 1\n', npband1_10m_inunmap, '\n\n1m InunMap Band 1\n', npband1_1m_inunmap,
      '\n\n10m Binary Band 1\n', npband1_10m_binary, '\n\n1m Binary Band 1\n', npband1_1m_binary,
      '\n\nMinus\n', npMinus, '\n\nConditional\n', npConditional)
```

```
10m InunMap Band 1
 [[-3.e+38 -3.e+38 -3.e+38 ... -3.e+38 -3.e+38 -3.e+38]
 [-3.e+38 -3.e+38 -3.e+38 ... -3.e+38 -3.e+38 -3.e+38]
 [-3.e+38 -3.e+38 -3.e+38 ... -3.e+38 -3.e+38 -3.e+38]
 ...
 [-3.e+38 -3.e+38 -3.e+38 ... -3.e+38 -3.e+38 -3.e+38]
 [-3.e+38 -3.e+38 -3.e+38 ... -3.e+38 -3.e+38 -3.e+38]
 [-3.e+38 -3.e+38 -3.e+38 ... -3.e+38 -3.e+38 -3.e+38]]

1m InunMap Band 1
 [[-3.e+38 -3.e+38 -3.e+38 ... -3.e+38 -3.e+38 -3.e+38]
 [-3.e+38 -3.e+38 -3.e+38 ... -3.e+38 -3.e+38 -3.e+38]
 [-3.e+38 -3.e+38 -3.e+38 ... -3.e+38 -3.e+38 -3.e+38]
 ...
 [-3.e+38 -3.e+38 -3.e+38 ... -3.e+38 -3.e+38 -3.e+38]
 [-3.e+38 -3.e+38 -3.e+38 ... -3.e+38 -3.e+38 -3.e+38]
 [-3.e+38 -3.e+38 -3.e+38 ... -3.e+38 -3.e+38 -3.e+38]]

10m Binary Band 1
 [[0 0 0 ... 0 0 0]
 [0 0 0 ... 0 0 0]
 [0 0 0 ... 0 0 0]
 ...
 [0 0 0 ... 0 0 0]
 [0 0 0 ... 0 0 0]
 [0 0 0 ... 0 0 0]]

1m Binary Band 1
 [[0 0 0 ... 0 0 0]
 [0 0 0 ... 0 0 0]
 [0 0 0 ... 0 0 0]
 ...
 [0 0 0 ... 0 0 0]
 [0 0 0 ... 0 0 0]
 [0 0 0 ... 0 0 0]]

Minus
 [[-3.4028235e+38 -3.4028235e+38 -3.4028235e+38 ... -3.4028235e+38
  -3.4028235e+38 -3.4028235e+38]
 [-3.4028235e+38 -3.4028235e+38 -3.4028235e+38 ... -3.4028235e+38
  -3.4028235e+38 -3.4028235e+38]
 [-3.4028235e+38 -3.4028235e+38 -3.4028235e+38 ... -3.4028235e+38
  -3.4028235e+38 -3.4028235e+38]
 ...
 [-3.4028235e+38 -3.4028235e+38 -3.4028235e+38 ... -3.4028235e+38
  -3.4028235e+38 -3.4028235e+38]
 [-3.4028235e+38 -3.4028235e+38 -3.4028235e+38 ... -3.4028235e+38
```

Figure A.7

```
  -3.4028235e+38 -3.4028235e+38]
 [-3.4028235e+38 -3.4028235e+38 -3.4028235e+38 ... -3.4028235e+38
  -3.4028235e+38 -3.4028235e+38]]

Conditional
 [[-9999. -9999. -9999. ... -9999. -9999. -9999.]
 [-9999. -9999. -9999. ... -9999. -9999. -9999.]
 [-9999. -9999. -9999. ... -9999. -9999. -9999.]
 ...
 [-9999. -9999. -9999. ... -9999. -9999. -9999.]
 [-9999. -9999. -9999. ... -9999. -9999. -9999.]
 [-9999. -9999. -9999. ... -9999. -9999. -9999.]]
```

## NaN and non-NaN counts

```
# NaN count = sum of all pixels less than NaN threshold
# Non-NaN count = total cell count - NaN count

nancount_10m_inunmap = (npband1_10m_inunmap < -9998).sum()
nonnancount_10m_inunmap = inunmap_10m_dataset_cellcount - nancount_10m_inunmap
print('10m inunmap:\n', 'NaN count =', nancount_10m_inunmap, '\n non-Nan count =', nonnancount_10m_inunmap)

nancount_1m_inunmap = (npband1_1m_inunmap < -9998).sum()
nonnancount_1m_inunmap = inunmap_1m_dataset_cellcount - nancount_1m_inunmap
print('\n1m inunmap:\n', 'NaN count =', nancount_1m_inunmap, '\n non-Nan count =', nonnancount_1m_inunmap)

nancount_10m_binary = (npband1_10m_binary < -9998).sum()
nonnancount_10m_binary = inunmap_10m_binary_dataset_cellcount - nancount_10m_binary
print('\n10m binary:\n', 'NaN count =', nancount_10m_binary, '\n non-Nan count =', nonnancount_10m_binary)

nancount_1m_binary = (npband1_1m_binary < -9998).sum()
nonnancount_1m_binary = inunmap_1m_binary_dataset_cellcount - nancount_1m_binary
print('\n1m binary:\n', 'NaN count =', nancount_1m_binary, '\n non-Nan count =', nonnancount_1m_binary)

nancount_minus = (npMinus < -9998).sum()
nonnancount_minus = inunmap_minus_dataset_cellcount - nancount_minus
print('\nMinus:\n', 'NaN count =', nancount_minus, '\n non-Nan count =', nonnancount_minus)

nancount_conditional = (npConditional < -9998).sum()
nonnancount_conditional = inunmap_conditional_dataset_cellcount - nancount_conditional
print('\nConditional:\n', 'NaN count =', nancount_conditional, '\n non-Nan count =', nonnancount_conditional)
```

```
10m inunmap:
 NaN count = 2942239
 non-Nan count = 168209

1m inunmap:
 NaN count = 267869277
 non-Nan count = 31517221

10m binary:
```

Figure A.8

```
 NaN count = 0
 non-Nan count = 3110448

1m binary:
 NaN count = 0
 non-Nan count = 299386498

Minus:
 NaN count = 285625917
 non-Nan count = 13760581

Conditional:
 NaN count = 265407851
 non-Nan count = 33978647
```

## Convert NaN placeholders with np.nan

```
# Pixels with value less than NaN threshold converted to np.NaN

npband1_10m_inunmap[npband1_10m_inunmap < -9998] = np.nan
npband1_1m_inunmap[npband1_1m_inunmap < -9998] = np.nan
npMinus[npMinus < -9998] = np.nan
npConditional[npConditional < -9998] = np.nan

print('npband1_10m_inunmap\n', npband1_10m_inunmap, '\n\nnpband1_1m_inunmap\n', npband1_1m_inunmap,
      '\n\nnpMinus\n', npMinus, '\n\nnpConditional\n', npConditional)
```

```
npband1_10m_inunmap
 [[nan nan nan ... nan nan nan]
 [nan nan nan ... nan nan nan]
 [nan nan nan ... nan nan nan]
 ...
 [nan nan nan ... nan nan nan]
 [nan nan nan ... nan nan nan]
 [nan nan nan ... nan nan nan]]

npband1_1m_inunmap
 [[nan nan nan ... nan nan nan]
 [nan nan nan ... nan nan nan]
 [nan nan nan ... nan nan nan]
 ...
 [nan nan nan ... nan nan nan]
 [nan nan nan ... nan nan nan]
 [nan nan nan ... nan nan nan]]

npMinus
 [[nan nan nan ... nan nan nan]
 [nan nan nan ... nan nan nan]
 [nan nan nan ... nan nan nan]
 ...
 [nan nan nan ... nan nan nan]
 [nan nan nan ... nan nan nan]
```

Figure A.9

```
 [nan nan nan ... nan nan nan]]

npConditional
 [[nan nan nan ... nan nan nan]
 [nan nan nan ... nan nan nan]
 [nan nan nan ... nan nan nan]
 ...
 [nan nan nan ... nan nan nan]
 [nan nan nan ... nan nan nan]
 [nan nan nan ... nan nan nan]]
```

## Display input rasters

```
plt.rcParams['font.size']=14
fig= plt.figure(figsize=(20,20))

# 10-meter inundation map
ax1 = fig.add_subplot(3,2,1)
ax1.set_facecolor('gray')
plt.imshow(npband1_10m_inunmap, extent=[xOrigin_10m, xOrigin_10m+inunmap_10m_dataset.width,
                                        yOrigin_10m, yOrigin_10m+inunmap_10m_dataset.height], cmap='Blues')
plt.ticklabel_format(axis='both', style='sci', scilimits=(0,0))
plt.title('10-meter Inundation Map')
cb = plt.colorbar()
cb.set_label('Inundation depth (m)')
plt.xlabel('Easting [m]')
plt.ylabel('Northing [m]');

# 1-meter inundation map
ax2 = fig.add_subplot(3,2,2)
ax2.set_facecolor('gray')
plt.imshow(npband1_1m_inunmap, extent=[xOrigin_1m, xOrigin_1m+inunmap_1m_dataset.width,
                                       yOrigin_1m, yOrigin_1m+inunmap_1m_dataset.height], cmap='Blues')
plt.ticklabel_format(axis='both', style='sci', scilimits=(0,0))
plt.title('1-meter Inundation Map')
cb = plt.colorbar()
cb.set_label('Inundation depth (m)')
plt.xlabel('Easting [m]')
plt.ylabel('Northing [m]');

# 10-meter binary inundation extent
ax3 = fig.add_subplot(3,2,3)
plt.imshow(npband1_10m_binary, extent=[xOrigin_10m, xOrigin_10m+inunmap_10m_dataset.width,
                                       yOrigin_10m, yOrigin_10m+inunmap_10m_dataset.height], cmap='binary')
plt.ticklabel_format(axis='both', style='sci', scilimits=(0,0))
plt.title('10-meter Binary Inundation Extent')
black_patch = pltpatches.Patch(facecolor='black', label='Inundated')
white_patch = pltpatches.Patch(facecolor='white', label='Not Inundated', edgecolor='k')
plt.legend(handles=[black_patch, white_patch], loc='best')
plt.xlabel('Easting [m]')
```

Figure A.10

```
plt.ylabel('Northing [m]');

# 1-meter binary inundation extent
ax4 = fig.add_subplot(3,2,4)
plt.imshow(npband1_1m_binary, extent=[xOrigin_1m, xOrigin_1m+inunmap_1m_dataset.width,
                                      yOrigin_1m, yOrigin_1m+inunmap_1m_dataset.height], cmap='binary')
plt.ticklabel_format(axis='both', style='sci', scilimits=(0,0))
plt.title('1-meter Binary Inundation Extent')
black_patch = pltpatches.Patch(facecolor='black', label='Inundated')
white_patch = pltpatches.Patch(facecolor='white', label='Not Inundated', edgecolor='black')
plt.legend(handles=[black_patch, white_patch], loc='best')
plt.xlabel('Easting [m]')
plt.ylabel('Northing [m]');

# Minus
divnorm = colors.TwoSlopeNorm(vmin=np.min(npMinus), vcenter=0, vmax=np.max(npMinus)) # Set divergent colormap with center at zero,

ax5 = fig.add_subplot(3,2,5)
ax5.set_facecolor('black')
plt.imshow(npMinus, extent=[xOrigin_1m, xOrigin_1m+inunmap_1m_dataset.width,
                            yOrigin_1m, yOrigin_1m+inunmap_1m_dataset.height], norm=divnorm, cmap='bwr')
plt.ticklabel_format(axis='both', style='sci', scilimits=(0,0))
plt.title('1-meter minus 10-meter')
cb = plt.colorbar()
cb.set_label('Minus (m)')
plt.xlabel('Easting [m]')
plt.ylabel('Northing [m]');

# Conditional
ax6 = fig.add_subplot(3,2,6)
ax6.set_facecolor('black')
plt.imshow(npConditional, extent=[xOrigin_1m, xOrigin_1m+inunmap_1m_dataset.width,
                                  yOrigin_1m, yOrigin_1m+inunmap_1m_dataset.height], cmap='bwr')
plt.ticklabel_format(axis='both', style='sci', scilimits=(0,0))
plt.title('Conditional')
cb = plt.colorbar()
cb.set_ticks([-1, 0, 1])
cb.set_ticklabels(['DW', 'WW', 'WD'])
plt.xlabel('Easting [m]')
plt.ylabel('Northing [m]');

# plt.savefig("C:\\Users\\ras6399\\Documents\\NOAA_Research\\Projects\\1mvs10mComparison\\Figures\\Brazos_HUC_2_InputSet.png", dpi=
```

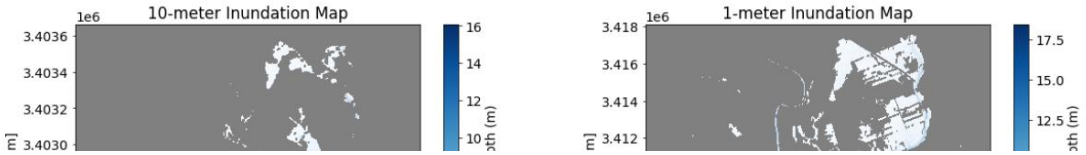


Figure A.11

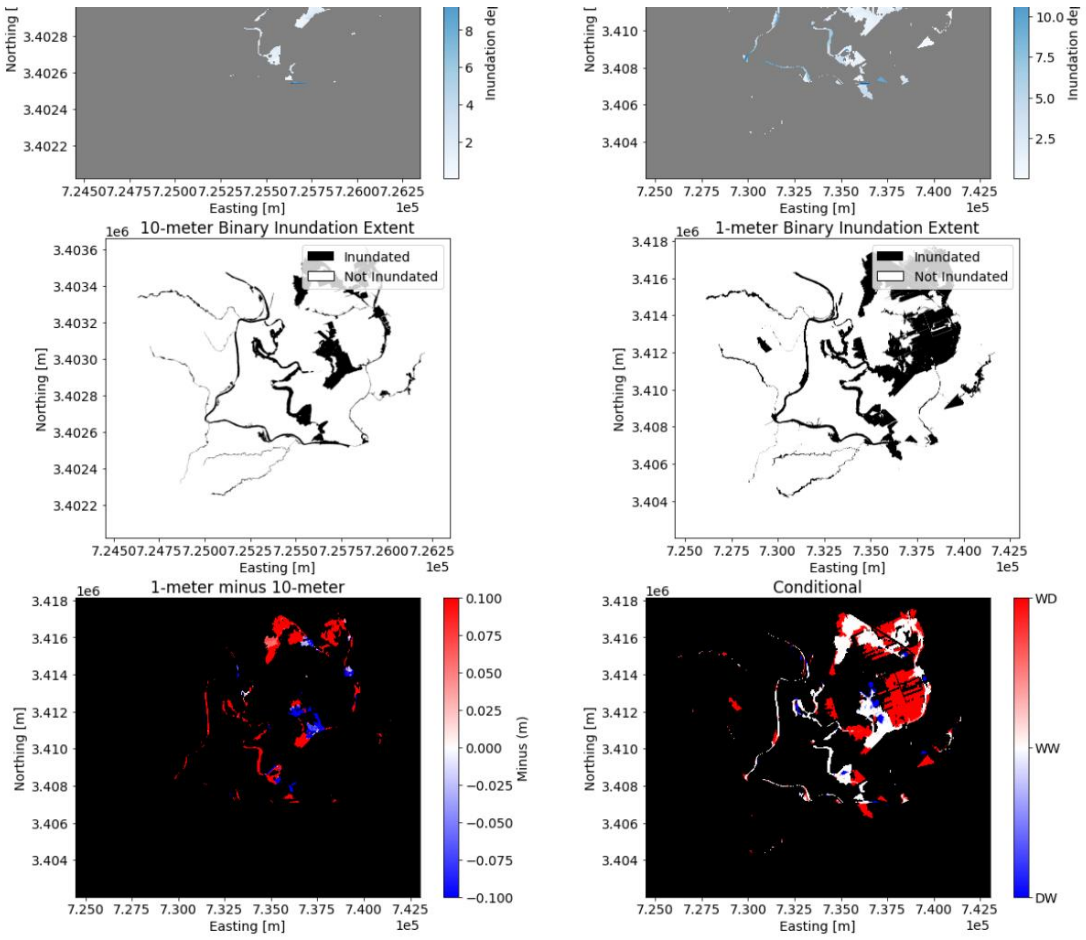
Northing [
Inundation dep
Easting [m]
1e5
1e6
10-meter Binary Inundation Extent
Inundated
Not Inundated
Northing [m]
1-meter Binary Inundation Extent
1-meter minus 10-meter
Minus (m)
Conditional
WD
WW
DW

Figure A.12

## Raster Comparison

### Calculate extent metrics

```
# 1m wet and 10 wet
WW = np.count_nonzero(npConditional == 0)

# 1m wet and 10m dry
WD = np.count_nonzero(npConditional == 1)

# 1m dry and 10m wet
DW = np.count_nonzero(npConditional == -1)

# 1m dry and 10m dry
DD = np.count_nonzero(npConditional == np.nan)

# 1m wet
W1 = WW + WD

# 10m wet
W10 = WW + DW

# Area Ratio
arearatio = W1/W10

# Accurate
accurate = WW/(WW+WD+DW)

# Underestimate
underestimate = WD/(WW+WD+DW)

# Overestimate
overestimate = DW/(WW+WD+DW)

print('WW =', WW, '\nWD =', WD, '\nDW =', DW, '\nDD =', DD,
      '\nW1 =', W1, '\nW10 =', W10, '\nArea Ratio =', arearatio,
      '\nAccurate =', accurate, '\nUnderestimate =', underestimate,
      '\nOverestimate =', overestimate)
```

```
WW = 13760581
WD = 17756640
DW = 2461426
DD = 0
W1 = 31517221
W10 = 16222007
Area Ratio = 1.9428681666824579
Accurate = 0.4049773082489129
Underestimate = 0.5225823147107652
Overestimate = 0.07244037704032183
```

Figure A.13

### Calculate depth metrics

```
# Root mean square error
RMSE = np.sqrt(np.nanmean(npMinus**2))
print('Root mean square error =', RMSE)
# Mean absolute error
MAE = np.nanmean(np.abs(npMinus))
print('Mean absolute error =', MAE)
# Mean error
ME = np.nanmean(npMinus)
print('Mean error =', ME)
```

```
Root mean square error = 2.2778742
Mean absolute error = 1.1638448
Mean error = 0.8347928
```

### Statistics Function

```
def rastercomparisonstatistics(dir_in_10m_inunmap_raster, dir_in_1m_inunmap_raster,
                               dir_in_10m_binary_raster, dir_in_1m_binary_raster, dir_in_minus_raster,
                               dir_in_conditional_raster, NaNthreshold):

    """
    rastercomparisonstatistics takes arguments:

    county
    mod
    number
    dir_in_10m_inunmap_raster
    dir_in_1m_inunmap_raster
    dir_in_10m_binary_raster
    dir_in_1m_binary_raster
    dir_in_minus_raster
    dir_in_conditional_raster
    NaNthreshold

    rastercomparisonstatistics returns:

    Statistics DataFrame
    """

    ### Initialize statistics DataFrame

    stats_dataframe = pd.DataFrame()

    ### Define statistics list

    stat_type = []
    resolution = []
```

Figure A.14

```
dataset = []
stat_value = []

### Define inunmap metadata

stat_type.extend(['X_Origin', 'Y_Origin', 'Pixel_Width', 'Pixel_Height',
                  'X_Origin', 'Y_Origin', 'Pixel_Width', 'Pixel_Height'])
resolution.extend([10, 10, 10, 10, 1, 1, 1, 1])
dataset.extend(['InunMap', 'InunMap', 'InunMap', 'InunMap', 'InunMap', 'InunMap', 'InunMap', 'InunMap'])

# Open 10-meter inundation raster using GDAL
inunmap_10m_dataset_gdal = gdal.Open(dir_in_10m_inunmap_raster)

# Extract transform data from 10-meter inundation raster
transform_10m = inunmap_10m_dataset_gdal.GetGeoTransform() # Extract transform data
xOrigin_10m = transform_10m[0] # Extract x-origin
yOrigin_10m = transform_10m[3] # Extract y-origin
pixelWidth_10m = transform_10m[1] # Extract pixel width
pixelHeight_10m = -transform_10m[5] # Extract pixal height

# Open 1-meter inundation raster using GDAL
inunmap_1m_dataset_gdal = gdal.Open(dir_in_1m_inunmap_raster)

# Extract transform data from 1-meter inundation raster
transform_1m = inunmap_1m_dataset_gdal.GetGeoTransform() # Extract transform data
xOrigin_1m = transform_1m[0] # Extract x-origin
yOrigin_1m = transform_1m[3] # Extract y-origin
pixelWidth_1m = transform_1m[1] # Extract pixel width
pixelHeight_1m = -transform_1m[5] # Extract pixel height

stat_value.extend([xOrigin_10m, yOrigin_10m, pixelWidth_10m, pixelHeight_10m,
                   xOrigin_1m, yOrigin_1m, pixelWidth_1m, pixelHeight_1m])

### Read in rasters using rasterio

inunmap_10m_dataset = rasterio.open(dir_in_10m_inunmap_raster) # 10-meter inundation raster
inunmap_1m_dataset = rasterio.open(dir_in_1m_inunmap_raster) # 1-meter inundation raster
inunmap_10m_binary_dataset = rasterio.open(dir_in_10m_binary_raster) # 10-meter binary raster
inunmap_1m_binary_dataset = rasterio.open(dir_in_1m_binary_raster) # 1-meter binary raster
inunmap_minus_dataset = rasterio.open(dir_in_minus_raster) # 1-meter minus 10-meter raster
inunmap_conditional_dataset = rasterio.open(dir_in_conditional_raster) # Conditional raster

### Extract dimension data from rasters

# Band

stat_type.extend(['Band_Count', 'Band_Count', 'Band_Count', 'Band_Count', 'Band_Count', 'Band_Count'])
resolution.extend([10, 1, 10, 1, 'Combo', 'Combo'])
dataset.extend(['InunMap', 'InunMap', 'Binary', 'Binary', 'Minus', 'Conditional'])

inunmap_10m_dataset_band = int(inunmap_10m_dataset.count)
```

Figure A.15

```
inunmap_1m_dataset_band = int(inunmap_1m_dataset.count)
inunmap_10m_binary_dataset_band = int(inunmap_10m_binary_dataset.count)
inunmap_1m_binary_dataset_band = int(inunmap_1m_binary_dataset.count)
inunmap_minus_dataset_band = int(inunmap_minus_dataset.count)
inunmap_conditional_dataset_band = int(inunmap_conditional_dataset.count)

stat_value.extend([inunmap_10m_dataset_band,
inunmap_1m_dataset_band,
inunmap_10m_binary_dataset_band,
inunmap_1m_binary_dataset_band,
inunmap_minus_dataset_band,
inunmap_conditional_dataset_band])

# Width

stat_type.extend(['Width', 'Width', 'Width', 'Width', 'Width', 'Width'])
resolution.extend([10, 1, 10, 1, 'Combo', 'Combo'])
dataset.extend(['InunMap', 'InunMap', 'Binary', 'Binary', 'Minus', 'Conditional'])

inunmap_10m_dataset_width = int(inunmap_10m_dataset.width)
inunmap_1m_dataset_width = int(inunmap_1m_dataset.width)
inunmap_10m_binary_dataset_width = int(inunmap_10m_binary_dataset.width)
inunmap_1m_binary_dataset_width = int(inunmap_1m_binary_dataset.width)
inunmap_minus_dataset_width = int(inunmap_minus_dataset.width)
inunmap_conditional_dataset_width = int(inunmap_conditional_dataset.width)

stat_value.extend([inunmap_10m_dataset_width,
inunmap_1m_dataset_width,
inunmap_10m_binary_dataset_width,
inunmap_1m_binary_dataset_width,
inunmap_minus_dataset_width,
inunmap_conditional_dataset_width])

# Height

stat_type.extend(['Height', 'Height', 'Height', 'Height', 'Height', 'Height'])
resolution.extend([10, 1, 10, 1, 'Combo', 'Combo'])
dataset.extend(['InunMap', 'InunMap', 'Binary', 'Binary', 'Minus', 'Conditional'])

inunmap_10m_dataset_height = int(inunmap_10m_dataset.height)
inunmap_1m_dataset_height = int(inunmap_1m_dataset.height)
inunmap_10m_binary_dataset_height = int(inunmap_10m_binary_dataset.height)
inunmap_1m_binary_dataset_height = int(inunmap_1m_binary_dataset.height)
inunmap_minus_dataset_height = int(inunmap_minus_dataset.height)
inunmap_conditional_dataset_height = int(inunmap_conditional_dataset.height)

stat_value.extend([inunmap_10m_dataset_height,
inunmap_1m_dataset_height,
inunmap_10m_binary_dataset_height,
inunmap_1m_binary_dataset_height,
inunmap_minus_dataset_height,
```

Figure A.16

```
inunmap_conditional_dataset_height])

# Total Cell Count
# Cell count = pixel width * pixel height

stat_type.extend(['Total_Cell_Count', 'Total_Cell_Count', 'Total_Cell_Count', 'Total_Cell_Count',
                  'Total_Cell_Count', 'Total_Cell_Count'])
resolution.extend([10, 1, 10, 1, 'Combo', 'Combo'])
dataset.extend(['InunMap', 'InunMap', 'Binary', 'Binary', 'Minus', 'Conditional'])

inunmap_10m_dataset_cellcount = int(inunmap_10m_dataset_width*inunmap_10m_dataset_height)
inunmap_1m_dataset_cellcount = int(inunmap_1m_dataset_width*inunmap_1m_dataset_height)
inunmap_10m_binary_dataset_cellcount = int(inunmap_10m_binary_dataset_width*inunmap_10m_binary_dataset_height)
inunmap_1m_binary_dataset_cellcount = int(inunmap_1m_binary_dataset_width*inunmap_1m_binary_dataset_height)
inunmap_minus_dataset_cellcount = int(inunmap_minus_dataset_width*inunmap_minus_dataset_height)
inunmap_conditional_dataset_cellcount = int(inunmap_conditional_dataset_width*inunmap_conditional_dataset_height)

stat_value.extend([inunmap_10m_dataset_cellcount,
inunmap_1m_dataset_cellcount,
inunmap_10m_binary_dataset_cellcount,
inunmap_1m_binary_dataset_cellcount,
inunmap_minus_dataset_cellcount,
inunmap_conditional_dataset_cellcount])

### Convert to Numpy array

npband1_10m_inunmap = inunmap_10m_dataset.read(1)
npband1_1m_inunmap = inunmap_1m_dataset.read(1)
npband1_10m_binary = inunmap_10m_binary_dataset.read(1)
npband1_1m_binary = inunmap_1m_binary_dataset.read(1)
npMinus = inunmap_minus_dataset.read(1)
npConditional = inunmap_conditional_dataset.read(1).astype(float)


### Convert NaN placeholders to np.nan
# Pixels with value less than NaN threshold converted to np.NaN

npband1_10m_inunmap[npband1_10m_inunmap < NaNthreshold] = np.nan
npband1_1m_inunmap[npband1_1m_inunmap < NaNthreshold] = np.nan
npMinus[npMinus < NaNthreshold] = np.nan
npConditional[npConditional < NaNthreshold] = np.nan

### NaN and non-NaN Cell Count
# NaN count = sum of all pixels less than NaN threshold
# Non-NaN count = total cell count - NaN count

stat_type.extend(['NaN_Count', 'non-NaN_Count','NaN_Count', 'non-NaN_Count'])
resolution.extend([10, 10, 1, 1])
dataset.extend(['Binary', 'Binary', 'Binary', 'Binary'])
```

Figure A.17

```
nancount_10m_binary = (npband1_10m_binary < 1).sum()
nonnancount_10m_binary = inunmap_10m_binary_dataset_cellcount - nancount_10m_binary
nancount_1m_binary = (npband1_1m_binary < 1).sum()
nonnancount_1m_binary = inunmap_1m_binary_dataset_cellcount - nancount_1m_binary


stat_value.extend([nancount_10m_binary,
nonnancount_10m_binary,
nancount_1m_binary,
nonnancount_1m_binary])

### Calculate areas

stat_type.extend(['Total_Raster_Area [m2]', 'Total_Raster_Area [m2]', 'Total_Raster_Area [m2]', 'Total_Raster_Area [m2]',
                  'Inundated_Area [m2]', 'Inundated_Area [m2]', 'Total_AreaRatio_1mto10m', 'Total_AreaRatio_1mto10m',
                  'Inun_AreaRatio_1mto10m', 'Inun_AreaRatio_10mto1m'])
resolution.extend([10, 1, 10, 1, 10, 1, 'Combo', 'Combo', 'Combo', 'Combo'])
dataset.extend(['Inunmap', 'Inunmap', 'Binary', 'Binary', 'Binary', 'Binary', 'Inunmap', 'Binary', 'Binary', 'Binary'])

total_raster_area_10m_inunmap = inunmap_10m_dataset_cellcount*pixelWidth_10m*pixelHeight_10m
total_raster_area_1m_inunmap = inunmap_1m_dataset_cellcount*pixelWidth_1m*pixelHeight_1m
total_raster_area_10m_binary = inunmap_10m_binary_dataset_cellcount*pixelWidth_10m*pixelHeight_10m
total_raster_area_1m_binary = inunmap_1m_binary_dataset_cellcount*pixelWidth_1m*pixelHeight_1m
inun_area_10m = pixelWidth_10m*pixelHeight_10m*nonnancount_10m_binary
inun_area_1m = pixelWidth_1m*pixelHeight_1m*nonnancount_1m_binary
total_raster_area_1mDIV10m_inunmap = total_raster_area_1m_inunmap/total_raster_area_10m_inunmap
total_raster_area_1mDIV10m_binary = total_raster_area_1m_binary/total_raster_area_10m_binary
inun_area_1mDIV10m = inun_area_1m/inun_area_10m
inun_area_10mDIV1m = inun_area_10m/inun_area_1m

stat_value.extend([total_raster_area_10m_inunmap, total_raster_area_1m_inunmap,
                   total_raster_area_10m_binary, total_raster_area_1m_binary,
                   inun_area_10m, inun_area_1m,
                   total_raster_area_1mDIV10m_inunmap, total_raster_area_1mDIV10m_binary,
                   inun_area_1mDIV10m, inun_area_10mDIV1m])

### Calculate extent metrics

stat_type.extend(['WW', 'WD', 'DW', 'DD', 'W1', 'W10', 'Area_Ratio_1mto10m', 'Area_Ratio_10mto1m',
                  'Accurate', 'Underestimate', 'Overestimate'])
resolution.extend(['Combo', 'Combo', 'Combo', 'Combo', 1, 10, 'Combo', 'Combo', 'Combo', 'Combo', 'Combo'])
dataset.extend(['Conditional', 'Conditional', 'Conditional', 'Conditional', 'Conditional',
                'Conditional', 'Conditional', 'Conditional', 'Conditional', 'Conditional', 'Conditional'])

# 1m wet and 10 wet
WW = int(np.count_nonzero(npConditional == 0))
# 1m wet and 10m dry
WD = int(np.count_nonzero(npConditional == 1))
# 1m dry and 10m wet
DW = int(np.count_nonzero(npConditional == -1))
# 1m dry and 10m dry
```

Figure A.18

```
DD = int(inunmap_conditional_dataset_cellcount-(WW+WD+DW))
# 1m wet
W1 = int(WW + WD)
# 10m wet
W10 = int(WW + DW)
# Area Ratio
arearatio1to10 = float(W1/W10)
arearatio10to1 = float(W10/W1)
# Accurate
accurate = float(WW/(WW+WD+DW))
# Underestimate
underestimate = float(WD/(WW+WD+DW))
# Overestimate
overestimate = float(DW/(WW+WD+DW))

stat_value.extend([WW, WD, DW, DD, W1, W10, arearatio1to10, arearatio10to1, accurate, underestimate, overestimate])

### Calculate depth metrics

stat_type.extend(['RMSE', 'MAE', 'ME'])
resolution.extend(['Combo', 'Combo', 'Combo'])
dataset.extend(['Minus', 'Minus', 'Minus'])

# Root mean square error
RMSE = float(np.sqrt(np.nanmean(npMinus**2)))
# Mean absolute error
MAE = float(np.nanmean(np.abs(npMinus)))
# Mean error
ME = float(np.nanmean(npMinus))

stat_value.extend([RMSE, MAE, ME])

# Create graphics

plt.rcParams['font.size']=14
fig= plt.figure(figsize=(20,20))

# 10-meter inundation map
ax1 = fig.add_subplot(3,2,1)
ax1.set_facecolor('gray')
plt.imshow(npband1_10m_inunmap, extent=[xOrigin_10m, xOrigin_10m+inunmap_10m_dataset.width,
                                        yOrigin_10m, yOrigin_10m+inunmap_10m_dataset.height], cmap='Blues')
plt.ticklabel_format(axis='both', style='sci', scilimits=(0,0))
plt.title('10-meter Inundation Map')
cb = plt.colorbar()
cb.set_label('Inundation depth (m)')
plt.xlabel('Easting [m]')
plt.ylabel('Northing [m]');

# 1-meter inundation map
ax2 = fig.add_subplot(3,2,2)
```

Figure A.19

```
ax2.set_facecolor('gray')
plt.imshow(npband1_1m_inunmap, extent=[xOrigin_1m, xOrigin_1m+inunmap_1m_dataset.width,
                                       yOrigin_1m, yOrigin_1m+inunmap_1m_dataset.height], cmap='Blues')
plt.ticklabel_format(axis='both', style='sci', scilimits=(0,0))
plt.title('1-meter Inundation Map')
cb = plt.colorbar()
cb.set_label('Inundation depth (m)')
plt.xlabel('Easting [m]')
plt.ylabel('Northing [m]');

# 10-meter binary inundation extent
ax3 = fig.add_subplot(3,2,3)
plt.imshow(npband1_10m_binary, extent=[xOrigin_10m, xOrigin_10m+inunmap_10m_dataset.width,
                                       yOrigin_10m, yOrigin_10m+inunmap_10m_dataset.height], cmap='binary')
plt.ticklabel_format(axis='both', style='sci', scilimits=(0,0))
plt.title('10-meter Binary Inundation Extent')
black_patch = pltpatches.Patch(facecolor='black', label='Inundated')
white_patch = pltpatches.Patch(facecolor='white', label='Not Inundated', edgecolor='k')
plt.legend(handles=[black_patch, white_patch], loc='best')
plt.xlabel('Easting [m]')
plt.ylabel('Northing [m]');

# 1-meter binary inundation extent
ax4 = fig.add_subplot(3,2,4)
plt.imshow(npband1_1m_binary, extent=[xOrigin_1m, xOrigin_1m+inunmap_1m_dataset.width,
                                      yOrigin_1m, yOrigin_1m+inunmap_1m_dataset.height], cmap='binary')
plt.ticklabel_format(axis='both', style='sci', scilimits=(0,0))
plt.title('1-meter Binary Inundation Extent')
black_patch = pltpatches.Patch(facecolor='black', label='Inundated')
white_patch = pltpatches.Patch(facecolor='white', label='Not Inundated', edgecolor='black')
plt.legend(handles=[black_patch, white_patch], loc='best')
plt.xlabel('Easting [m]')
plt.ylabel('Northing [m]');

# Minus
divnorm = colors.TwoSlopeNorm(vmin=np.min(npMinus), vcenter=0, vmax=np.max(npMinus)) # Set divergent colormap with center at ze

ax5 = fig.add_subplot(3,2,5)
ax5.set_facecolor('black')
plt.imshow(npMinus, extent=[xOrigin_1m, xOrigin_1m+inunmap_1m_dataset.width,
                                      yOrigin_1m, yOrigin_1m+inunmap_1m_dataset.height], norm=divnorm, cmap='bwr')
plt.ticklabel_format(axis='both', style='sci', scilimits=(0,0))
plt.title('1-meter minus 10-meter')
cb = plt.colorbar()
cb.set_label('Minus (m)')
plt.xlabel('Easting [m]')
plt.ylabel('Northing [m]');

# Conditional
ax6 = fig.add_subplot(3,2,6)
ax6.set_facecolor('black')
```

Figure A.20

```
    plt.imshow(npConditional, extent=[xOrigin_1m, xOrigin_1m+inunmap_1m_dataset.width,
                                      yOrigin_1m, yOrigin_1m+inunmap_1m_dataset.height], cmap='bwr')
    plt.ticklabel_format(axis='both', style='sci', scilimits=(0,0))
    plt.title('Conditional')
    cb = plt.colorbar()
    cb.set_ticks([-1, 0, 1])
    cb.set_ticklabels(['DW', 'WW', 'WD'])
    plt.xlabel('Easting [m]')
    plt.ylabel('Northing [m]');

    # Return statistics lists and figure

    return stat_type, resolution, dataset, stat_value, fig
```

## Calculate statistics for individual HUC12

```
stats_dataframe = pd.DataFrame()

i = 2
county = 'Brazos'

print(f'{county} {i}')
print(f'Setting Directories')
dir_in_10m_inunmap_raster, dir_in_1m_inunmap_raster, dir_in_10m_binary_raster, \
dir_in_1m_binary_raster, dir_in_minus_raster, dir_in_conditional_raster \
= rastercomparisondirectories(county, '', i, 'Alec')
print(f'Directories Complete')

start_time = time.time()
print(f'Calculating statistics')
stat_type, resolution, dataset, stat_value, fig = rastercomparisonstatistics(dir_in_10m_inunmap_raster, \
    dir_in_1m_inunmap_raster, dir_in_10m_binary_raster, dir_in_1m_binary_raster, dir_in_minus_raster, \
    dir_in_conditional_raster, -9998)

total_time = time.time() - start_time
print('Time to complete statistics = {0:8.5f} seconds'.format(total_time))

stats_dataframe['Stats_Type'] = stat_type
stats_dataframe['Resolution'] = resolution
stats_dataframe['Dataset'] = dataset
stats_dataframe[f'{county}_HUC_{i}'] = stat_value

pd.set_option("display.max_rows", None, "display.max_columns", None)
stats_dataframe
```

```
Brazos 2
Setting Directories
Directories Complete
Calculating statistics
Time to complete statistics = 85.46209 seconds
```

Figure A.21

| | Stats_Type | Resolution | Dataset | Brazos_HUC_2 |
|---|---|---|---|---|
| **0** | X_Origin | 10 | InunMap | 7.244532e+05 |
| **1** | Y_Origin | 10 | InunMap | 3.402018e+06 |
| **2** | Pixel_Width | 10 | InunMap | 9.820378e+00 |
| **3** | Pixel_Height | 10 | InunMap | 9.820378e+00 |
| **4** | X_Origin | 1 | InunMap | 7.244620e+05 |
| **5** | Y_Origin | 1 | InunMap | 3.402010e+06 |
| **6** | Pixel_Width | 1 | InunMap | 1.000000e+00 |
| **7** | Pixel_Height | 1 | InunMap | 1.000000e+00 |
| **8** | Band_Count | 10 | InunMap | 1.000000e+00 |
| **9** | Band_Count | 1 | InunMap | 1.000000e+00 |
| **10** | Band_Count | 10 | Binary | 1.000000e+00 |
| **11** | Band_Count | 1 | Binary | 1.000000e+00 |
| **12** | Band_Count | Combo | Minus | 1.000000e+00 |
| **13** | Band_Count | Combo | Conditional | 1.000000e+00 |
| **14** | Width | 10 | InunMap | 1.892000e+03 |
| **15** | Width | 1 | InunMap | 1.856200e+04 |
| **16** | Width | 10 | Binary | 1.892000e+03 |
| **17** | Width | 1 | Binary | 1.856200e+04 |
| **18** | Width | Combo | Minus | 1.856200e+04 |
| **19** | Width | Combo | Conditional | 1.856200e+04 |
| **20** | Height | 10 | InunMap | 1.644000e+03 |
| **21** | Height | 1 | InunMap | 1.612900e+04 |
| **22** | Height | 10 | Binary | 1.644000e+03 |
| **23** | Height | 1 | Binary | 1.612900e+04 |
| **24** | Height | Combo | Minus | 1.612900e+04 |
| **25** | Height | Combo | Conditional | 1.612900e+04 |
| **26** | Total_Cell_Count | 10 | InunMap | 3.110448e+06 |
| **27** | Total_Cell_Count | 1 | InunMap | 2.993865e+08 |

Figure A.22

| | Stats_Type | Resolution | Dataset | Brazos_HUC_2 |
|---|---|---|---|---|
| **28** | Total_Cell_Count | 10 | Binary | 3.110448e+06 |
| **29** | Total_Cell_Count | 1 | Binary | 2.993865e+08 |
| **30** | Total_Cell_Count | Combo | Minus | 2.993865e+08 |
| **31** | Total_Cell_Count | Combo | Conditional | 2.993865e+08 |
| **32** | NaN_Count | 10 | Binary | 2.942239e+06 |
| **33** | non-NaN_Count | 10 | Binary | 1.682090e+05 |
| **34** | NaN_Count | 1 | Binary | 2.678693e+08 |
| **35** | non-NaN_Count | 1 | Binary | 3.151722e+07 |
| **36** | Total_Raster_Area [m2] | 10 | Inunmap | 2.999711e+08 |
| **37** | Total_Raster_Area [m2] | 1 | Inunmap | 2.993865e+08 |
| **38** | Total_Raster_Area [m2] | 10 | Binary | 2.999711e+08 |
| **39** | Total_Raster_Area [m2] | 1 | Binary | 2.993865e+08 |
| **40** | Inundated_Area [m2] | 10 | Binary | 1.622205e+07 |
| **41** | Inundated_Area [m2] | 1 | Binary | 3.151722e+07 |
| **42** | Total_AreaRatio_1mto10m | Combo | Inunmap | 9.980512e-01 |
| **43** | Total_AreaRatio_1mto10m | Combo | Binary | 9.980512e-01 |
| **44** | Inun_AreaRatio_1mto10m | Combo | Binary | 1.942863e+00 |
| **45** | Inun_AreaRatio_10mto1m | Combo | Binary | 5.147042e-01 |
| **46** | WW | Combo | Conditional | 1.376058e+07 |
| **47** | WD | Combo | Conditional | 1.775664e+07 |
| **48** | DW | Combo | Conditional | 2.461426e+06 |
| **49** | DD | Combo | Conditional | 2.654079e+08 |
| **50** | W1 | 1 | Conditional | 3.151722e+07 |
| **51** | W10 | 10 | Conditional | 1.622201e+07 |
| **52** | Area_Ratio_1mto10m | Combo | Conditional | 1.942868e+00 |
| **53** | Area_Ratio_10mto1m | Combo | Conditional | 5.147030e-01 |
| **54** | Accurate | Combo | Conditional | 4.049773e-01 |
| **55** | Underestimate | Combo | Conditional | 5.225823e-01 |

Figure A.23

| | Stats_Type | Resolution | Dataset | Brazos_HUC_2 |
|---|---|---|---|---|
| **56** | Overestimate | Combo | Conditional | 7.244038e-02 |
| **57** | RMSE | Combo | Minus | 2.277874e+00 |
| **58** | MAE | Combo | Minus | 1.163845e+00 |
| **59** | ME | Combo | Minus | 8.347928e-01 |

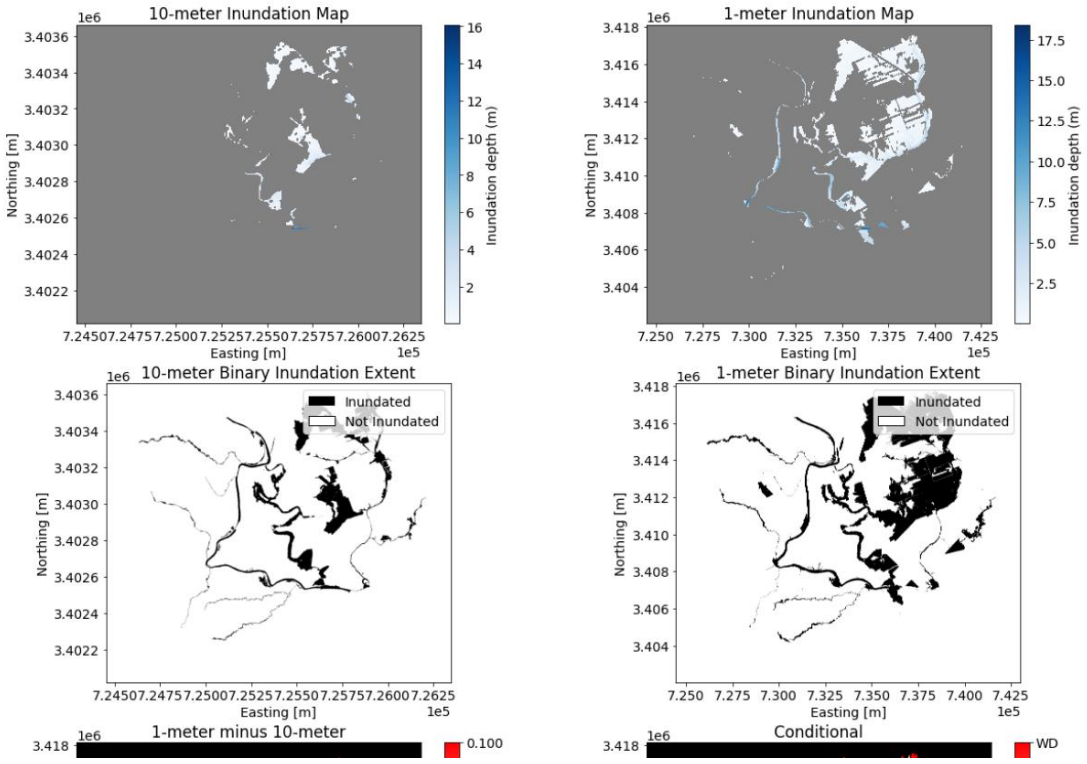


Figure A.24

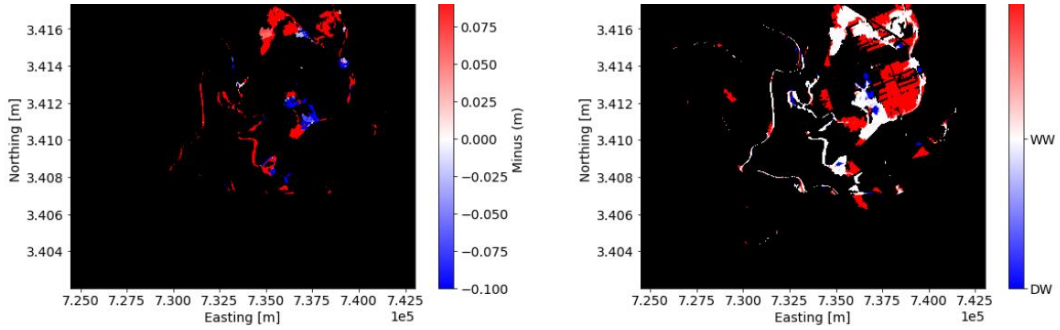


**Batch Statistics and DataFrame Build Function**

```
def rastercomparisonstatsbatch(county, mod, start_value, end_value, forlooptype, user, NaNthreshold):
    first = True
    stats_dataframe = pd.DataFrame()
    county = county
    mod = mod
    start = start_value
    end = end_value
    forlooptype = forlooptype
    user = user
    NaNthreshold = NaNthreshold

    if forlooptype == 'numeric':
        for i in range(start, end, 1):

            print(f'{county} {mod}{i}')
            print(f'Setting Directories')
            dir_in_10m_inunmap_raster, dir_in_1m_inunmap_raster, dir_in_10m_binary_raster, \
            dir_in_1m_binary_raster, dir_in_minus_raster, dir_in_conditional_raster \
            = rastercomparisondirectories(county, mod, i, user)
            print('Directories Complete')

            start_time = time.time()
            print(f'Calculating statistics')
            stat_type, resolution, dataset, stat_value, fig = rastercomparisonstatistics(dir_in_10m_inunmap_raster, \
                dir_in_1m_inunmap_raster, dir_in_10m_binary_raster, dir_in_1m_binary_raster, dir_in_minus_raster, \
                dir_in_conditional_raster, NaNthreshold)

            total_time = time.time() - start_time
            print('Time to complete statistics = {0:8.5f} seconds'.format(total_time))
```

Figure A.25

```
            if first:
                stats_dataframe['Stats_Type'] = stat_type
                stats_dataframe['Resolution'] = resolution
                stats_dataframe['Dataset'] = dataset
                stats_dataframe[f'{county}_HUC_{mod}{i}'] = stat_value
                first = False

            else:
                stats_dataframe[f'{county}_HUC_{mod}{i}'] = stat_value

    if forlooptype == 'alphabetic':
        for i in [chr(i) for i in range(ord(start),ord(end))]:

            print(f'{county} {mod}{i}')
            print(f'Setting Directories')
            dir_in_10m_inunmap_raster, dir_in_1m_inunmap_raster, dir_in_10m_binary_raster, \
            dir_in_1m_binary_raster, dir_in_minus_raster, dir_in_conditional_raster \
            = rastercomparisondirectories(county, mod, i, user)
            print('Directories Complete')

            start_time = time.time()
            print(f'Calculating statistics')
            stat_type, resolution, dataset, stat_value = rastercomparisonstatistics(dir_in_10m_inunmap_raster, \
                dir_in_1m_inunmap_raster, dir_in_10m_binary_raster, dir_in_1m_binary_raster, dir_in_minus_raster, \
                dir_in_conditional_raster, NaNthreshold)

            total_time = time.time() - start_time
            print('Time to complete statistics = {0:8.5f} seconds'.format(total_time))

            if first:
                stats_dataframe['Stats_Type'] = stat_type
                stats_dataframe['Resolution'] = resolution
                stats_dataframe['Dataset'] = dataset
                stats_dataframe[f'{county}_HUC_{mod}{i}'] = stat_value
                first = False

            else:
                stats_dataframe[f'{county}_HUC_{mod}{i}'] = stat_value

    # DataFrame summary statistics calculations
    stats_dataframe['Min'] = stats_dataframe.min(stats_dataframe.iloc[45, 4:])
    stats_dataframe['Max'] = stats_dataframe.max(stats_dataframe.iloc[45, 4:-1])
    stats_dataframe['Mean'] = stats_dataframe.mean(stats_dataframe.iloc[45, 4:-2])
    stats_dataframe['STD'] = stats_dataframe.std(stats_dataframe.iloc[45, 4:-3])

    stats_dataframe.to_csv(rf'C:\Users\ras6399\Documents\NOAA_Research\Projects\1mvs10mComparison\Stats\{county}{mod}_Stats.csv')

    pd.set_option("display.max_rows", None, "display.max_columns", None)
    stats_dataframe
```

Figure A.26

```
    return stats_dataframe
```

### Run Batch Stats

```
stats_dataframe = rastercomparisonstatsbatch('Brazos', '', 0, 23, 'numeric', 'Alec', -9998)
stats_dataframe
```

Figure A.27

# References

Afshari, S., Tavakoly, A.A., Rajib, M.A., Zheng, X., Follum, M.L., Omranian, E., and Fekete, B. (2018). Comparison of new generation low-complexity flood inundation mapping tools with a hydrodynamic model. Journal of Hydrology, Volume 556, 2018, Pages 539-556, ISSN 0022-1694. https://doi.org/10.1016/j.jhydrol.2017.11.036.

Barták, Vojtěch (2009). How to extract river networks and catchment boundaries from DEM: A review of digital terrain analysis techniques. Journal of Landscape Studies, 2, Pages 57-68.

Blake, E.S., and Zelinsky, D.A. (2018). Hurricane Harvey, National Oceanic and Atmospheric Administration, National Hurricane Center Tropical Cyclone Report. Page 76. https://www.nhc.noaa.gov/data/tcr/AL092017_Harvey.pdf.

Brunner, G.W., and United States Army Corps of Engineers Hydrologic Engineering Center (2020). HEC-RAS River Analysis System User's Manual Version 6.0 Beta. https://www.hec.usace.army.mil/software/hec-ras/documentation.aspx.

Carruthers, A. (2020). The assessment, improvement, and application of the GeoFlood flood inundation mapping framework. University of Texas at Austin

Master's Thesis.

Chang, J.L., Mohamed, Z.S., Peik, A.L.S., and Razali, S.F.M. (2016). Flood forecasting model using empirical method for a small catchment area. Journal of Engineering Science and Technology, 11, Pages 666-672.

Dewitz, J. (2019). National Land Cover Database (NLCD) 2016 Products: U.S. Geological Survey data release. https://doi.org/10.5066/P96HHBIE.

Fagan, C. (2015). NFIE-Geo Texas-Gulf Region. HydroShare. http://www.hydroshare.org/resource/1d78964652034876b1c190647b21a77d.

Fagan, C. (2015). NFIE-Geo Mississippi Region. HydroShare. http://www.hydroshare.org/resource/126bb28f05224636a8bc8b3d1bdad6b5.

Federal Emergency Management Administration (2020). Federal Emergency Management Administration - Harvey Flood Depths Grid. HydroShare. http://www.hydroshare.org/resource/e8768f4cb4d5478a96d2b1cbd00d9e85.

Federal Emergency Management Administration (2020). Federal Emergency Management Administration - Risk Mapping, Assessment and Planning (Risk MAP). https://www.fema.gov/flood-maps/tools-resources/risk-map.

Godbout, L., Zheng, J., Dey, S., Eyelade, D., Maidment, D., and Passalacqua, P. (2019). Error assessment for height above the nearest drainage inundation mapping. Journal of the American Water Resources Association, 55(4), 952–963. https://doi.org/10.1111/1752-1688.12783.

GRASS Development Team (2021). Geographic Resources Analysis Support System (GRASS GIS) Software, Version 7.8.6. Open Source Geospatial Foundation. http://grass.osgeo.org.

Jafarzadegan, K., and Merwade, V. (2018) Probabilistic floodplain mapping using HAND-based statistical approach. Geomorphology (Amsterdam, Nether-

lands), 324, 48–61. https://doi.org/10.1016/j.geomorph.2018.09.024.

Jamali, B., Löwe, R., Bach, P.M., Urich, C., Arnbjerg-Nielsen, K., and Deletic, A. (2018). A rapid urban flood inundation and damage assessment model. Journal of Hydrology, Volume 564, 2018, Pages 1085-1098, ISSN 0022-1694. https://doi.org/10.1016/j.jhydrol.2018.07.064.

Johansen, K., Grove, J., Denham, R., and Phinn, S. R. (2013). Assessing stream bank condition using airborne LiDAR and high spatial resolution image data in temperate semirural areas in Victoria, Australia. Journal of Applied Remote Sensing, 7(1), 073492. https://doi.org/10.1117/1.JRS.7.073492.

Johnson, J. M., Munasinghe, D., Eyelade, D., and Cohen, S. (2019). An integrated evaluation of the National Water Model (NWM)–Height Above Nearest Drainage (HAND) flood mapping methodology. Natural Hazards Earth System Sciences, 19, Pages 2405–2420. https://doi.org/10.5194/nhess-19-2405-2019.

Koenig, T.A., Bruce, J.L., O'Connor, J.E., McGee, B.D., Holmes, R.R., Jr., Hollins, Ryan, Forbes, B.T., Kohn, M.S., Schellekens, M.F., Martin, Z.W., and Peppler, M.C. (2016). Identifying and preserving high-water mark data. U.S. Geological Survey Techniques and Methods, Book 3, Chapter A24, Page 47. http://dx.doi.org/10.3133/tm3A24.

Lashermes, B., Foufoula-Georgiou, E., and Dietrich, W. E. (2007). Channel network extraction from high resolution topography using wavelets. Geophysical Research Letters, 34(23), L23S04. https://doi.org/10.1029/2007GL031140.

Liu, Y.Y., Maidment, D.R., Tarboton, D.G., Zheng, X., Yildirim, A, Sazib, N.S., and Wang, S. (2016). A CyberGIS approach to generating high-resolution Height Above Nearest Drainage (HAND) raster for national

flood mapping. CyberGIS 16, The Third International Conference on CyberGIS and Geospatial Data Science, Urbana, Illinois, July 26-28. http://dx.doi.org/10.13140/RG.2.2.24234.41925.

National Oceanic and Atmospheric Administration (2018). Hurricane Harvey Information. http://www.weather.gov/hgx/hurricaneharvey.

National Oceanic and Atmospheric Administration (2018). Billion-dollar weather and climate disasters: Table of events. http://www.ncdc.noaa.gov/billions/events.

National Oceanic and Atmospheric Administration (2018). Federal Funding Opportunity 2018 Joint Technology Transfer Initiative. https://www.grants.gov/web/grants/view-opportunity.html?oppId=300187.

National Oceanic and Atmospheric Administration and National Water Center (2020). National Oceanic and Atmospheric Administration National Water Center - Harvey National Water Model Streamflow Forecasts. HydroShare. http://www.hydroshare.org/resource/35d4502200764c2985c24ae5c8836ab9.

Nobre, A.D., Cuartas, L.A., Hodnett, M., Rennó, C.D., Rodrigues, G., Silveira, A., Waterloo, M., and Saleska, S. (2011). Height Above the Nearest Drainage – a hydrologically relevant new terrain model. Journal of Hydrology, Volume 404, Issues 1–2, 2011, Pages 13-29, ISSN 0022-1694. https://doi.org/10.1016/j.jhydrol.2011.03.051.

National Oceanic and Atmospheric Administration and Office of Water Prediction (2020). National Oceanic and Atmospheric Administration, Office of Water Prediction: The National Water Model. https://water.noaa.gov/about/nwm.

Orlandini, S., Tarolli, P., Moretti, G., and Dalla Fontana, G. (2011). On the prediction of channel heads in a complex alpine terrain using gridded elevation data. Water Resources Research, 47(2), W02538. https://doi.org/10.1029/2010WR009648.

Passalacqua, P., T. Do Trung, E. Foufoula-Georgiou, G. Sapiro, and W. E. Dietrich (2010). A geometric framework for channel network extraction from lidar: Nonlinear diffusion and geodesic paths. Journal of Geophysical Research, 115, F01002. doi:10.1029/2009JF001254.

Passalacqua, P., Belmont, P., and Foufoula-Georgiou, E. (2012). Automatic geomorphic feature extraction from lidar in flat and engineered landscapes. Water Resources Research, 48(3). https://doi.org/10.1029/2011WR010958.

Pelletier, J. D. (2013). A robust, two-parameter method for the extraction of drainage networks from high-resolution digital elevation models (DEMs): Evaluation using synthetic and real-world DEMs. Water Resources Research, 49, Pages 75 – 89. https://doi.org/10.1029/2012WR012452.

Perona, P., and Malik, J. (1990). Scale-Space and Edge Detection Using Anisotropic Diffusion. IEEE Transactions on Pattern Analysis and Machine Intelligence, 12(7), 629–639. https://doi.org/10.1109/34.56205

Robson, A.J., Moore, R.J., Wells, S.C., Rudd, A., Cole, S.J., and Mattingley, P.S. (2017). Understanding the performance of flood forecasting models. Report - SC130006/R. ISBN: 978-1-84911-408-0. https://assets.publishing.service.gov.uk/government/uploads/system/uploads/attachment_da
_report.pdf.

Rodda, H.J.E. (2005). The development and application of a flood risk model for the Czech Republic. Natural Hazards (Dordrecht), 36(1), Pages 207–220.

https://doi.org/10.1007/s11069-004-4549-4.

Rennó, C.D., Nobre, A.D., Cuartas, L.A., Soares, J.V., Hodnett, M.G., Tomasella, J., and Waterloo, M.J. (2008). HAND, a new terrain descriptor using SRTM-DEM: Mapping terra-firme rainforest environments in Amazonia. Remote Sensing of Environment, 112(9), Pages 3469–3481. https://doi.org/10.1016/j.rse.2008.03.018.

Rosser, J., Leibovici, D., and Jackson, M. (2017). Rapid flood inundation mapping using social media, remote sensing and topographic data. Natural Hazards, 87(25), Pages 103-120. https://link.springer.com/content/pdf/10.1007/s11069-017-2755-0.pdf.

Sämann, R., Graf, T., Neuweiler, I. (2019) Modeling of contaminant transport during an urban pluvial flood event – The importance of surface flow. Journal of Hydrology, Volume 568, 2019, Pages 301-310, ISSN 0022-1694. https://doi.org/10.1016/j.jhydrol.2018.10.002.

Sangireddy, H., Stark, C., Kladzyk, A., and Passalacqua, P. (2016). GeoNet: An open source software for the automatic and objective extraction of channel heads, channel network, and channel morphology from high resolution topography data. Environmental Modelling & Software, Volume 83, 2016, Pages 58-73. https://doi.org/10.1016/j.envsoft.2016.04.026.

Teng, J., Jakeman, A.J., Vaze, J., Croke, B.F.W., Dutta, D., and Kim, S. (2017) Flood inundation modelling: A review of methods, recent advances and uncertainty analysis. Environmental Modelling & Software, Volume 90, 2017, Pages 201-216, ISSN 1364-8152. https://doi.org/10.1016/j.envsoft.2017.01.006.

Tesfa, T.K., Tarboton, D.G., Watson, D.W., Schreuders, K.A.T., Baker,

M.E., and Wallace, R.M. (2011). Extraction of hydrological proximity measures from DEMs using parallel processing. Environmental Modelling & Software: with Environment Data News, 26(12), Pages 1696–1709. https://doi.org/10.1016/j.envsoft.2011.07.018.

Tarboton, D. G. (1997). A new method for the determination of flow directions and upslope areas in grid digital elevation models. Water Resources Research, 33(2), Pages 309-319. https://doi.org/10.1029/96WR03137.

Tarboton, D.G. (2015). Utah State University, TauDEM Web page. http://hydrology.usu.edu/taudem/taudem5/index.html.

Texas Department of Transportation, Transportation Planning and Programming (2019). Texas County Boundaries. https://services.arcgis.com/KTcxiTD9dsQw4r7Z/arcgis/rest/services/Texas_County_Boundar

Texas Natural Resources Information System, A Division of the Texas Water Development Board (2020). StratMap: Elevation - Lidar. https://tnris.org/stratmap/elevation-lidar/.

United States Geological Survey (2020). The National Map 3D Elevation Program. https://www.usgs.gov/core-science-systems/national-geospatial-program/national-map.

United States Census Bureau (2021). QuickFacts. https://www.census.gov/quickfacts/fact/table/US/PST045219?.

United States Geological Survey (2020). National Hydrography: Watershed Boundary Dataset. https://www.usgs.gov/core-science-systems/ngp/national-hydrography/watershed-boundary-dataset?qt-science_support_page_related_con=4#qt-science_support_page_related_con.

United States Geological Survey (2020). NHD Medium Resolution.

https://www.usgs.gov/core-science-systems/ngp/hydrography/about/nhd-medium-resolution.

United States Geological Survey (2020). National Hydrography: NHDPlus High Resolution. https://www.usgs.gov/core-science-systems/ngp/national-hydrography/nhdplus-high-resolution.

Watson, K.M., Harwell, G.R., Wallace, D.S., Welborn, T.L., Stengel, V.G., and McDowell, J.S. (2018). Characterization of peak streamflows and flood inundation of selected areas in southeastern Texas and southwestern Louisiana from the August and September 2017 flood resulting from Hurricane Harvey. U.S. Geological Survey Scientific Investigations Report 2018–5070, Page 44. https://doi.org/10.3133/sir20185070.

Wing, O.E.J., Sampson, C.C., Bates, P.D., Quinn, N., Smith, A.M., and Neal, J.C. (2019). A flood inundation forecast of Hurricane Harvey using a continental-scale 2D hydrodynamic model. Journal of Hydrology X, Volume 4, 2019, 100039, ISSN 2589-9155. https://doi.org/10.1016/j.hydroa.2019.100039.

Zheng, X., Maidment, D. R., Tarboton, D. G., Liu, Y. Y., and Passalacqua, P. (2018). GeoFlood: large-scale flood inundation mapping based on high-resolution terrain analysis. Water Resources Research, 54, Pages 10,013-10,033. https://doi. org/10.1029/2018WR023457.

Zheng, X., Tarboton, D. G., Maidment, D. R., Liu, Y. Y., and Passalacqua, P. (2018). River channel geometry and rating curve estimation using height above nearest drainage. Journal of the American Water Resources Association, 54(4), Pages 785-806. https://doi.org/10.1111/1752-1688.12661.